Nuno Filipe Ferreira Lopes

Licenciado em Ciências de Engenharia

Development and implementation of strategies for the incorporation of reinforcing elements in aluminium alloys by solid state processing

Dissertação para obtenção do Grau de Mestre em Engenharia Mecânica

Orientador: Professora Doutora Rosa Maria Mendes Miranda
Co-orientador: Professor Doutor Telmo Jorge Gomes dos Santos

FACULDADE DE CIÊNCIAS E TECNOLOGIA
UNIVERSIDADE NOVA DE LISBOA

Março de 2012

Copyright

Development and implementation of strategies for the incorporation of reinforcing elements in aluminium alloys by solid state processing

©Nuno Filipe Ferreira Lopes, FCT-UNL, 2012

A Faculdade de Ciências e Tecnologia e a Universidade Nova de Lisboa têm o direito, perpétuo e sem limites geográficos, de arquivar e publicar esta dissertação através de exemplares impressos reproduzidos em papel ou de forma digital, ou por qualquer outro meio conhecido ou que venha a ser inventado, e de a divulgar através de repositórios científicos e de admitir a sua cópia e distribuição com objectivos educacionais ou de investigação, não comerciais, desde que seja dado crédito ao autor e editor.

Agradecimentos

A realização deste trabalho apenas foi possível graças ao contributo, empenho e apoio de várias pessoas às quais é imprescindível agradecer.

Em primeiro um especial agradecimento à minha Orientadora, Professora Rosa Maria Mendes Miranda pela oportunidade de realizar este desafiante trabalho, assim como, pela disponibilidade, empenho e interesse no desenvolvimento deste trabalho

Um sincero obrigado ao meu Co-Orientador, Professor Telmo Santos, pelo seu apoio, orientação e tempo disponibilizado na realização prática deste trabalho, assim como pela amizade demonstrada.

Um sincero obrigado a todos os Professores do Núcleo de Tecnologia Industrial, pelo interesse demonstrado e pelas ajudas preciosas na realização deste trabalho.

Um especial agradecimento aos Srs. António Campos e Paulo Magalhães por toda a sua assistência técnica neste trabalho, assim como pelo apoio e grande amizade sempre demonstrada. Não podia deixar de agradecer também ao Mestre João Gonzalez, por toda a ajuda prestada.

Uma especial abraço ao meu colega João Russo pela amizade demonstrada durante a realização deste trabalho, assim como os necessários momentos de distracção.

Aos meus colegas e amigos, também futuros engenheiros, um muito obrigado pela ajuda e força demonstrada no decorrer desta vida académica. Um especial abraço para os meus amigos Filipe Marques, Jorge Bernardo, Hélder Guerra, Rodrigo Pires, Gonçalo Sorger, Duarte Lousa, João Violante, Luís Almeida e Tiago Baptista.

A toda à minha família em especial, aos meus País e Irmão um muito obrigado por todo o apoio e carinho demonstrado durante todos estes anos.

Aos meus grandes amigos de sempre um profundo obrigado por todos os momentos de distracção e apoio durante estes anos de faculdade, e principalmente durante a realização deste trabalho.

Resumo

Este trabalho visou estudar diferentes estratégias de processamento de superfícies por fricção linear para a produção de compósitos de matriz metálica A primeira consistiu numa pré deposição de partículas sobre o material base e posterior processamento. Na segunda utilizaram-se pinos consumíveis preenchidos com partículas de reforço. Em cada uma destas estratégias usou-se corrente eléctrica num processo sob patente.

Como substrato utilizou-se alumínio AA5083-H111 e como reforço, partículas de carboneto de silício e alumina com tamanhos médios de 35 e 45 µm.

A pré deposição de partículas de reforço revelou-se mais eficaz que o uso de ferramentas consumíveis com partículas. Estes últimos produziram revestimentos com uma distribuição não homogénea de partículas e baixa interligação entre o substrato e o reforço.

Pré depositando partículas de alumina, observou-se maior extensão e profundidade com um aumento de dureza no reforço de 60 %, enquanto que com partículas de carboneto silício o aumento de dureza foi de 300 %, embora com extensões e profundidades da camada reforçada menores que os observados para a alumina nas mesmas condições processuais e menor homogeneidade dos revestimentos.

Com a passagem de corrente eléctrica verificou-se um aumento de extensão e profundidade (500 e 40 % respectivamente), mas um decréscimo de dureza (10 %), com a mesma estratégia de deposição sem corrente.

Abstract

This investigation aimed to study new surface processing strategies to produce reinforced surface metal matrix composites by Friction Stir Processing. The first consisted on pre-placing reinforcing particles over the surface, while the second used consumables drilled holes filled with reinforcing particles. Each strategy was investigated using an electric current in a process under patenting.

Aluminium AA5083-H111 plates were used as base material. Silicon carbide and alumina particles with median sizes of 35 and 45 μm, respectively, were used.

Pre deposition of reinforcing particles proved to be more effective than the use of consumable tools packed with particles. The last ones produced coatings with a non homogeneous distribution and poor bonding between the substrate and the reinforcing coating.

The pre deposition of alumina produced a higher extension and depth of reinforced layer and an increase in hardness of 60%, while silicon carbide produced an increase in hardness of 300 %, though in a smaller extension and depth than alumina under the same processing conditions.

Using the electric current a significant raise of 500% and 40% was observed in extension and depth respectively, but hardness decreased by 10 %.

Palavras Chave

Processamento por fricção linear

AA5083-H111

Carboneto silício

Alumina

Depósito por fricção linear

Compósitos superficiais de matriz metálica

Keywords

Friction stir processing

AA5083-H111

Silicon carbide

Alumina

Friction stir deposition

Surface metal matrix composite

Índice

Table index

Figure index

Abbreviations and Symbols

Al_2O_3	Alumina
AS	Advancing side
BM	Base material
EDS	Energy dispersive X-ray spectroscopy
FGM	Functionally graded material
FSP	Friction stir processing
FSW	Friction stir wending
HAZ	Heat affected zone
MMC	Metal matrix composite
RS	Retreating side
SEM	Scanning electron microscopy
SMMC	Surface metal matrix composite
TMAZ	Thermo-mechanically affected zone

.

1 Introduction

Attention has been given to aluminium alloys in applications where low weight is required. However, aluminium alloys have limited mechanical strength. The incorporation of reinforcing particles on the surface or in the bulk would benefit this material for high demanding applications. So, an investigation was conducted aiming to assess the potential to use solid state processing techniques to reinforce aluminium alloys enhancing mechanical properties, specially on the surface. Friction Stir Processing (FSP) was considered for this study.

FSP is a technique based on the fundamentals of Friction Stir Welding (FSW), and in the last years, an increased in this technique has been verified for applications in manufacturing industries, that allows the reinforcing of material surfaces. This technique, in theory, is considered less expensive and more versatile than other competing technologies, for achieving surface reinforcement composites. However, FSP process has the disadvantage of lack in process control, in terms of particle distributions. This lack of control is due to unpredictability in viscoplastic material flow during FSP process. So, investigation is needed to identify parameter control and their effect on surface characteristics but also on new strategies to reinforce the surfaces leading to the production fo materials with a chemical, structural and functional gradient as FGMs.

However, limited work exist on this matter, thus investigation is needed to identify the best strategies for reinforcing Al, the effect of processing parameters on particle distribution and surface characteristics.

1.1 Objectives

This study was conducted in the framework of a research project funded by FCT/MCTES "Technology developments of friction stir processing to produce functionally graded materials and improve surfaces for advance engineering applications – FRISURF".

The main objective was to investigate different strategies based on convectional FSP, with the purpose of surface reinforcing a ductile alloy adding hard ceramic particles improving FSP reinforcement techniques.

The following specific objectives can be highlighted:

1. deposit reinforcing particles on aluminium alloys by different techniques and process the surfaces by FSP
2. produce surface layers with hard ceramic particles- SiC and Al_2O_3;
3. assess the use of assisting techniques to FSP process, namely with electric current;
4. characterize mechanical and structurally the metal matrix composites surfaces produced.

1.2 Structure

The present work is structured in five chapters.

Chapter 2 describes the state of the art addressing process concepts for the subsequent result analysis.

Chapter 3 presents the experimental procedure adopted including set-up and test planning. A brief description of material and reinforcements strategies is done, as well as, the techniques and procedures used for surface characterization.

Chapter 4 reports the results and discussion and is divided in four main subjects, concerning the characterization reinforcements by strategy and material tested. Results from metallography, image processing, SEM/EDS and hardness are presented.

Main conclusions and proposals for future work developments and presented in Chapter 5.

2 State of art

Materials with improved mechanical properties have become of great importance for engineering nowadays. Surface metal matrix composites (SMMC) are a unique class of these materials.

Much attention has been paid to Friction Stir Processing (FSP) as a way to produce SMMC as reinforcements elements to ductile alloys. This technique is based on Friction Stir Welding (FSW). Most studies on this area focus on using FSP to process base materials such as aluminum, copper, magnesium, and a number of polymers.

Materials can be added during FSP to improve base materials tribological and mechanical properties for surface reinforcements of aluminium alloys, magnesium alloys, and copper. Details of the benefits and limitations of FSP will be presented, along with examples of potential applications.

2.1 Base Materials

As said previously the base material (BM) used on studies for reinforcement are aluminium, magnesium, copper and polymer nanocomposites. These materials are used do to their unique mechanical properties that make them an object of intense studies for a very wide applications in advance engineering.

2.1.1 Aluminum alloys

Aluminium alloys are present in a wide variety of industrial applications due to their good relation weight/volume due to low density, high resistance to corrosion, good formability that ensures that these alloys can be used in various objects, and also this material can be recycled.

In automobile and aerospace industries, this material ensures a good performance and lower fuel consumptions, due to a low relation weight/volume. Due to corrosion resistance, naval and chemical industries have also a high interest in this alloys.

A vast range of aluminium alloys exist, each one with different composition and properties. Aluminium alloys are presented in Table 2.1. Alloys from series 2XXX, 6XXX and 7XXX are thermally treated [1] while the others can be mechanically worked.

Table 2.1 – Series of aluminium alloys and main alloying elements [1].

Series	Main Elements	Other elements
1XXX	Pure aluminium	-
2XXX	Cu	Mg, Li
3XXX	Mn	
4XXX	Si	
5XXX	Mg	
6XXX	Mg, Si	
7XXX	Zn	
8XXX	Li, Sn, Fe, Cu and Mn	

According to ulterior treatments, the alloys have a number of designations. Table 2.2 depicts the designation of treatments in Al alloys.

Table 2.2 – Treatments specifications [1].

Designation treatment	Specification
F	Without any treatments
O	Annealed
H	Mechanical treatments
Fist digit specification	Specification
H1X	Cold deformation
H2X	Cold deformation and partial annealed
H3X	Cold deformation and stabilization
T	Thermal treatments

Due to the high interest in these alloys, a number of techniques is being studied to improve its properties and increase their applications. FSP with reinforcement particles is one of these techniques. Mishra et al [2] was the first to use FSP to successful manufacture a SiC

surface aluminium based composites, and showed that SiC particles were well distributed in the Al matrix and good bounding with the Al matrix was achieved. Later, Lim et al [3] found that the addition of SiC particles into an aluminium matrix lead to an increase in wear resistance.

2.1.2 Magnesium alloys

Magnesium alloys are also object of studies for the same reasons as aluminium alloys, but also because magnesium allows show good possibilities in substituting aluminium in aerospace, automobile industries, and plastic in the electronic and computer industries for their weight saving and good thermal and electric conductivity. However, mechanical properties such as hardness are not sufficient to enhance their applications [3]. Magnesium alloy such AZ31 has been studied for reinforcement in order to enhance mechanical properties [3-8]. Lee et al. [9] added SiC particles by FSW of a magnesium alloy and reported an improvement in hardness and wear characteristics of the weld zone. Chen et al. [10] investigated the wear properties of a AZ91 magnesium alloy and identified two main wear regimes, a mild wear regime and a severe wear regime. Most of recent researches have demonstrates that surface reinforcing is achievable, and that magnesium alloys properties were increased [3,4,11].

2.1.3 Copper alloys

Copper is mostly used for various thermal and electronic applications, such as electronic packaging, electrical contacts and resistance welding electrodes. This is due to the good thermal electric conductivity, high plasticity, excellent resistance to corrosion and oxidation [12]. However, low mechanical stench and undesirable wear resistance limit the applications for this material [13-17]. Do to the electrolytic co-deposition of ceramic particles for fabrication of metal matrix composites; these studies are very interesting for a larger field of industrials applications, especially in cases where high abrasive and protective characteristics are needed [12,15].

2.2 Solid Processing

FSP is a solid state process that can generate localized heating, plastic deformation and stirring in a relatively short duration [18-20]. FSP was first developed by Misha et al. [2] using the basic principles of Friction Stir Welding (FSW).

FSP technique has a wide range of applications, for example, to eliminate defects in cast parts, reduce weight in vehicles enhancing performance [11, 22-25], repair equipment in naval industry, where the material used is subjected to high corrosion [26].

FSP uses a non-consumable rotating tool and a pin of different geometries and profiles, and a shoulder constraining the material plasticized by the pin. The friction between the rotational tool and the work piece produces localized heating, and when the proper thermal and

mechanical conditions are achieved, the tool initiates a translation movement as represented in Figure 2.1

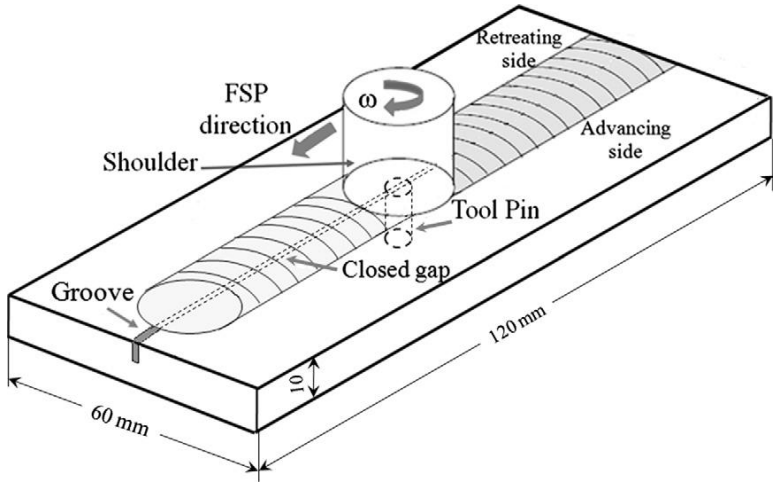

Figure 2.1 - Schematic illustration of FSP [27].

Plastic deformation imposed by the pin and shoulder rotation, generates friction heat that softens the material without reaching its melting point, making possible the translation movement. The material is moved around the pin and constricted by the shoulder.

Both FSW and FSP have the advantages summarized in Table 2.1 [28].

Table 2.3 - Key benefits of friction stir welding and friction stir processing [28].

Metallurgical benefits	Technical benefits	Environmental benefits	Energy benefits
• Solid state process; • Low distortion of workpiece; • No loss of alloying elements; • Excellent metallurgical properties at the processed area; • Fine microstructure; • Absent of cracking.	• Depth of the processed zone can be adjusted simply by changing the length of the pin; • Processing results can be accurately controlled by optimizing tool design and process parameters; • One-step technique; • Good dimensional stability and repeatability regardless of atmospheric conditions, worker`s experience and number of parts to produce; • Automated process.	• No shielding gas is required; • Eliminate griding wastes; • Eliminate solvents required for surface degreasing and cleaning; • Reduced noise; • Consumable materials saving, such as rugs, wire or other gases.	• Low energy consumption since heat input comes from friction and plastic deformation; • Improve materials use (e.g.. joining thickness) allows reduction in weight; • Low energy needed than is fusion processing; • FSW replaces fastener use in joining of "non-weldable" alloys thereby reducing the weight of aircraft, automobile or ship, which leads to a lower fuel consumption

2.2.1 Process parameters

Process parameters are very important, because they determinate the amount of heat generated and plastic deformation, affecting material flow around the non-consumable tool, thus determining the results obtained. For these reasons, it is necessary a deep understanding of these parameters so that better control of the process can be achieved.

The most important parameters are:

- Tool geometry – As previous studies [29-35] tool geometry can be considered the key factor for controlling the material flow and the homogeneity of particle distribution within the stirred zone. Different pin profiles are available, some of which are depicted in Figure 2.2.

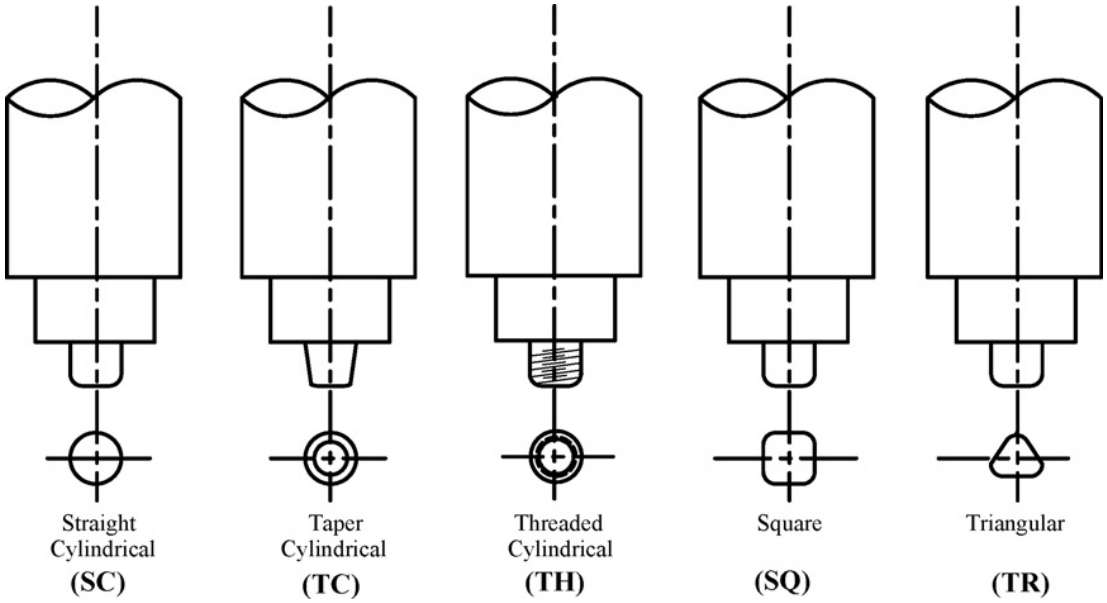

Figure 2.2 - FSP tool pin profiles exemples [20].

For a better comprehension of pin profiles influence in FSP intense investigation has been conducted. This investigation focus on the influence of the pin profile in particle distribution, grain size and hardness, and the behavior of viscoplastic material flow around the pin.

Elangovan et. al. [20] showed relative improvement in microhardness with certain pin profiles, pins with live edges like square and triangular profiles show better results than straight cylindrical and taper cylindrical. Threaded cylindrical profiles also show good results as showed in Figure 2.3

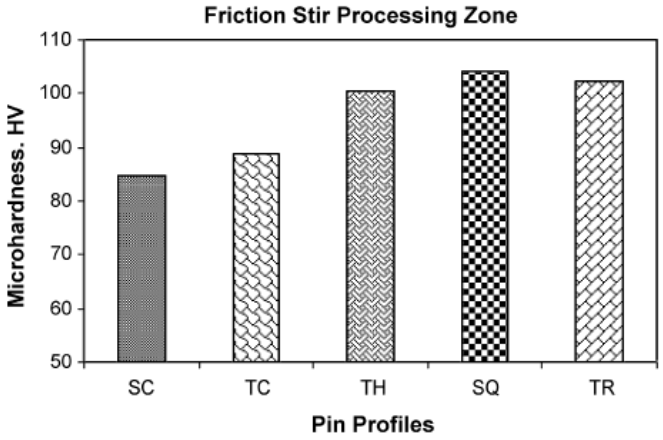

Figure 2.3 - Effect of pin profiles on FSP zone hardness [20].

Mahmoud et al. [36] studied the pin profiles influence, combined with rotation and advancing speeds in multipass processing. Figure 2.4 shows macroscopic aspects of nugget cross sections produced by different pin profiles at different rotating speeds. The authors observed that using a square pin, SiC particles were more homogeneously distributed in the nugget zone, while with other pin profiles large clustering areas of SiC were observed.

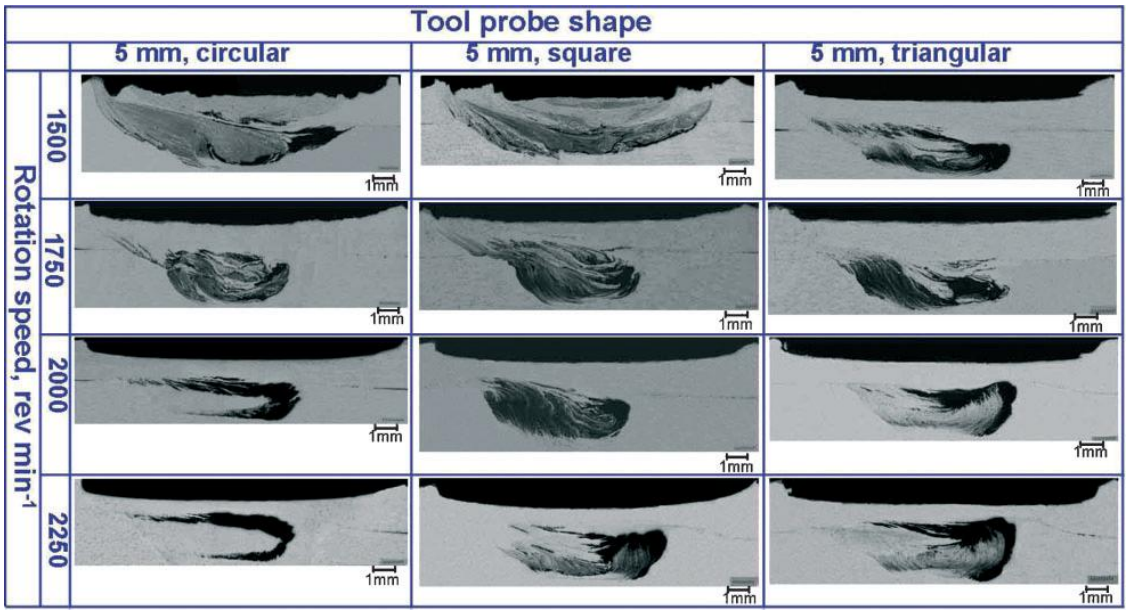

Figure 2.4 – Macrographs of cross sections of nugget zone after first pass with different pin profiles [36].

The authors also performed hardness profiles in tests with different pin profiles at a rotational speed of 1500 rev/min and with three passes, and showed that with a square pin a more stable profile and higher values were achieved in comparison with circular and triangular profiles, as depicted in Figure 2.5. In conclusion the authors reported that better

results are obtained with a square pin profile, but wear rate of this tool is much higher compromising tool life and process costs.

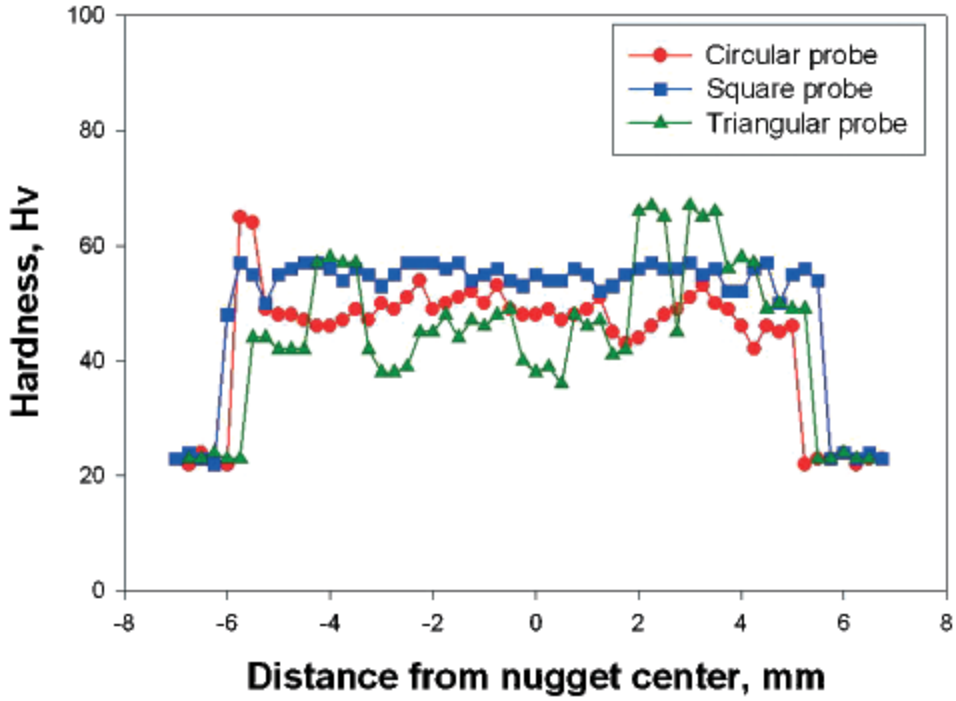

Figure 2.5 – Hardness profiles across FSP stirred zones after three passes with different tool profiles at a rotating speed of 1500 rev/min [36].

Shoulder profiles are also of great importance especially in FSP, as they are responsible for the improvement of the interaction shoulder/work piece, by entrapping plasticized material. Thus, the amount of plastic deformation increases, resulting in an enhancement of material mixing [37]. According to Rajiv et al [38] several shoulder profiles can be used, as showed in Figure 2.6.

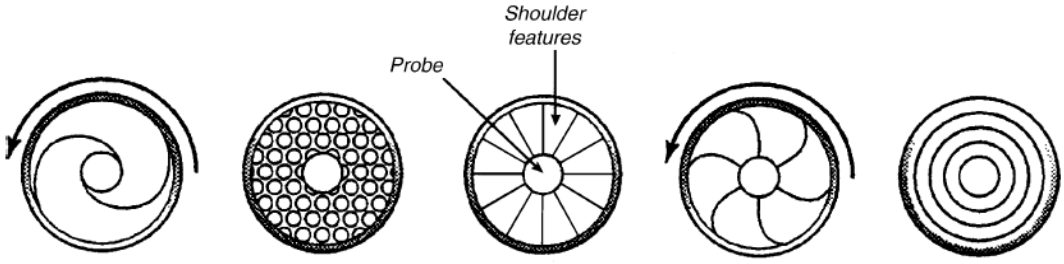

Figure 2.6 - Shoulder geometries [38].

- Tool rotation rate – As spindle speed rises, material plastic deformation becomes more intense, increasing heat input, which enables more material mixing. Therefore, it is possible to achieve a greater grain size refinement, equiaxial grains, material homogeneity and precipitate solution [28]. Mahmoud et al.[36] reported that producing

a SiC particle reinforced composite on a aluminum surface, rotational speed of 1500 rev/min was not enough to form a sound nugget when pin diameter where 3 and 7 mm, and the height and width of the nugget zone tend to increase with the rotation speed.

- Transverse speed – Affects mainly the time of exposure to friction heat and material viscosity provoked by the rotation speed of the tool. Low speeds result in larger exposing time to high temperatures that may not by desirable, originating some defects, such grain growth and severe clusters. However, high speed may result in lower heat input that causes lack of stirring in friction processed zone yielding poor tensile resistance. Elangovan et al. [34] showed that with a speed of 0.76 mm/s superior tensile properties can be obtained regardless of pin profiles. However, transverse speeds depend of the rotation speed chosen, meaning that transverse speed depends of the rotational speed chosen.
- Tilt angle – It defines the angle between the tool axis and the work piece as shown in Figure 2.7. A good choice of the tilt angle ensures that the shoulder moves the material more efficiently from the front to the back of the pin, and improves the quality of the surface finish. Usually, a maximum of 5º angle is used in FSP process.

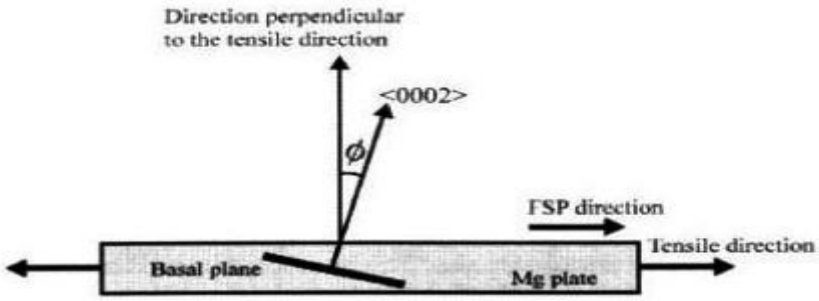

Figure 2.7 - Tilt angle definition [27].

- Tool vertical force – This force is applied by the tool shoulder in the axial direction of the tool, and is responsible for the amount of plasticized material and material consolidation. Very high or too low forces, lead to undesirable defeats such as, grain growth, coarsening during cooling and shear lips for high forces, and poor material consolidation for low forces. Tool vertical force is responsible for the amount of material deposition in the BM surface.

2.2.2 Multiple-Pass FSP

Multiple passes of FSP consists in passing more than one time with FSP tool over the same track on the BM. This is done to improve several characteristics of FSP. Yang et al. [39] used multiple FSP passes with alumina particles achieving a larger composite zone and a more

homogeneous distribution of ceramic particles. Authors produced a Al6061/Al_2O_3 nano-composite surface layer, with multiple passes of FSP as depicted in Figure 2.8.

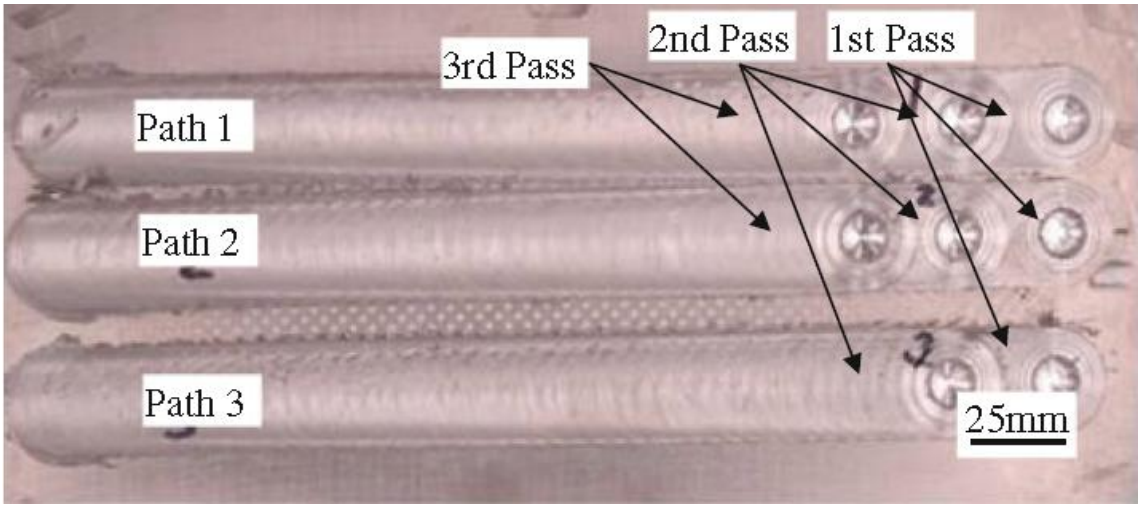

Figure 2.8 - Multiple passes of FSP [39].

They also concluded that an increased number of passes causes a more uniforme dispersion of fine clusters and a good distribution of Al_2O_3 particles as shown in Figure 2.9. that represents cross sections of tracks with one, two and three passes of FSP. Analyses from a) to c) represents one to three passes respectively, and from d) to f) the interface zone is observed from one to three passes respectively.

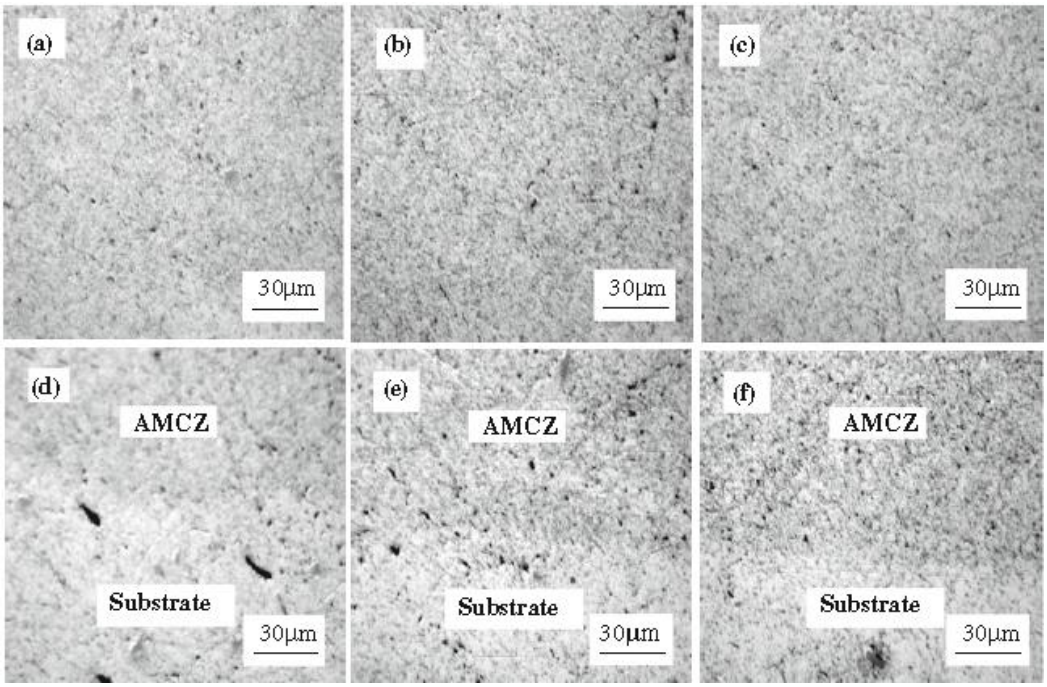

Figure 2.9 - Optical microscopic images of samples processed by different passes in AMCZ and transition region from composite coating to aluminium alloy substrate: a) AMCZ after one pass; b) AMCZ of two passes; c) AMCZ after three passes; d) transition region after one pass, e) transition region after two passes; and f) transition region after three passes (17.64 kN axial force) [39].

Nakata et al. [40] applied multiple passes of FSP and observed an increase of hardness profile of about 20 HV, and an increase in tensile strength (1.7 times higher), as shown in Figure 2.10, where the highest values were achieved in the left zone that correspond to the multi passes. Also hardness profile is more homogeneous than in the right side that corresponds to a simple FSP pass.

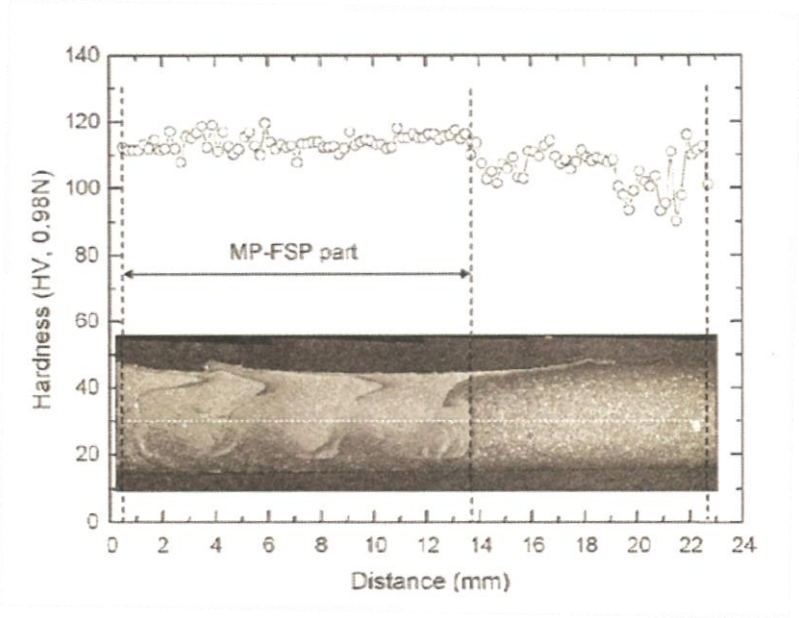

Figure 2.10 - Hardness profile of cross-section in a multi-pass FSP [40].

However, some studies [41,42] using multiple passes presented a lower ductility in comparison with single passes.

Multiple passes of FSP can improve homogeneity but can also be undesirable because some defects may appear, like low ductility.

2.3 Methods of reinforcement

Few methods of reinforcement have been reported and in most studies reinforcing powders are mixed with a small amount of volatile solvent such as methanol, in order to form a thin reinforcement layer, preventing the escape of reinforcing powders.

The most common method consists of machining grooves in the BM to insert the reinforcing particles. The dimensions of the groove have to do with the volume of reinforced powder to insert in the BM. The groove is normally aligned with the central line of the rotational pin as showed in Figure 2.11, to prevent sputtering of the reinforcing powders and its ejection from groove during the process.

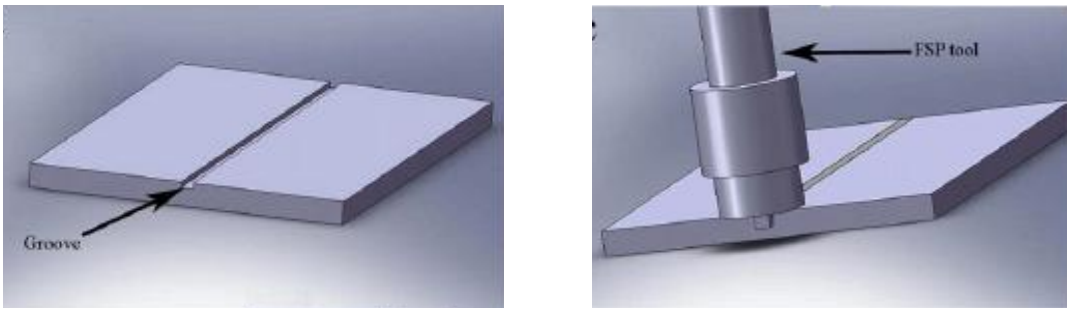

a) b)

Figure 2.11 - Schematic illustration of the groove FSP setup, a) groove, and b) toll aligned with groove [12].

Some methods consist in machining the groves and then closing these with one FSP pass without pin, in order to close an entrap the reinforcing particles, as depicted in Figure 2.12.

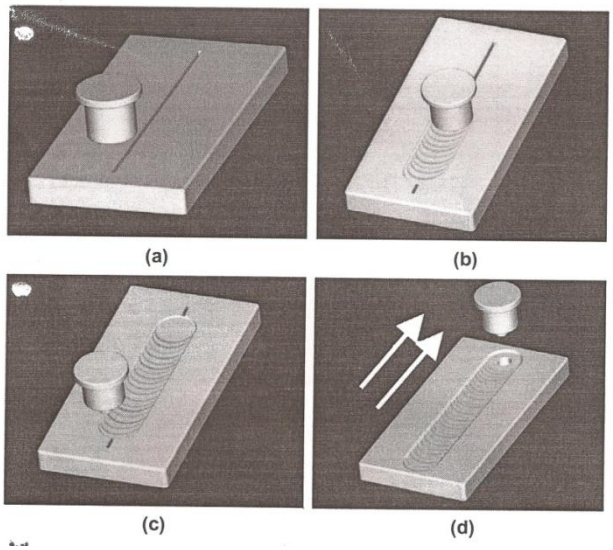

Figure 2.12 - FSP procedure: a) Cuter groove with inserted particles; b) Closing the groove with particles; c) FSP with pin tool; c) multiple passes of FSP [43].

Gandra et al [28] performed tests where the groove was aligned with the central line of the rotational tool, and also placed laterally to the tool on the advancing and retreating sides, and observed that in some samples where the groove was placed laterally, it was not possible to close the grooves as depicted in Figure 2.13 a) and c). The author also concluded that the material flow does not stir the channel, but rather deforms it.

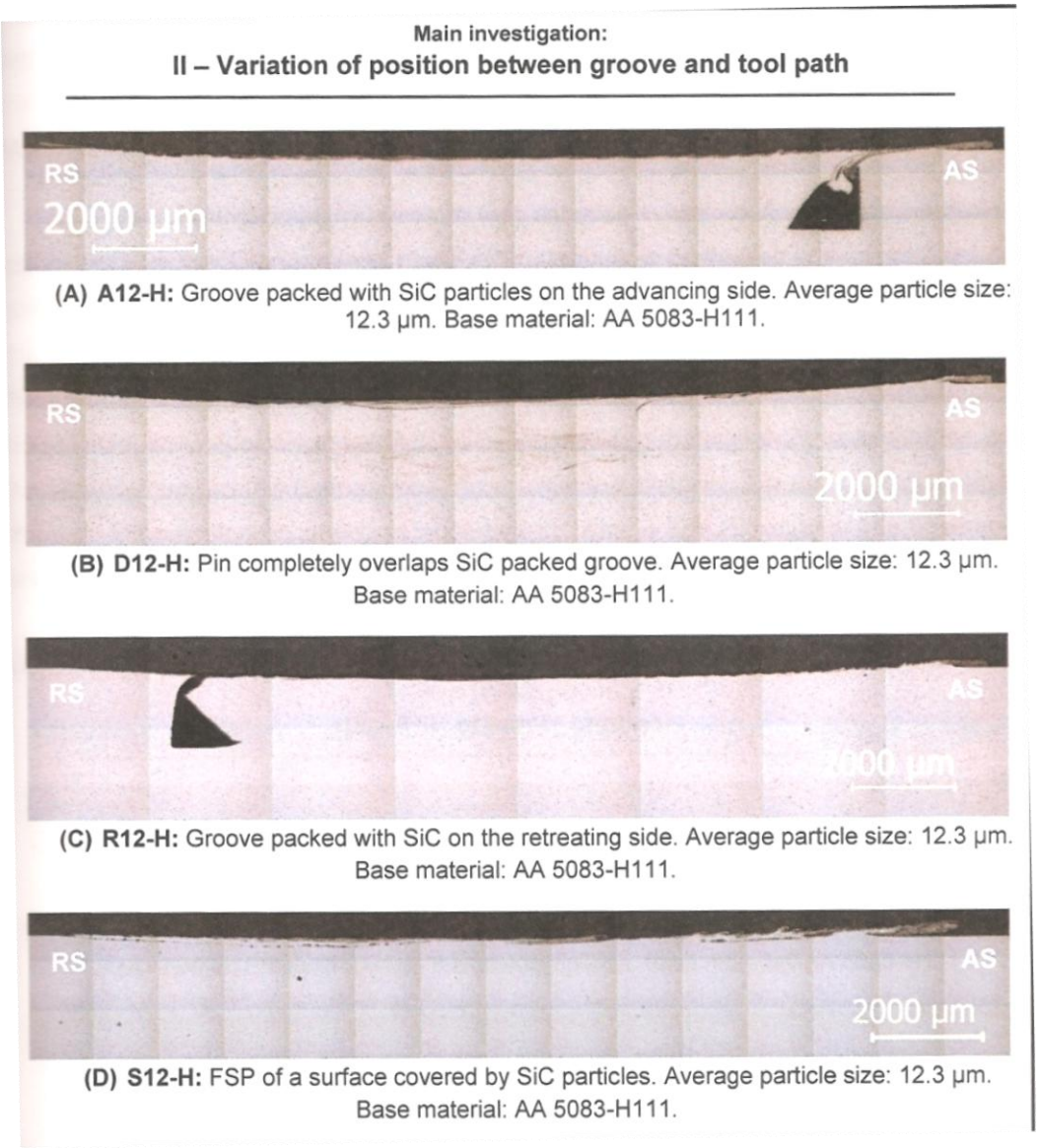

Figure 2.13 - Macrographs of bead cross section, with different placements of grooves [28].

Another method consists in machining holes in the BM to insert reinforcing powders as can be seen in Figure 2.14. The method uses holes in order to make a more uniform distribution of the reinforcing powders. However, the authors were not conclusive about the influence of using machined holes compared to other techniques, like grooves.

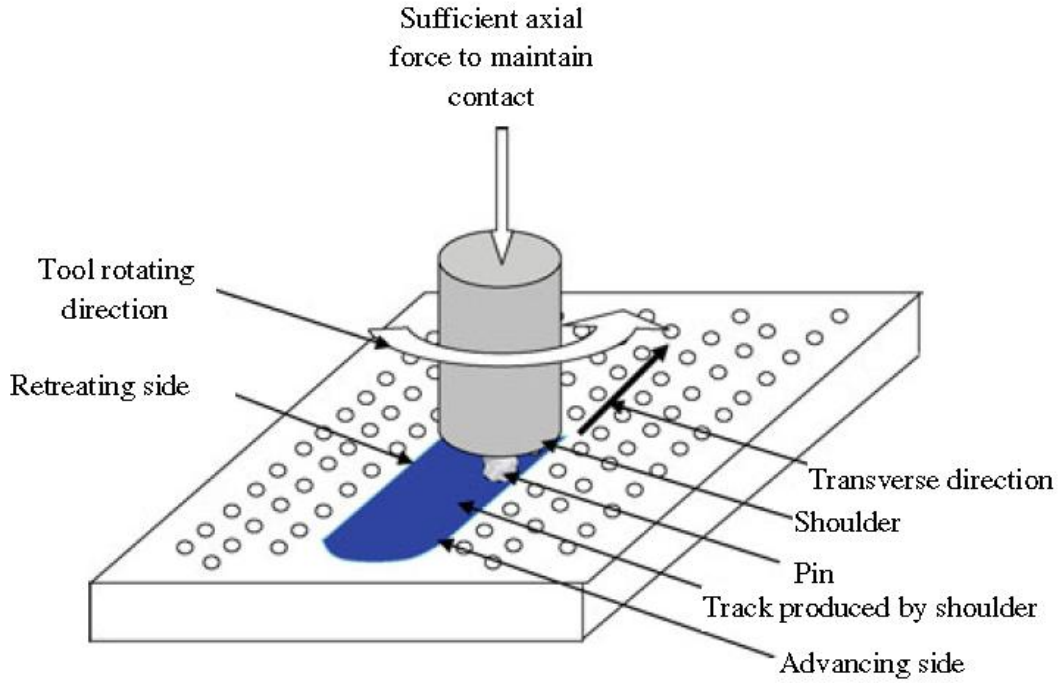

Figure 2.14 - Schematic representation of the drilled holes in surface reinforcing [6].

Spraying the particles over the surface of the BM is another strategy to introduce particles on FSP surfaces. A mixture of reinforcing particles with a small amount of volatile solvent like methanol is used. Another method is thermal spray where the BM is blasted with the reinforcing particles grits to a surface roughness of about 10μm, and in order to increase the surface roughness and therefore the adhesion of the coating to the substrate. A plasma spray (PS) system is normally used. Zahmatkesh et al. [44] used this technique with the following parameters, as showed in Table 2.2.

Table 2.4 - Process parameters [44].

Spray parameters	Unit
Stand off distance	10 cm
Plasma gas (Ar) flow rate	40 l/mim
Arc current	500 A
Voltage	44 V
Powder feed rate	30 g/min
Carrier gas (N_2) flow rate	3 l/min

2.4 Reinforcement materials

A large range of materials are used for surface reinforcements, the majority being hard ceramic particles. According to Devinder Yadav et al. the ceramic particles most used are SiC,

Al_2O_3, AlN . This allows improving BMs, as mentioned in chapter 2.1, as hardness and wear resistance.

2.4.1 Ceramic reinforcing

Hard ceramic particles have proved to increase hardness, wear resistance, and tensile properties of surface composites. For this, several studies have been conducted to understand and improve these reinforcements. Most of the studies performed with ceramic particles, use SiC and Al_2O_3. Mishra et al. [2] reported the first successful results on the fabrication of SMMC with ceramic particles. Mahmoud et al. [36] successfully produced a surface metal matrix reinforcement, Kurt et al. [47] reported that the higher micro hardness (150 HV) of the SiC was successfully obtained for a specimen under a rotating speed of 100 rpm and a travel speed of 15 mm/min.

SiC – These hard ceramic particles are widely used in the fabrication of SMMC using FSP, this is due to the properties of SiC particles (SiCp). As stated above, the first results on fabrication of SMMC were reported by Mishra et al. [46], where the SiCp were mixed with methanol and them applied to the surface of aluminium plates. The authors showed that the SiCp were well distributed in the aluminium matrix, and a good bounding was achieved. Garcia et al [48] noticed that the wear resistance of AA6061/SiCp composites increased with the volume fraction and size of reinforcements. Kurt et al. [47] incorporated SiCp in a AA1050 alloy, using FSP with various tool rotations and transverse speeds. The authors demonstrated that using the correct parameters, a decrease in grain size and increase in hardness of the BM can be achieved; also good interfacial condition between the SiCp and the BM was achieved. The authors reported that microhardeness improves with the increase of rotational speed, and reached maximum value of 150 HV with a rotational speed of 1000 rpm and a transverse speed of 15 mm/min. These high values of Al/SiC composites were attributed to the presence of the SiCp, which also improved the bending and yield strengths, which was 60 MPa to the plain specimen and 84 MPa for SiCp reinforced specimen.

Other studies [27,49] used SiC particles with the addition of solid lubricants like graphite and MoS_2, in order to improve the tribological properties of composites under sliding wear conditions. Alidokht et al. [27] reported a good dispersion of the SiC and MoS_2 particles, in a A356 aluminium alloy, and an increase in wear resistance, but a decrease in hardness in comparison with Al/SiC composites as shown in Figure 2.15. This decrease in hardness was due to the presence of MoS_2particles confirmed by SEM analysis in Figure 2.16.

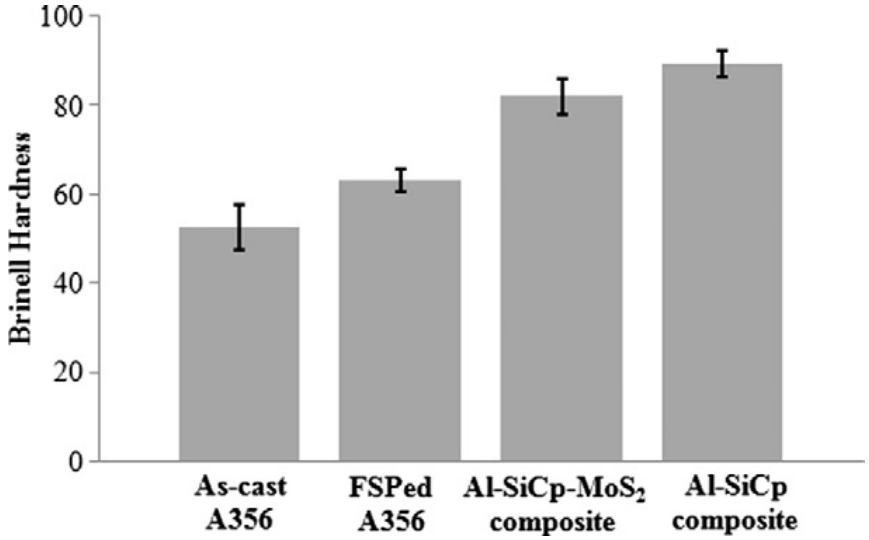

Figure 2.15 - Variation of Brinell hardness in as-cast, FSPed A356 and composite samples [27].

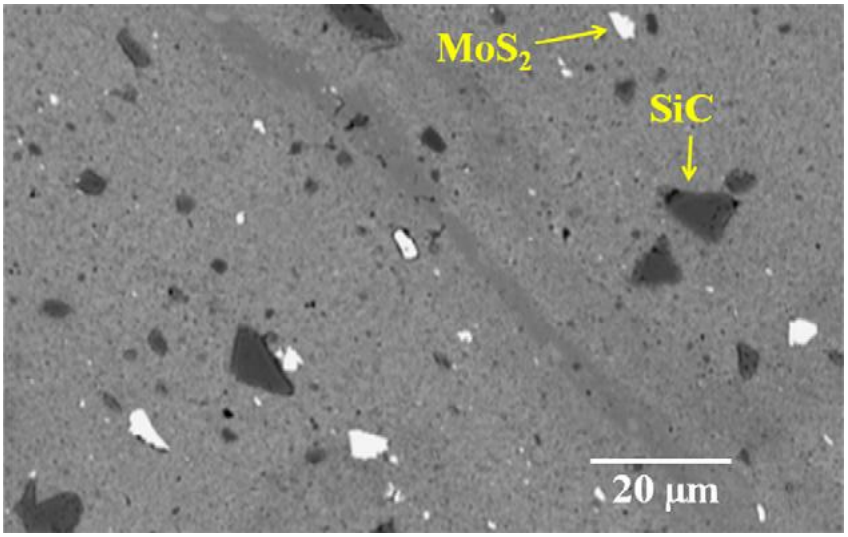

Figure 2.16 - SEM image of particle dispersion in hybrid composite produced by FSP [27].

In previous studies only aluminum alloys have been reinforced with SiCp, but this hard ceramic particles are also used to reinforce other materials, like magnesium and copper alloys. Morisada et al. [4] reported to have successfully dispersed SiCp in a AZ31 alloy with FSP, and concluded that the insertion of SiC particles promoted the grain refinement of the AZ31 matrix. The authors also noticed an increase in micro hardness of 80 HV in the stirred zone. An evaluation of the grain growth at elevated temperatures was also performed by the authors, who reported that the fine grain structure of the AZ31 produced by FSP was unstable above 300ºC, and with the SiC particles the fine grain structure was maintained at elevated temperatures around 400ºC.

Barmouz et al.[12] studied the production of a copper reinforced metal matrix composite by FSP, with SiC particles for thermal and electronic applications, and reported that in pure

copper without SiCp, the hardness increased in the nugget zone with the increase in transverse speed (**Erro! A origem da referência não foi encontrada.** a), reinforced with SiCp the hardness decreases with the increase in transverse speeds (Figure 2.17 b).

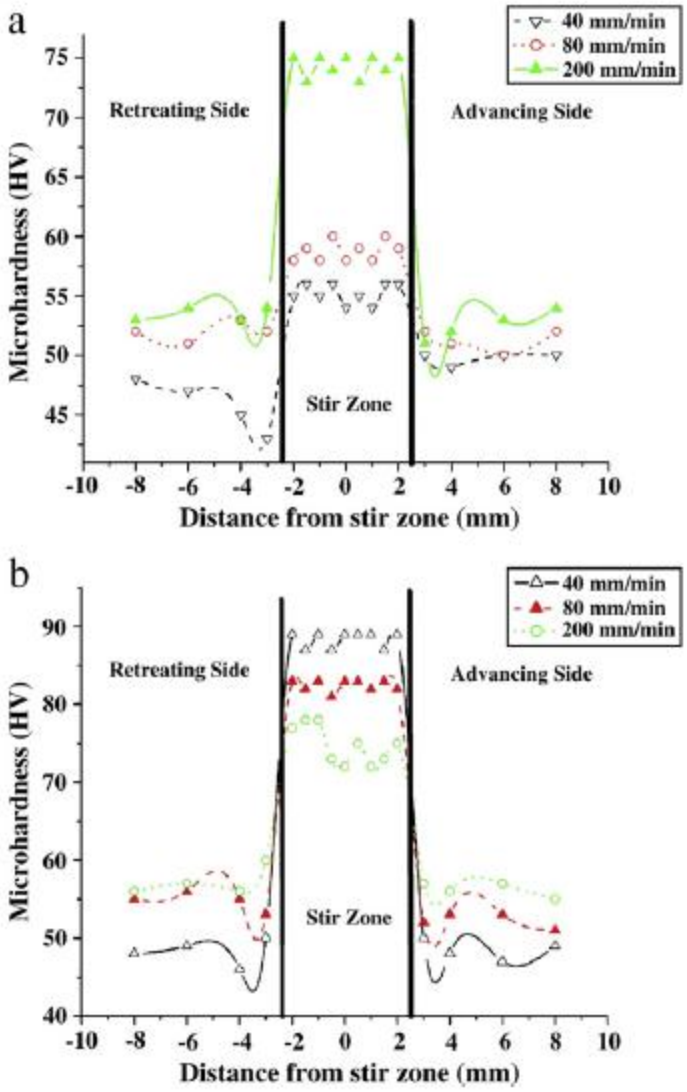

Figure 2.17 - Microhardness values of specimens FSPed a) without SiC particles and b) with SiC particles in different traverse speeds [12].

Al_2O_3 – These hard ceramic particles are also very used in the production of SMMC, for the same reasons as SiCp, and because alumina particles provoke less wear in FSP tools. Most studies performed on this subject reported a successful fabrication of SMMC with alumina hard ceramic particles [23,36,53].

Zahmatkesh et al. [43] reported that Al_2O_3 clusters were almost homogenously distributed in a nanocomposite surface layer without any evidence of structural defects. For an AA2024

aluminium alloy reinforced by a mixture of aluminium and Al_2O_3 powders, the authors observed an increase in the average microhardness about 230 HV and surface friction coefficient and wear rate dropped as depicted in Figure 2.18.

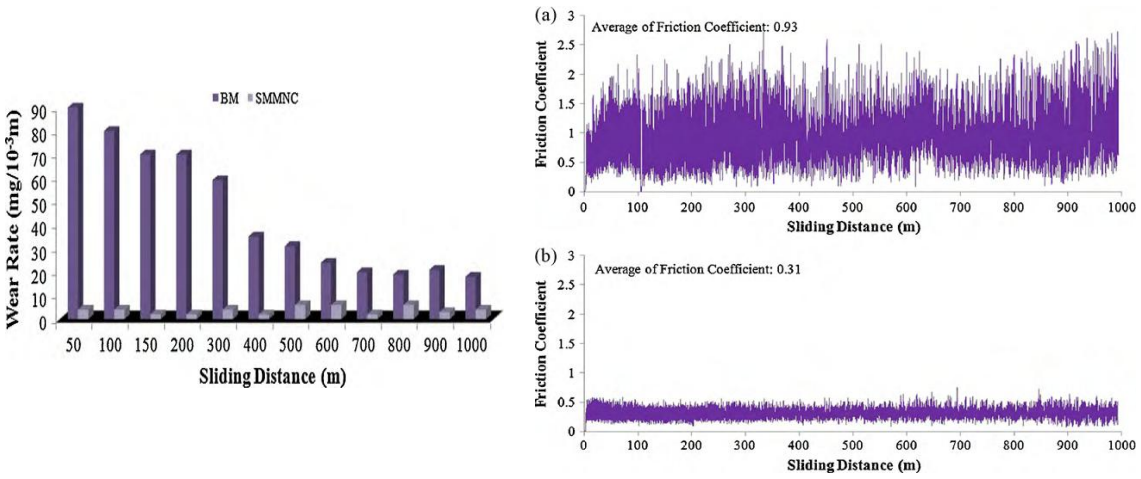

a) b)

Figure 2.18 - a) Wear rate of samples as a function of sliding distance for BS and SMMNC, b) Variation of friction coefficient BM and SMMNC [43].

Other studies [11,23,34,36] concluded that a good dispersion of nano-size Al_2O_3 particles varies with the number of FSP passes performed, normally a good dispersion is achieved in the surface composite layer produced by three and four passes. Shafiei-Zarghani et al. [23] applied multiple passes producing a Al/Al_2O_3 nano-composite surface layer and concluded that increasing the number of passes causes more uniform dispersion of fine clusters and a good distribution of Al_2O_3 particles as showed in Figure 2.19, where it is noticeable that, with one pass, some alumina particles concentrations are observed, and with three and four passes no particle clusters are observed.

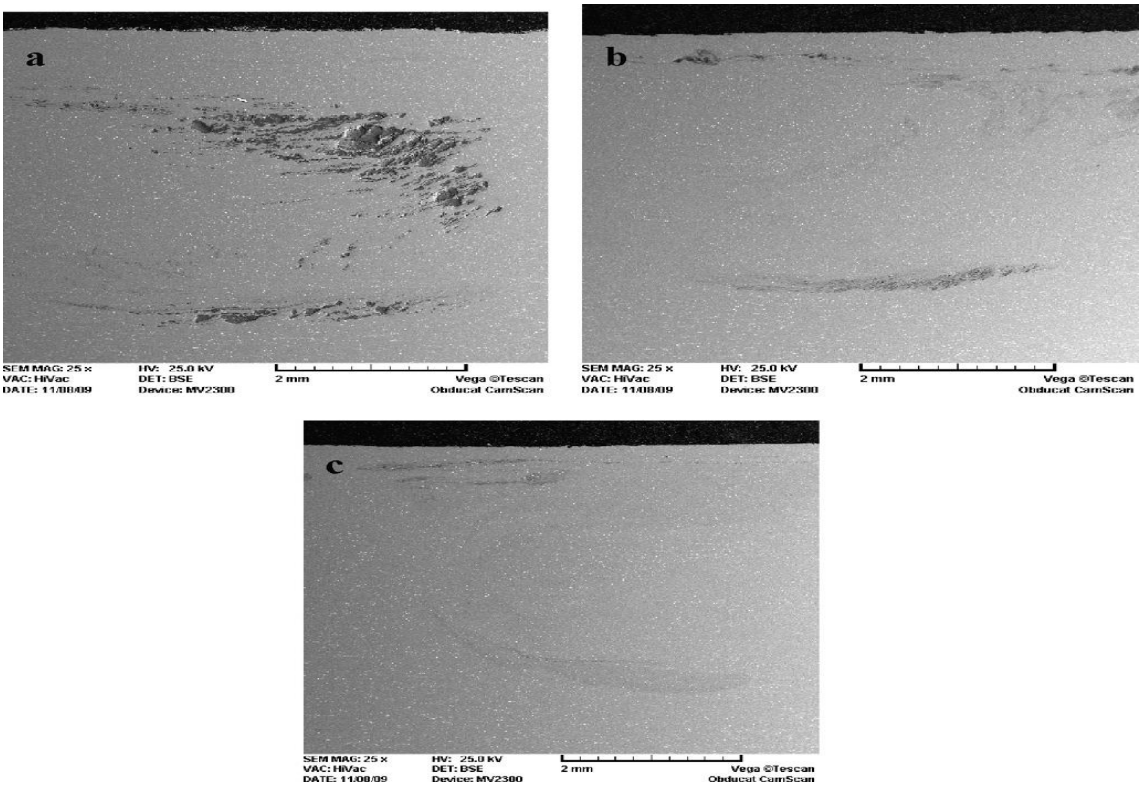

Figure 2.19 - Cross section micrographs of the SCL fabricated using one a), three b) or four c) FSP passes showing Al_2O_3 particles clustering/dispersion within the stirred zone [23].

In this study, the authors reported an increase in hardness with increasing number of FSP passes, using an AA6082 commercial Aluminium alloy, and concluded that such increase was due to a more uniform distribution of alumina particles and to a decrease in the matrix grain size as seen in Table 2.3. Maximum values of micro hardness were achieved with four passes (312 HV) and the wear resistance also increased.

Table 2.5 - Summary of the mean Al_2O_3 cluster size, Al matrix grain size and micro hardness value of the SCLs produced using various number of FSP passes [23].

Number of FSP passes	Mean Al_2O_3 cluster size (nm)	Mean matrix (Al) grain size (µm)	Zener limitinggrain size (µm)	Micor hardenss value (Hv)
1	476	5.1	2.11	159
2	254	2.44	1.13	186
3	125	0.75	0.56	267
4	76	0.48	0.34	312

Besides the improvements in hardness and wear, Sharifitabar et al. [25] found out that increasing the number of passes to four, led to the improvement of tensile and yield strengths, and also by increasing to three passes the elongation was improved, but with four passes the

elongation suffers a decrease, this is observed in specimens with and without reinforcing particles, has showed in Figure 2.20.

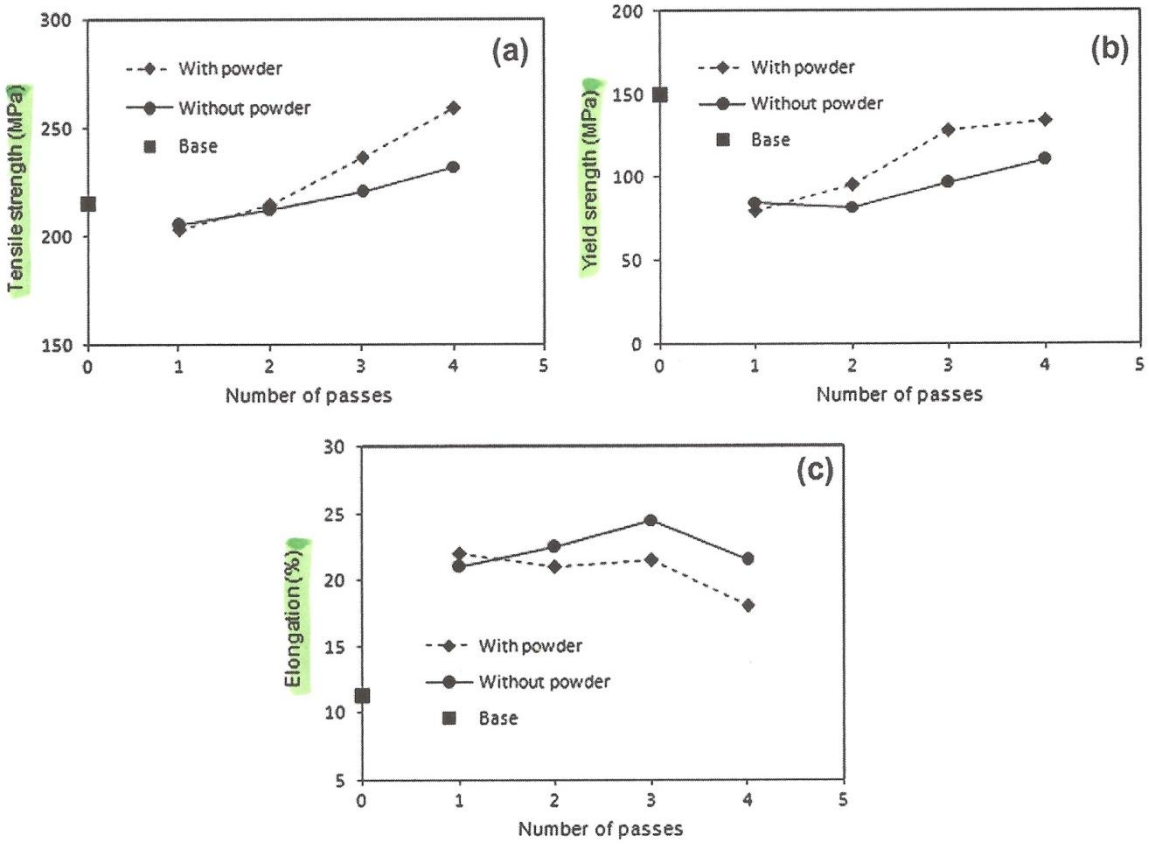

Figure 2.20 - Tensile properties of the composites and FSP materials produced by different passes [25].

Faraji et al. [11] investigated microstructure, wear properties and micro hardness of an AZ91 reinforced with Al_2O_3 by means of FSP, and concluded that grain size and particle distribution are highly affected by FSP parameters and the number of passes. Wear resistance increases significantly and the magnesium alloy passes from severe wear to mild wear, due to particle reinforcement as seen in Figure 2.21. This figure represents wear rate of a processed base material compared to samples reinforced with alumina particles with different pin profiles and with one and two passes.

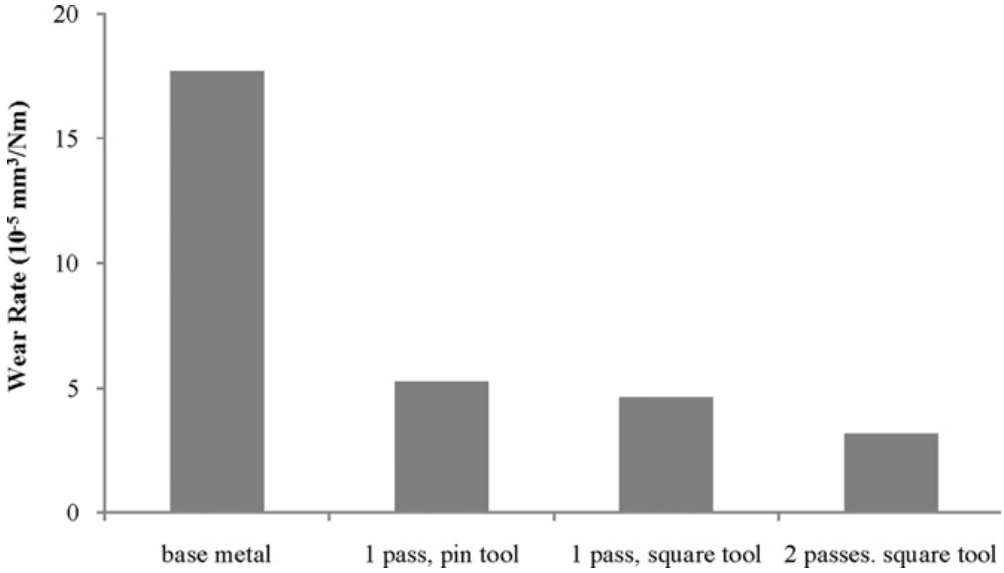

Figure 2.21 - Wear rate in the base metal and the friction stir processed specimens in different conditions [11].

Surface-hybrid-composites – Hybrid metal matrix composites are engineering materials reinforced by a combination of two or more different type and/or form of substance. This is done in an attempt to combine advantages from the different substances and provides a high degree of freedom in material design [55]. It was reported by Misha et al [20] that hybrid composites of SiC and Al_2O_3 exhibited better wear resistance than those with only SiC, and Al_2O_3. The advantage of using hybrids composites especially SiC and Al_2O_3 composites, is that both composites complement each other. Some studies documented that SiC is more effective than Al_2O_3 in wear resistance and in the increase of hardness, while Al_2O_3 is more stable and inert, providing a better tolerance to corrosion and a better temperature behaviour.

Mahmoud et al. [57] used different ratios of SiC and Al_2O_3 on a commercially pure aluminium AA1050-H24, to produce hybrid composites. The authors reported an almost homogenously distribution over the nugget zone by FSP without any defects except some small voids formed around the Al_2O_3 particles. It was also reported that the hardness increased to about 60 HV with SIC particles at 100% and decreased proportionally with the increase of Al_2O_3 particles. Friction coefficient decreases with the increase of Al_2O_3 particles as depicted in Figure 2.22 a) regardless the applied load. Wear characteristics were very random and depended on applied loads and SiC and Al_2O_3 ratios (Figure 2.22 b).

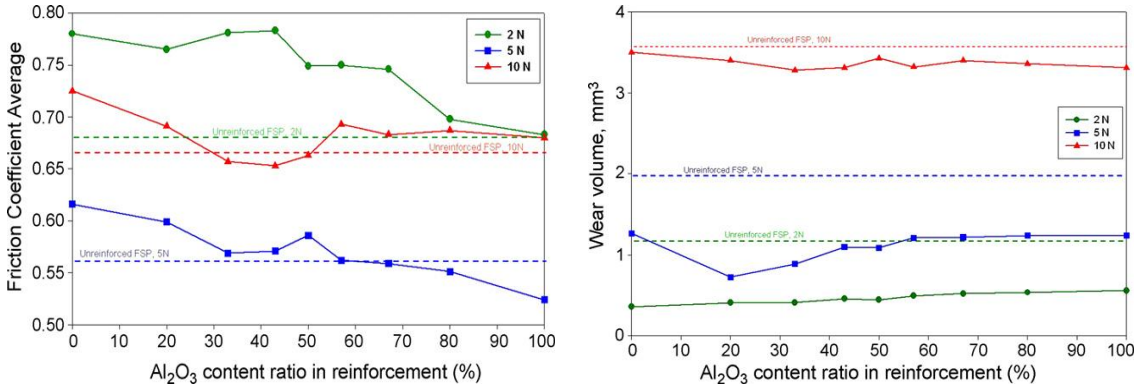

a) b)

Figure 2.22 - a) Effect of hybrid ratio of reinforcements on the average friction coefficient at normal applied loads of 2, 5, and 10 N, b) Effect of hybrid ratio of reinforcements on wear volume losses at normal applied loads of 2, 5, and 10 N [57].

2.4.2 Metallic reinforcements

Nickel – Hard ceramic particles are normally used as reinforcements in the metal matrix. However, these materials have some disadvantages like low ductility, poor wettability, and particle matrix debonding or presence of porosity or particle clusters. Many techniques were developed in order to prevent these defects, and an alternative approach was to substitute the hard ceramic particles by Nickel particles, that have high strength (400 MPa), high stiffness, good temperature properties, and good oxidation resistance. However, many studies struggle with the serious challenges of processing metallic particle reinforced MMC, most specifically Ni particles.

Normally, the processing of metallic particles is achieved by disintegrated metal deposition (DMD) [59], but FSP can be used instead of DMD. However, few studies have been made in this direction. Yadav et al. [24] studied a commercially AA1050 aluminium alloy with Ni particles, and concluded that Ni particles can be successfully embedded in aluminium and the process lead to a grain refinement of the matrix, and a three fold increase in 0.2% proof stress while an appreciable amount of ductility was retained. The authors also compared their work with results obtained with hard ceramic particles studies [58-61] as showed in Table.2.6. Another study [44] confirmed the previous results.

Table 2.6 - Tensile properties of the composite (standard deviations are shown in parenthesis) [24].

Material	0.2 Proof stress (MPa)	UTS (MPa)	% elongation	N
Base aluminium	35 (0.6)	72 (1)	39 (0.6)	0.37
FDPed Al	82 (2)	90 (3)	35 (2)	0.15
Al-7% Ni composites	104 (3.7)	127 (7)	25 (2.6)	0.2
Al-11.6% Al_2O_3	86	165	8	
Al-22% SiC	-	11	8	
Al-TiB2 in situ	128	164	6.3	

Nitinol (NiTi) – Nitinol is a nickel titanium alloy used due to its shape memory effect and superelasticity. Shape memory effect is the ability to undergo deformation at one temperature, and then recover its original [62, 63]. Studies reported on the use of NiTi wires, but few have been made in the dispersion of NiTi powders in a metal matrix. Dixit et al. [64] reported to have successfully produced a NiTi reinforced AA1100 composite using FSP, and that the particles were uniformly distributed as can be seen in Figure 2.23. Good bonding with the matrix was achieved and no interfacial products were formed during FSP. The authors suggest that under adequate processing, the shape memory effect of NiTi particles can be used to induce residual stress in the parent matrix. Most importantly, experimental samples in this study show an improvement in mechanical properties such as micro hardness.

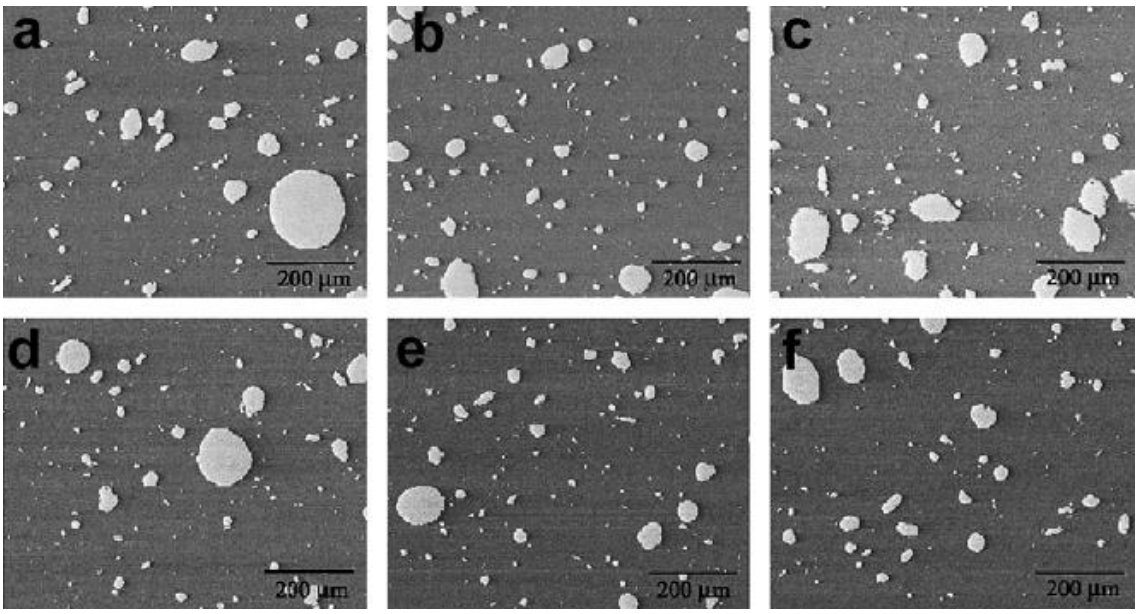

Figure 2.23 - SEM images showing uniformly distributed NiTi particles in various parts of the nugget region of FSP composites a)–c) and of annealed composites d)–f) [64].

Iron – Iron reinforcing is very attractive for high temperature applications, because these particles are stable at elevated temperatures. Normally these alloys are achieved by rapid solidification and mechanical alloying, but FSP can be a suitable substitute of these techniques. According to Lee et al. [13] a Al-10 at. and using a %Fe powder in their work, the authors showed that FSP can be applied to produce aluminium base nanocomposites from powder mixtures, the composite produce was fully dense with enhanced modulus of 91 GPa, and tensile strengths of 217 MPa. However, the authors suggested that more work is needed in the optimization of FSP parameters in order to further improve the mechanical properties.

2.4.3 Nanotubes

Multi-walled carbon nanotubes (MWCNT) – The addition of MWCNT into a number of metallic materials as reinforcing fibres is topic of recent interest due to the unique mechanical and physical properties of this material, like very high tensile strengths [65-67]. FSP was used by Lim et al. [68] to produce a composite of aluminium alloy with MWCNT, and the author confirmed that nanotubes were embedded in the stirred zone and that the multi walled was retained. With tool rotational speeds of 1500 and 2500 rpm an increase in shoulder penetration is observed and consequently nanotubes distribution increases. However, a completely uniform distribution was not achieved when regular tangle nanotubes were used as base material, and its was also suggested to future works that multiple FSP pass should improve in the dispersion of the nanotubes.

With the objective of weigh reduction on several vehicles, FSP was used in the production of a MWCNT/AZ31 surface composite by Morisada et al. [5]. The authors concluded that MWCNT can be dispersed into a AZ31 matrix by FSP and that microhardness increases to values of 74 HV. The addition of MWCNT promotes a grain refinement by FSP.

2.4.4 Copper

Due to corrosion and constant wear, many navy weapons systems and other support equipments need constant repairs. These repairs are highly expensive and normally are made by laser-assisted direct metal deposition (DMD), et al [54] uses FSP on a multi-layered copper-nickel 70/30, in order to reduce the number of defects produced by DMD. The methodology is represented in Figure 2.24.

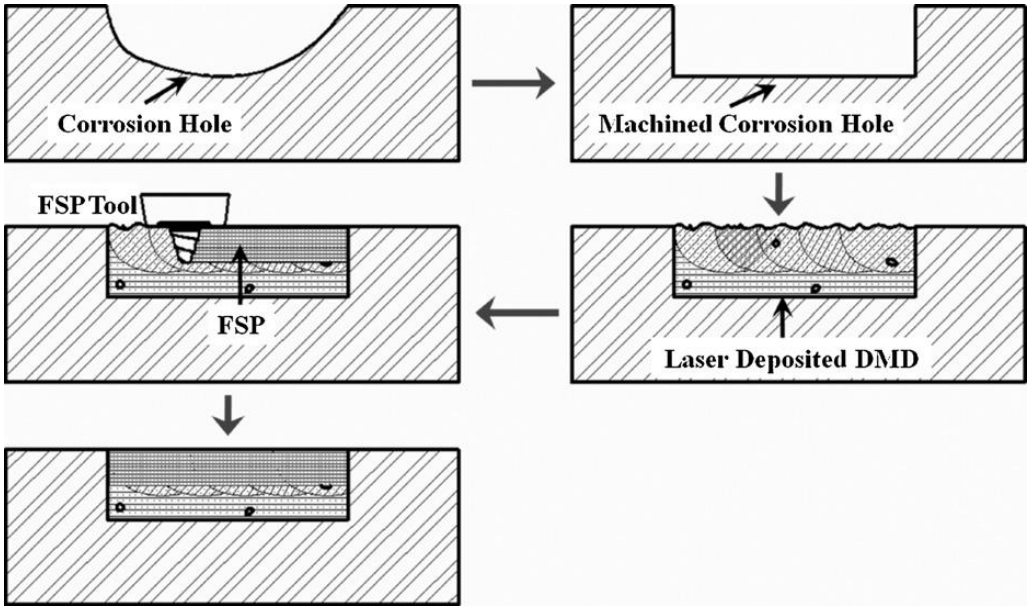

Figure 2.24 - Methodology of repair of copper–nickel 70/30 using DMD and FSP. First the corrosion hole is machined to a regular shape. This is followed by laser deposition and FSP. The surface is finally machine to disire finish. [55].

The authors concluded in this research that with FSP nugget porosity was approachably 0.35% compared with 3.3% and 1.3% in DMD, also that FSP homogenizes elemental composition. Tensile and corrosion tests revealed that FSP copper-nickel 7/30 had a higher yield-strength, lower ductility and higher corrosion rate than DMD copper-nickel 70/30.

2.5 Conclusion

Friction stir processing is a very attractive technology for solid state processing for the production of MMC and SMMC. Several authors successfully manufactured MMC and SMMC with significant improvements in BM properties, such as hardness, wear resistance, corrosion resistance, thus proving that FSP is a suitable technique for the reinforcement of a wide range of materials. Materials such as aluminium, magnesium and cooper have great impact in modern industry, in the substitution of other materials, especially due to weight reduction and high corrosion resistance. For this, a large investment is being made by the scientific and industrial communities.

Despite the intense studies on this subject, work is still to be done to optimize techniques and reduce defects, so that this technique can be applied in a larger scale. The optimization involves processing parameters and development of new variants for applying FSP to produce SMMC and MMC.

3 Experimental set-up

3.1 Materials characterization

A commercial AA5083 (AlMg 4.5 Mn 0.7) cold hardened was used as BM in this investigation.

The AA5083-H111 aluminium alloys were supplied by LANEMA, in plates with 200×150×8 mm dimensions. The mechanical, physical and chemical properties of the alloy were provided by the supplier and are summarized in the following tables:

Table 3.1 - AA5083 H111 chemical composition.

Chemical composition (weight %)								
Si	Fe	Cu	Mn	Mg	Cr	Zn	Ti+Zr	Al
			0,4	4	0,05			
0,4	0,4	0,1	1	4,9	0,025	0,25	0,15	

Table 3.2 - AA5083 H111 physical properties

Physical properties	
Density	2,66 g/cm^3
Modulus of elasticity	71000 MPa
Linear thermal expansion coef. (20°-100°)	23,8×10^{-6} K^{-1}
Thermal conductivity (20°C)	105-120 W/mK
Electric conductivity (20°C)	15-17 mS/m

Table 3.3 - AA5083-H111 mechanical properties

Mechanical properties			
Ultimate tensile strength UTS (MPa)		UTS0.2 (MPa)	Brinell Hardness
min.	max.	min.	
275	285	125	73

As reinforcing material SiC , and Al_2O_3 were used in grain sizes of 35 and 45 µm respectively.

Al AW 2007-H4 aluminium alloy was supplied by EUROFERRAMENTAS, in a rod with 20 mm diameter. The mechanical and chemical properties information for the AL AW 2007-H4 are summarized in the following tables:

Table 3.4 - AL AW 2007-H4 aluminium alloy physical properties

Chemical composition (weight %)								
Si	Fe	Cu	Mn	Mg	Cr	Zn	Ti+Zr	Al
0,491	0,649	3,664	0,568	0,562	0,042	0,112	0,039	

Table 3.5 - AL AW 2007-H4 alloy mechanical properties

Mechanical properties		
Yield Strenght (N/mm^2)	Yield point (N/mm^2)	Vickers Hardness
458,57	12,13	112

3.2 Equipment

The equipment used in this study is a milling cutter machine available at DEMI in Universidade Nova de Lisboa – Faculdade de Ciencias e Tecnlogia. The milling cutter comprises a moving framework were the working table is attached, moving in the X,Y,Z axis as depicted in Figure 3.2. Tool rotation and tilt angle were provided by the milling cutter head. This equipment allows the control of travelling speed (X,Y,Z) and tool rotation speed (C-axis). Since it has no vertical force control, processing can be preformed controlling the head position in Z axis.

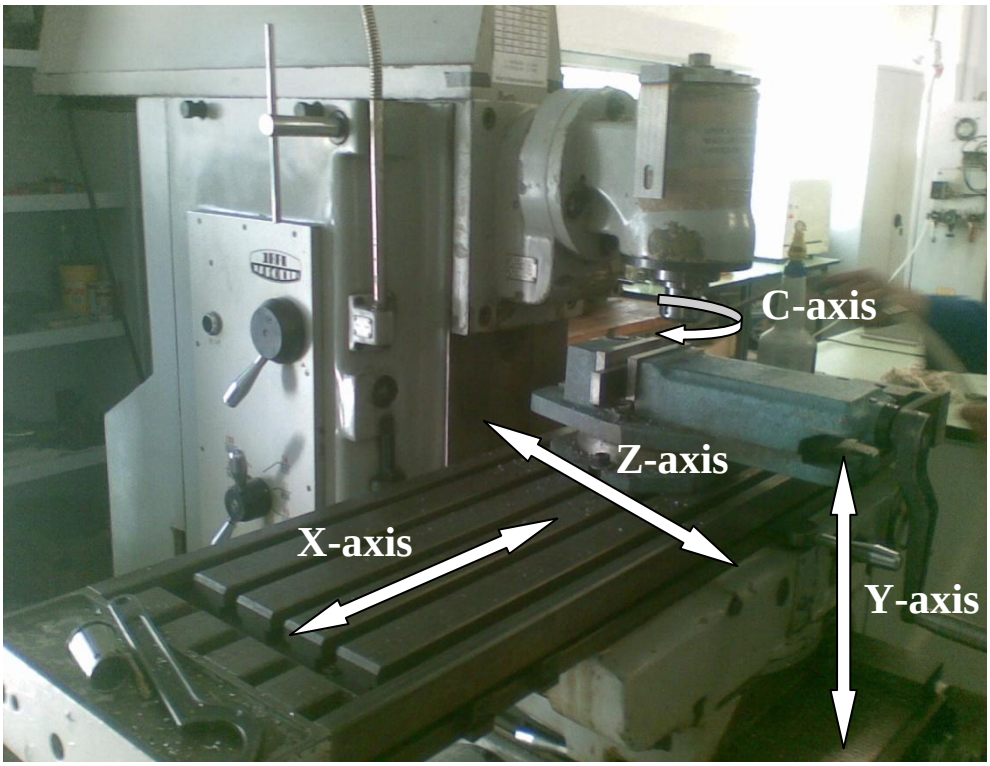

Figure 3.1 - Milling cotter at DEMI. Degrees of freedom representation

3.3 Clamping base system

Clamping system was developed, in order to test a variant of the process using electric current and to successfully clamp aluminium plates to the work piece.

Since this process is under patenting, limited information can be provided.

3.4 Electric system

In this investigation it was used a variant of process, consisting of applying an electric current to assist the conventional FSP softening the BM during FSP processing.

All the electric components of the process were adequately insulated in order to avoid any electric current into the milling cutter that could provoke damage.

Using software CST Studio Suit simulations were made, to determinate electric density passing through the system and the electric current flow. Materials for the different components of tool and fixing system were selected. Figure 4.1 represents the material chosen from the software database.

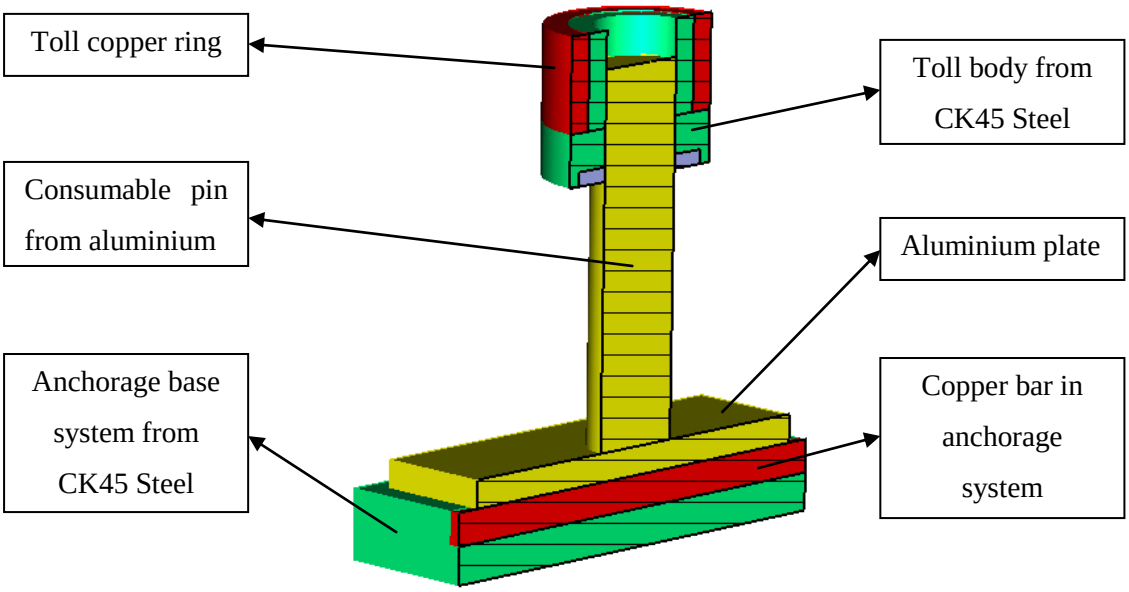

Figure 3.2 – Cross section of the simulated tool

Figure 3.3 shoes electric density that passes through the tool and fixing system. Point one represents the point chosen for the entry of current and point two represents the exit of current of the system.

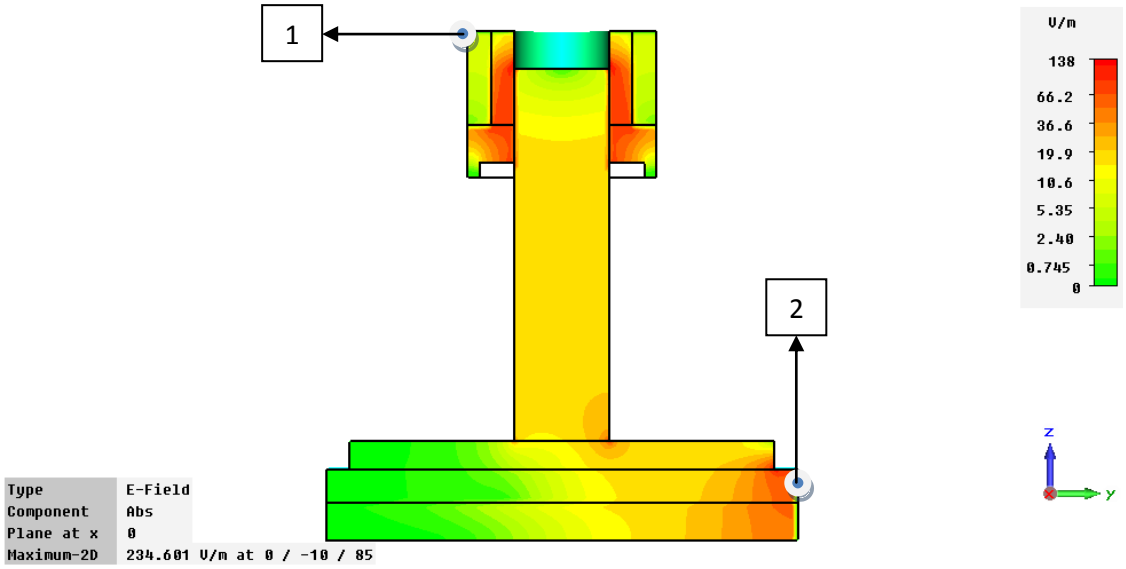

Figure 3.3 – Electric densety in process two.

This software also allows to determinate the electric current flux, and taking into account that electric current prefers the path with less resistance, Figure 3.4 is more a confirmation that all the parts of the system were well developed. Figure 3.4 shows electric current flux in the tool.

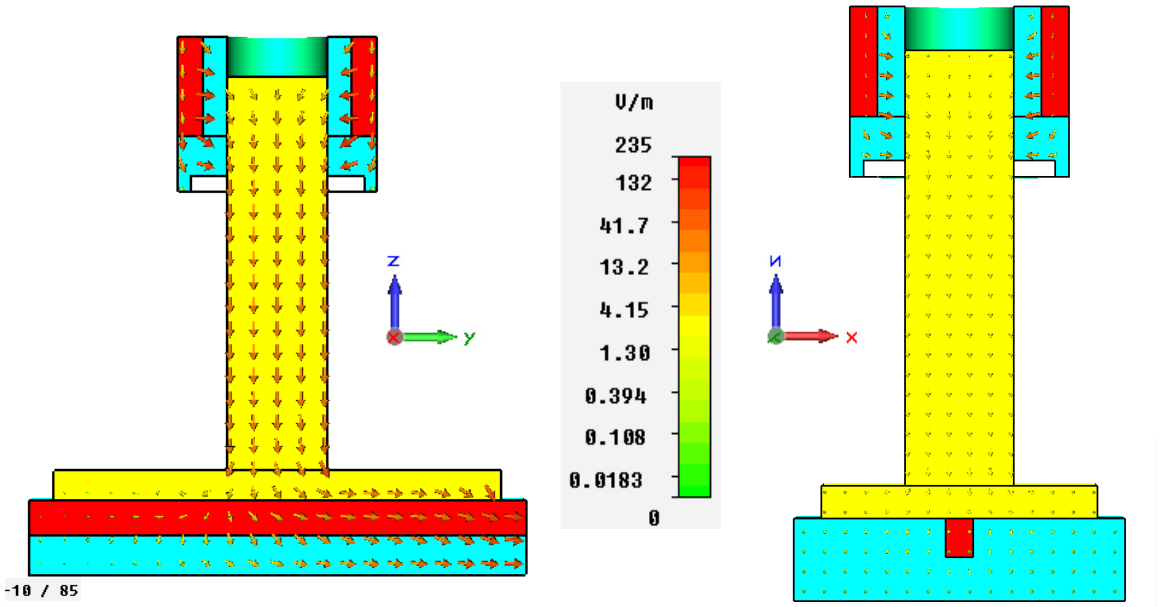

a) b)

Figure 3.4 – Electric flow in the tool.

A number of preliminary tests were performed using software Labview to evaluate heat contribution (ºC), current (A), and Voltage (V) to the process. Figure 3.5 depicts set up. These tests were performed with no speeds involved, temperature one was registered from thermocouple one placed in the aluminium plate, and temperature two was registered from thermocouple two placed in consumable tool. Both thermocouples were placed as close as possible to each other.

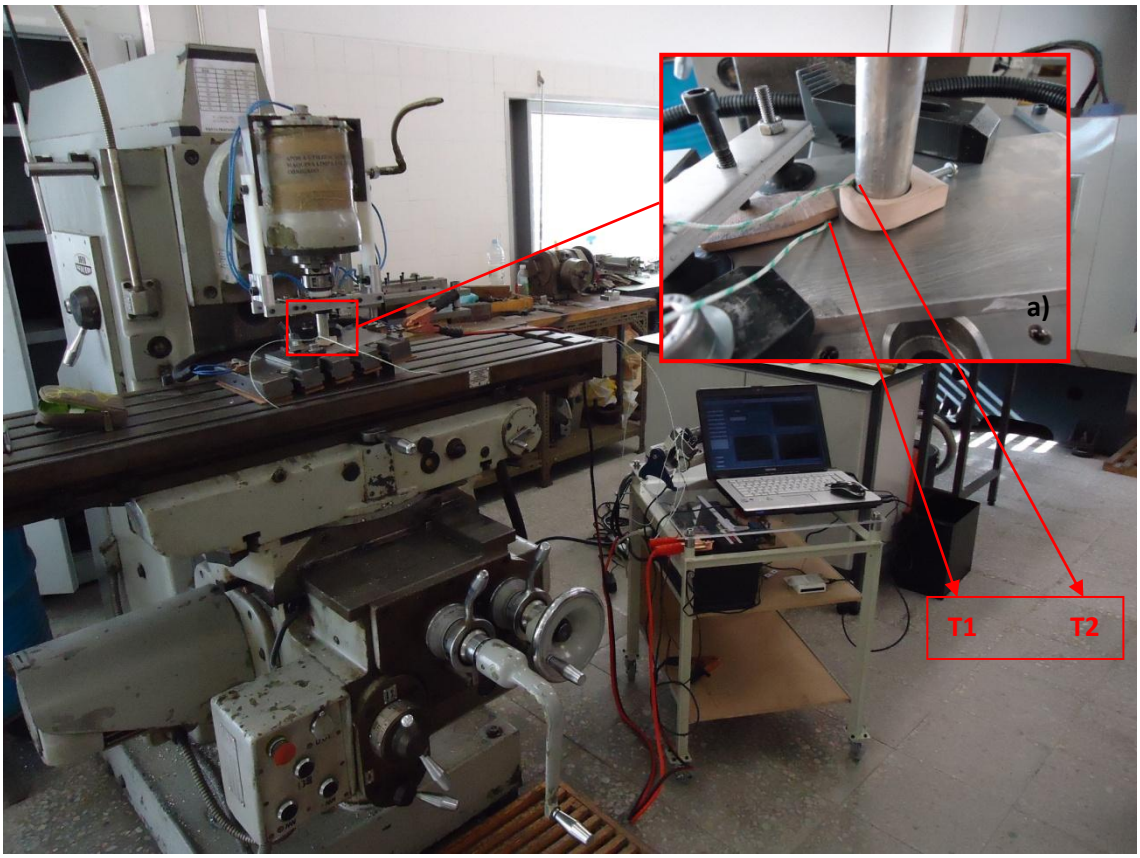

Figure 3.5 – Analysis montage. (A) Detail from interface between BM and consumable pin.

Figure 3.6 represents the front panel from software Labview, with a number of controls and graphics corresponding to acquisition of temperature, current and voltage for initial test. The control panel allows the control of all variants, and is prepared to accommodate AC and DC current.

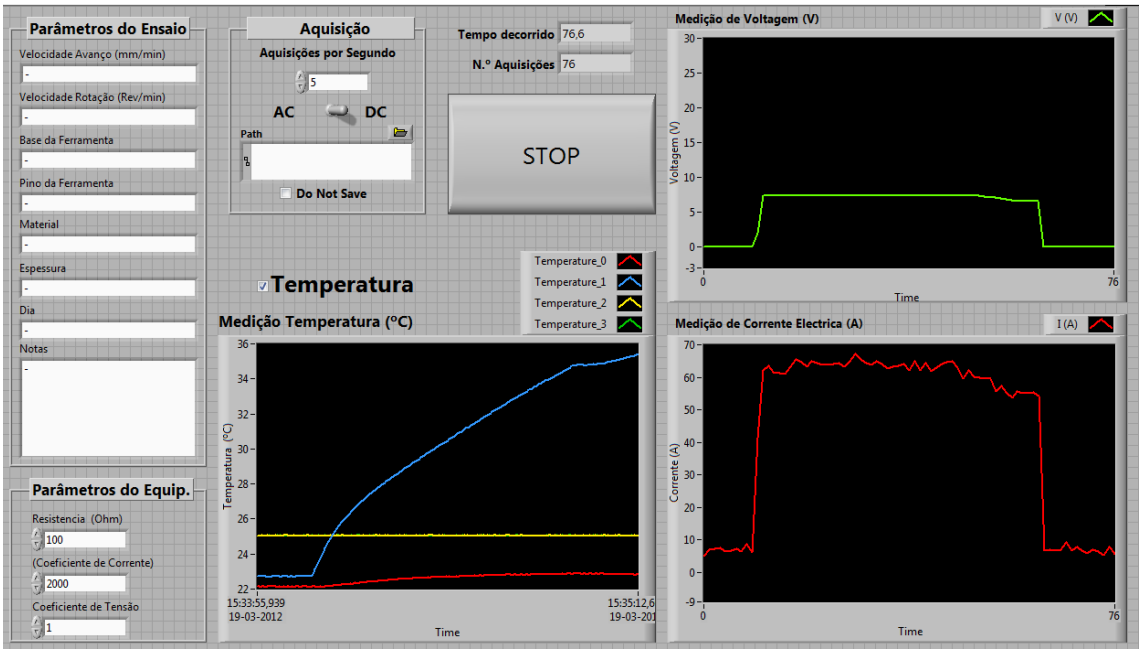

Figure 3.6 – Labview front panel.

3.5 Testing description

In order to produce a surface modification by FSP two different processes were tested. These processes have different tools designs, different way of applying reinforcement powders, and are organized in the following way.

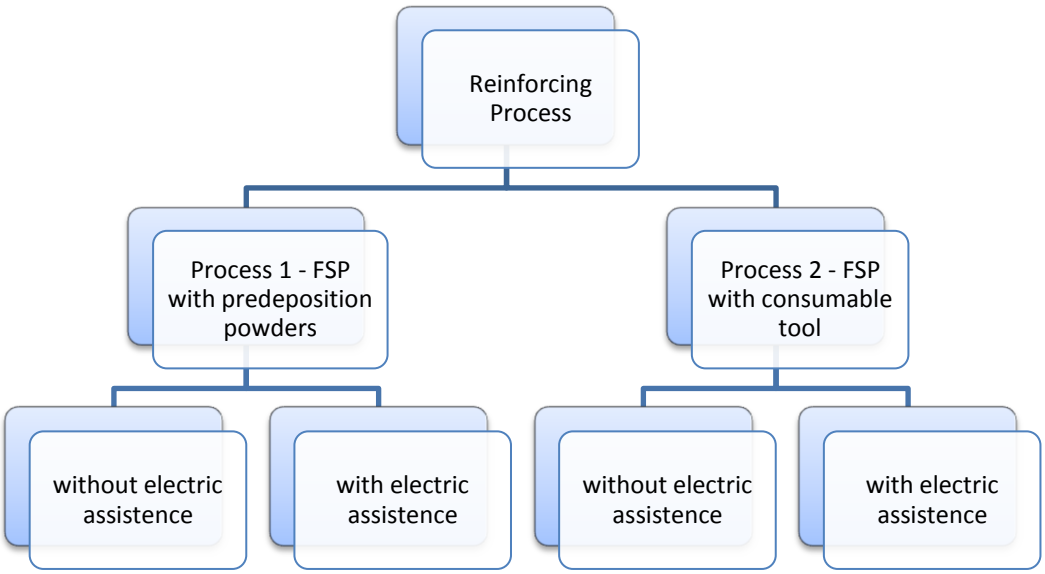

Test names were given according to the following nomenclature and according with the process in question, as depicted in Figure 3.7.

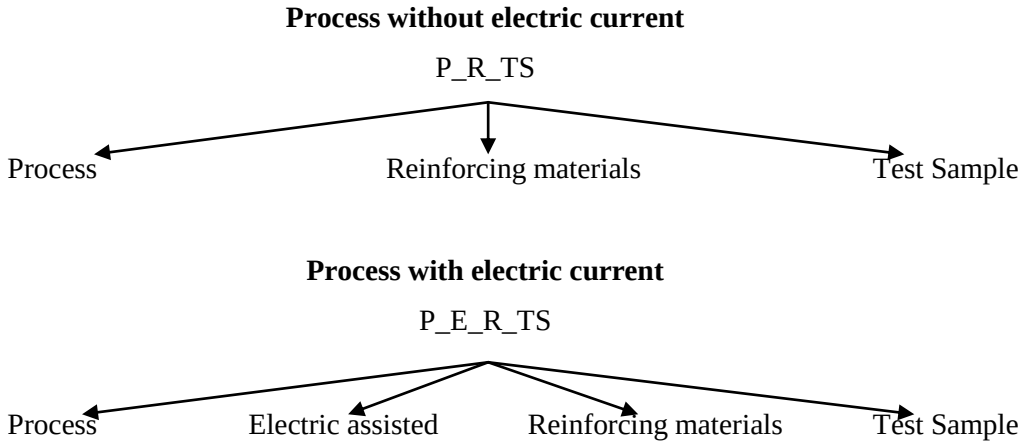

Figure 3.7 – Test names for investigation.

Example: P1_RS_TS1- means process 1, with SiC as reinforcing material, and test sample number 1. Another example P2_E_RA_TS4 means this is process 2, with electric variant, reinforced with alumina particles, and refers to test sample number 4.

3.5.1 Friction Stir Processing (FSP) with predeposition of reinforcing particles - Process P1

3.5.1.1 Methods of reinforcement

In this variant, and in order to successfully produce a SMMC, a thin layer of reinforcing material was predeposited and fixed to the unprocessed zone by a spray glue in the surface of AA5083-H111 BM (Figure 3.8). This process was repeated several times to reach a uniform thickness of reinforcing particles. For this method different thickness were used for Al_2O_3 and for SiCp.

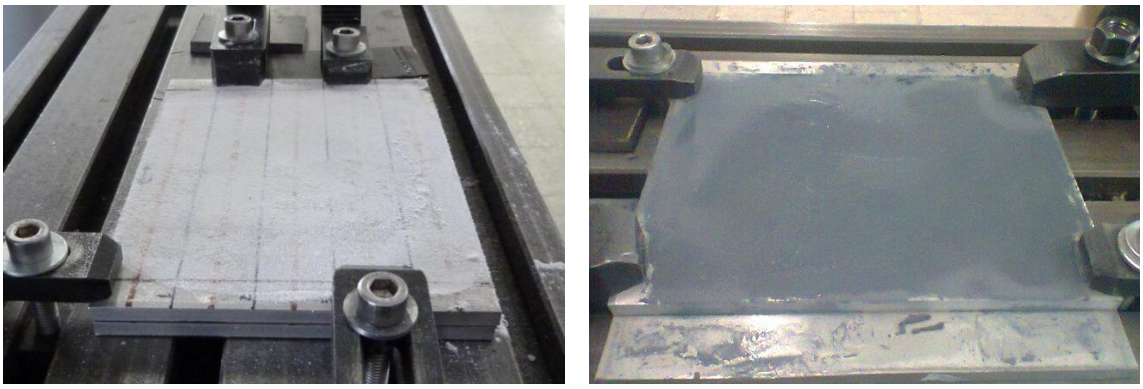

a) b)

Figure 3.8 - Methods of reinforcement. (A) With alumina particles, (B) with silicon carbide particles

3.5.1.2 Tool design

As stated before, tool geometry is a very important parameter in FSP, for this reason several tools were designed to improve this process. However, for each process a different tool was used, including for the electric variant.

For the process without electric current, a simple FSP tool was used depicted in Figure 3.9. For process 2, the tool had no pin.

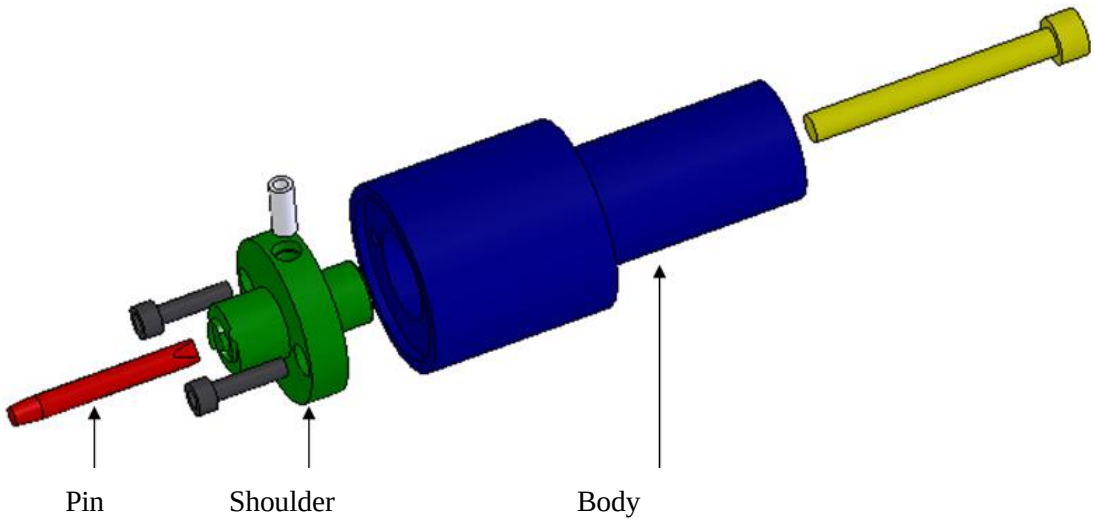

Figure 3.9 - Tool profile without electric current.

For the process with electric assistance special tool and dedicated equipment were designed. Aiming to maximize the electric current to increase the homogenously in the material.

Since this process is under patenting, limited information can be provided.

3.5.1.3 Testing description of process.

Table 3.4. presents the sequence of process variants tested and reinforcing material tested.

Table 3.6 - Trial group process one description. Conventional FSP with and without electric variant.

Main investigation: Process 1 - Conventional FSP assist by electric current			
Test name	Description	Base material	Reinforcing material
P1	Process 1	AA5083-H111	None
P1_S	Process 1	AA5083-H111	Silicon carbine particles
P1_A	Process 1	AA5083-H111	Alumina particles
P1_E	Process 1 assisted by electric current	AA5083-H111	None
P1_E_S	Process 1 assisted by electric current	AA5083-H111	Silicon carbine particles
P1_E_A	Process 1 assisted by electric current	AA5083-H111	Alumina particles

The first round of tests was preformed for comparison with other variants.

3.5.2 Friction Stir Processing (FSP) with consumable tool with drilled holes packed with particles-P2.

Do to restrictions in the milling cutter used in this process, in terms of load prescription and positioning, it has necessary to develop an assembly that could compensate the equipment restrictions. In Figure 3.11 it can be seen the assembly made, with the respective parameters. In

this case the parameters Ω, V_x and α are independent, as V_y is dependent from V_x and α (V_y=f(V_x,α)=$V_x \times \alpha$)

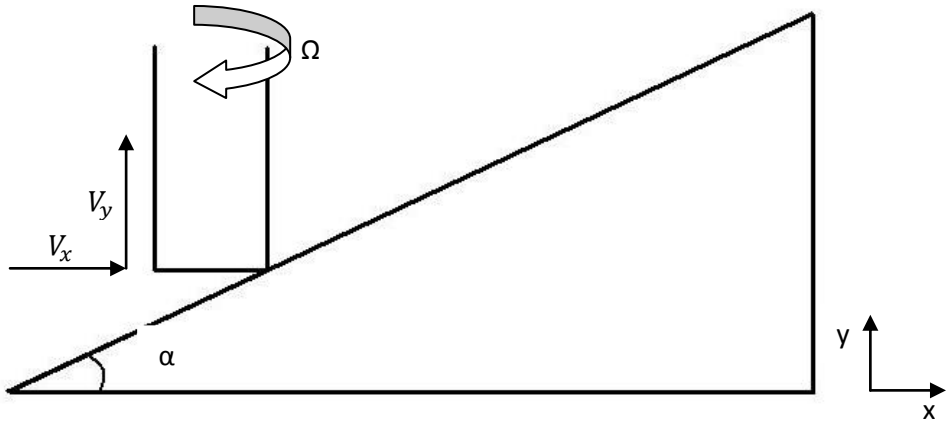

Figure 3.10 – Schematic procedure for process two.

3.5.2.1 Method of reinforcement

In this process the reinforcing material were placed and compress directly into the tool. The mixture of powders were compacted into the driller holes, this is only a precaution to avoid losing any material during the preparation of the tests. The objective with the consumable pin with the reinforcing material, is to produce a more homogeneous distribution on the SMMC.

3.5.2.2 Tool design

For this process different consumable tools were developed, the consumable pins are both for the process with and without electric. The tool made of Al1100 has several number of drilled holes to compact reinforced powders, the following consumable pins were developed, named and are presented in Table 3.8

Table 3.7 - Consumable pins developed and respective designation.

Toll designation	T_H1_HD2	T_H2_HD2	T_H1_HD4	T_H2_HD4	T_H4_HD4
Toll profiles	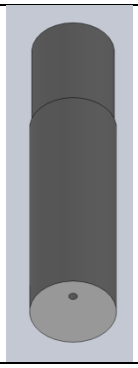	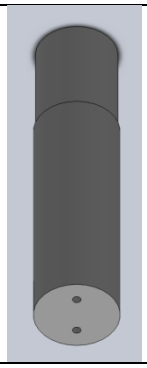	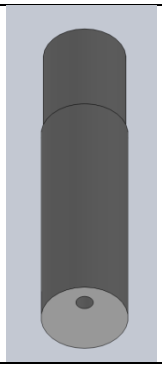	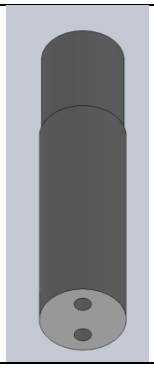	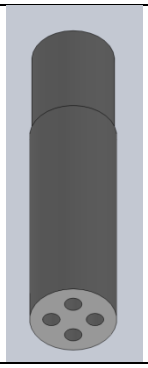
Nº holes	1	2	1	2	4
Height (mm)	85	85	85	85	85
External diameter (mm)	20	20	20	20	20
Hole diameter (mm)	2	2	4	4	4
Depth (mm)	25	25	45	45	45
Particle volume (mm^3)	78,53	157,08	565,49	1130,95	2261,95

For the variant with electric current the same base used in process 1 was also used in process 2, with the difference that shoulder and the pin were substituted by the consumable pin as showed in Figure 3.12. The reinforce powders were compacted into the several holes.

Figure 3.11 Tool section view.

As can be seen in pin profiles represented in Table 3.8 the powders entered into the holes and then were compacted. The particles have to be well compacted because the holes were not closed.

3.5.2.3 Testing description of process.

Like in process 1, a number of tests were run to assess the process as described in Table 3.8.

Table 3.8 - Process 2 description

Main investigation: Process 2 - Conventional FSD assisted by electric current			
Test name	Description	Base material	Reinforcing material
P2	Process 2	AA5083-H111	None
P2_S	Process 2	AA5083-H111	Silicon carbine particles
P2_A	Process 2	AA5083-H111	Alumina particles
P2_E	Process 2 assisted by electric current	AA5083-H111	None
P2_E_S	Process 2 assisted by electric current	AA5083-H111	Silicon carbine particles
P2_E_A	Process 2 assisted by electric current	AA5083-H111	Alumina particles

3.6 Characterization techniques

Test samples were removed from final sections of tracks, where the process is more stable. Macroscopic and microscopic characterizations were preformed in all test samples, and Vickers hardness tests were preformed in test samples that revealed interesting features under microscopic analysis.

Test samples from trial group P1 were etched with Keller modified reagent, to reveal thermal mechanical affected zones. In other tests etching was not preformed because it would be more difficult to observe reinforcing particles, especially SiC reinforced surface composites

Surface composites reinforced with alumina particles were observed under Scanning Electron Microscopy (SEM) and Energy Dispersive x-ray Spectroscopy (EDS) to confirm the presence of alumina particles, as well as, the fraction area and alumina particle distribution.

3.6.1 Polishing procedure

Polishing was performed using a Buehler grinder/polisher Phoenix Alpha with SiC grinding paper, with a increasing grip.

3.6.2 Metallography

Two different equipments were used to preformed a macro and microscopic analysis to evaluate possible defects generated by the process, as well as potential compositions, microstructural gradients and distributions of reinforcing particles

The first equipment, a Olympus microscope model CX40RF200 with a light source Olympus TH3 available at Department of Mechanical and Industrial Engineering, Faculdade de Ciências e Tecnologia, Universidade Nova de Lisboa, was used in the initial observation phase, to evaluate polish procedure and defects.

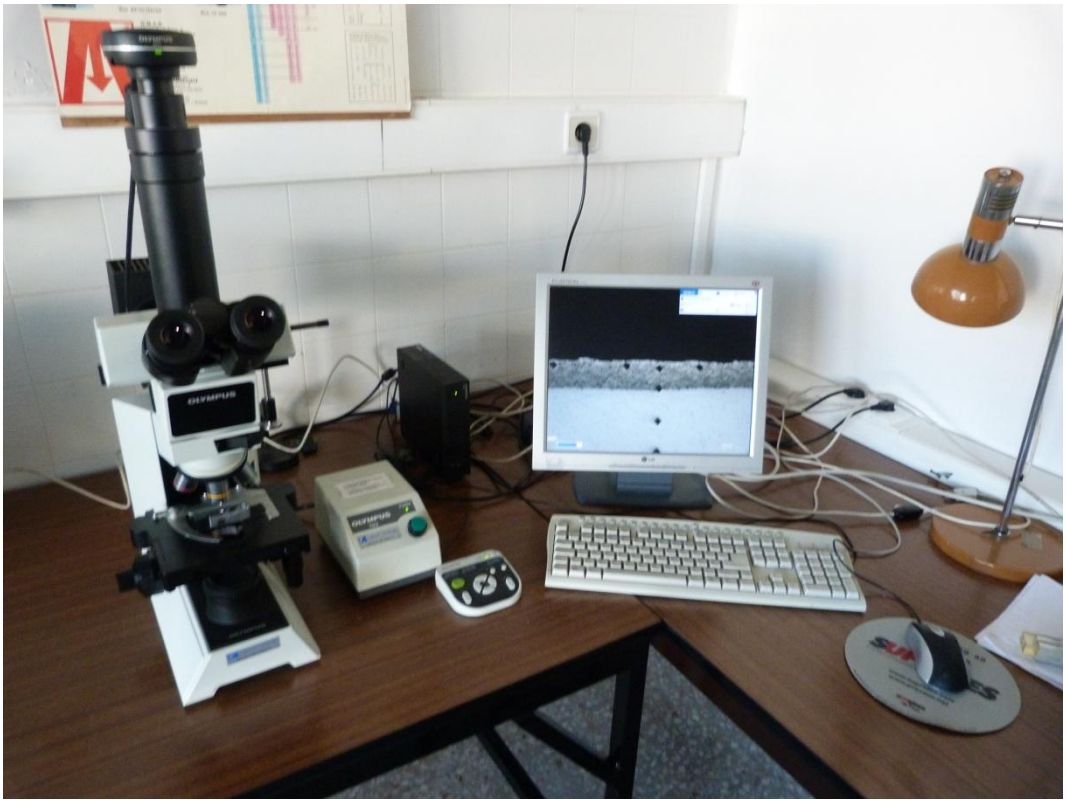

Figure 3.12 – Optical microscope from DEMI.

For a deeper analysis a second equipment was used, a Leica DMI 5000 M inverted optical microscope available at CENIMAT/i3N, Materials Science Department of Faculdade de Ciências e Tecnologia, Universidade Nova de Lisboa. This equipment has a motorized base that combined with a dedicated software allows a multi-step composition of images for mapping large areas in test samples.

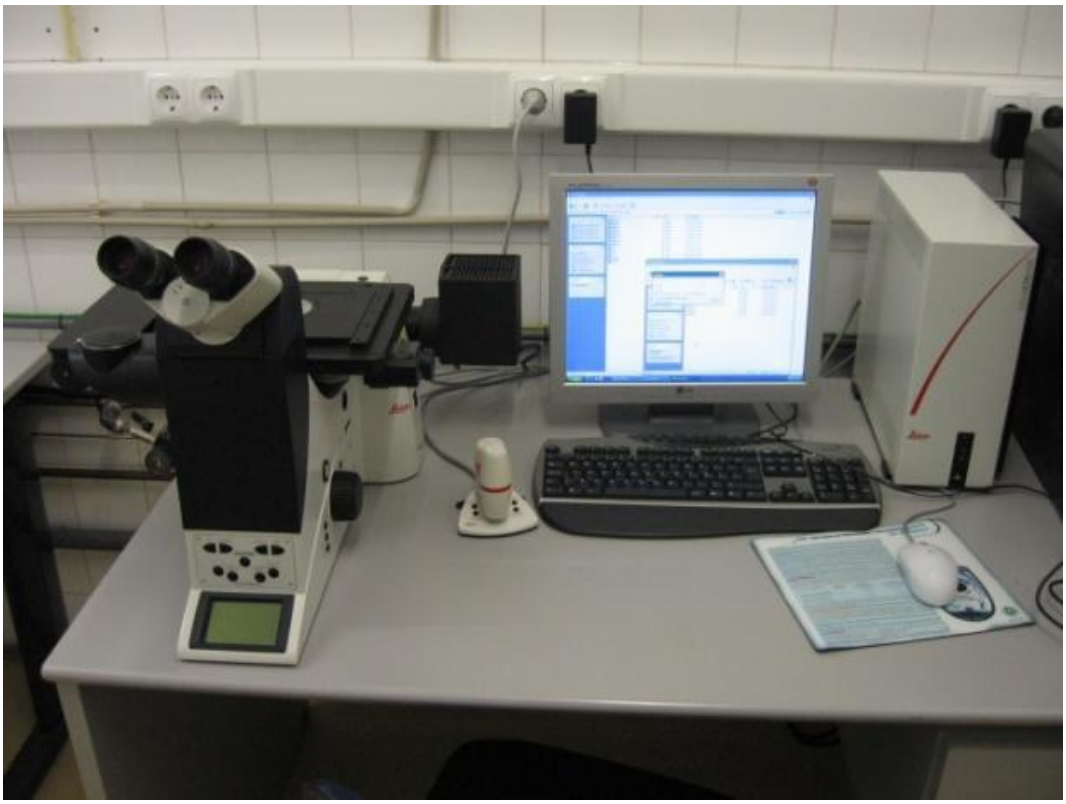

Figure 3.13 – Leica DWI 5000 M inverted geometry microscope used for both macroscopic and microscopic analysis.

3.6.3 SEM/EDS

Surface composites reinforced with alumina particles were observed under SEM and EDS, to confirm the presence of alumina particles. Analyses were made using SEM/EDS equipment available at CENIMAT/i3N, Material Science Departement of Faculdade de Ciências e Tecnologia, Universidade Nova de Lisboa

3.6.4 Hardness testing

Hardness testing was preformed using a Mitotoyo HM-112 Micro-Vickers Hardness Testing.

Figure 3.14 – Vickers Hardeness Testing Machine.

For trial group P1 micro-hardness indentions were preformed under a load of 200g. Hardness profiles were preformed along the depth in the cross test samples with a distance of 0,06 mm in reinforced layer and 0,2 mm in BM areas, and hardness profile along the bead surface were performed at a depth of 0,06 mm of the lowest region in cross sample as depicted in Figure 3.15. The distance between indentions was calculated to be higher than 2.5×D, where D is the distance between vertices from indention pyramid.

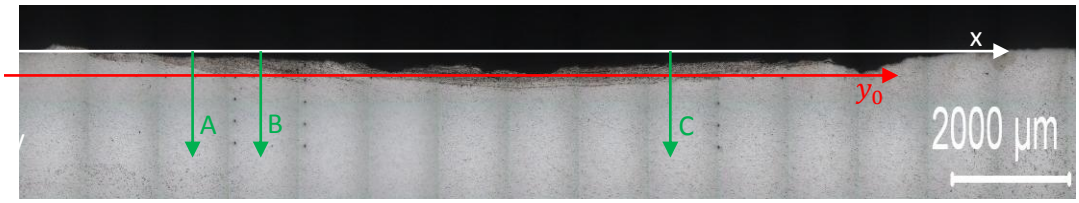

Figure 3.15 – Vickers hardness profiles for trial group P1.

For trial group P2 hardness profiles were preformed in depth with the specifications depicted in Figure 3.16. The indentions were made with a vertical line spaced of 0.17 mm and the vertical hardness profiles were preformed in zones where a good bounding between BM an consumable pin was observed.

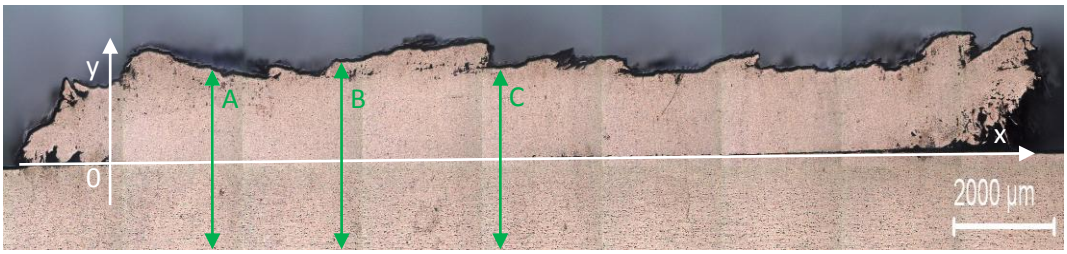

Figure 3.16 - Vickers hardness profiles for trial group P2

3.7 Conclusions

Samples were produced with two basic strategies for reinforcing aluminium surfaces: using predeposited particles processed with a non consumable tool, and using a consumable tool with drilled holes filled with reinforcing particles.

In each of these procedures, electrical current was applied to soften the base material and improve the process.

A set of samples was removed, prepared for metallographic analysis and hardness measurements

4 Results and discussion

The following chapter presents the results organized according to the deposition strategy adopted, and these are:

- Predeposition particles over the substrate.
- Consumable tool with drilled holes packed with particles.
- Electric current applied in the previous strategies.

4.1 Friction stir process with predeposition of reinforcing particles. (P1)

4.1.1 Evaluation of parameters in friction surfacing (P1_P).

According to the test description, tests P1 were run in order to determine the best window of parameters for this process.

Four tests were run, with the parameters listed in Table 4.1

Table 4.1 - Parameters of P1.

Test	ω(rev)	Vx (mm/min)	ω/Vx
P1_T1	1120	180	6,222
P1_T2	710	224	3,170
P1_T3	355	355	1,000
P1_T4	1800	180	10,000

Initial macroscopic and microscopic analyses were inconclusive in samples one to three, on sample four some macro defects were detected as shown in Figure 4.1. After a contrast of tests samples in P1 with Keller solution, it was visible by a microscopic analyses, a thermal

affected zone in test sample four, which was the test performed under the hottest conditions. No relevant defects were seen on the others test samples.

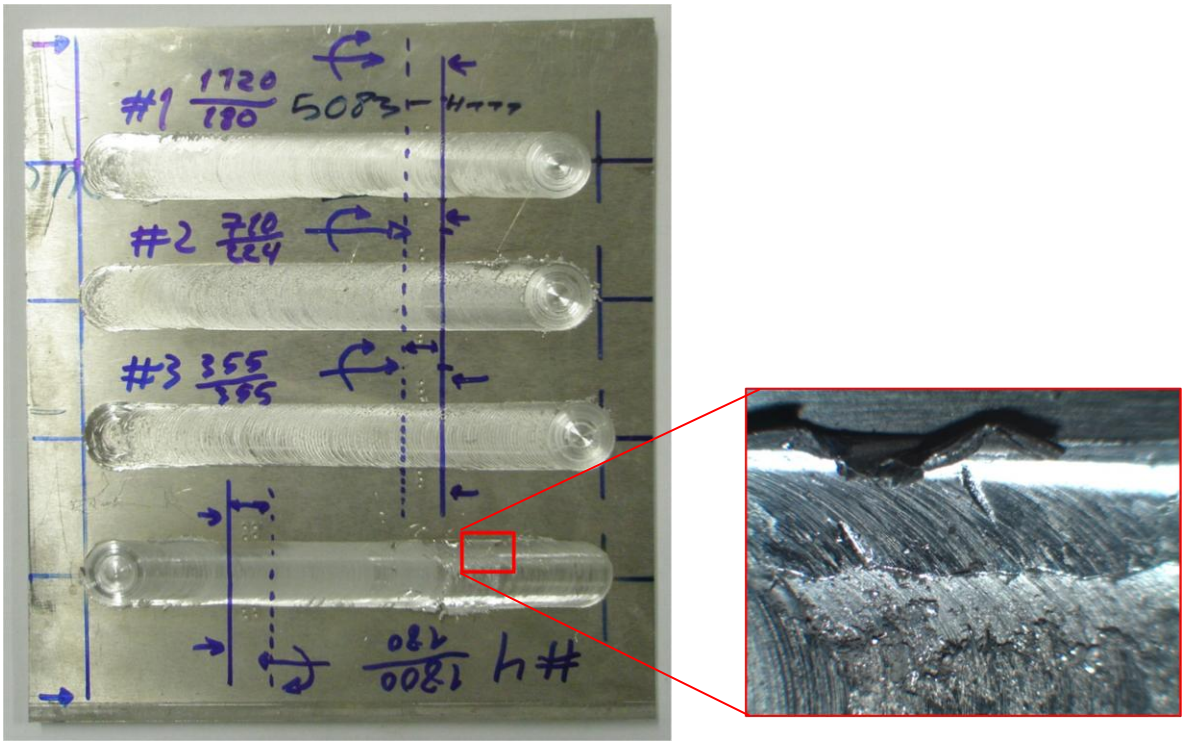

Figure 4.1 – Macrograph of tracks from test group P1_P.

4.1.2 Friction stir process reinforced with alumina particles (P1_A).

Test P1_A were preformed with the same parameters as P1_P depicted in Table 4.1.

4.1.2.1 Macroscopic characterization

Macroscopic characterization of all the tracks, shows that the surface beads have an almost absence of waviness, but a small burr is observed in the processed zone, as observed in Figure 4.2.

P1_RA_T1

P1_RA_T2

P1_RA_T3

P1_RA_T4

Figure 4.2 – Macrograph from tracks for trial group P1_A.

4.1.2.2 Microscopic characterization

Microscopic analysis on cross sections of test P1_RA were preformed; showing a thin reinforced zone in all the samples with some interesting differences between them, like depth, extension and particle distribution.

Figure 4.3 shows several micrographs of sample P1_A_TS1 cross section, with a thin layer of process zone with a maxim deep of 200 µm and an extension of 9.5 mm. This thin layer shows a homogeny distribution of alumina particles demonstrated on Figure 4.3 b), the alumina particles have fragmented in to smaller particles with an average size of 10 µm. The distribution and size of alumina particles are best seen in a dark field illumination mode as showed in Figure 4.3 b) to d). The interface zone, best observed in Figure 4.3 c) and d) shows a good bounding between the BM and processed zone, with no defects that can compromise the process zone. Macroscopically, it can be seen in the Figure 4.1 a) and b) a small burr. In this sample the reinforced layer is more pronounced in the RS.

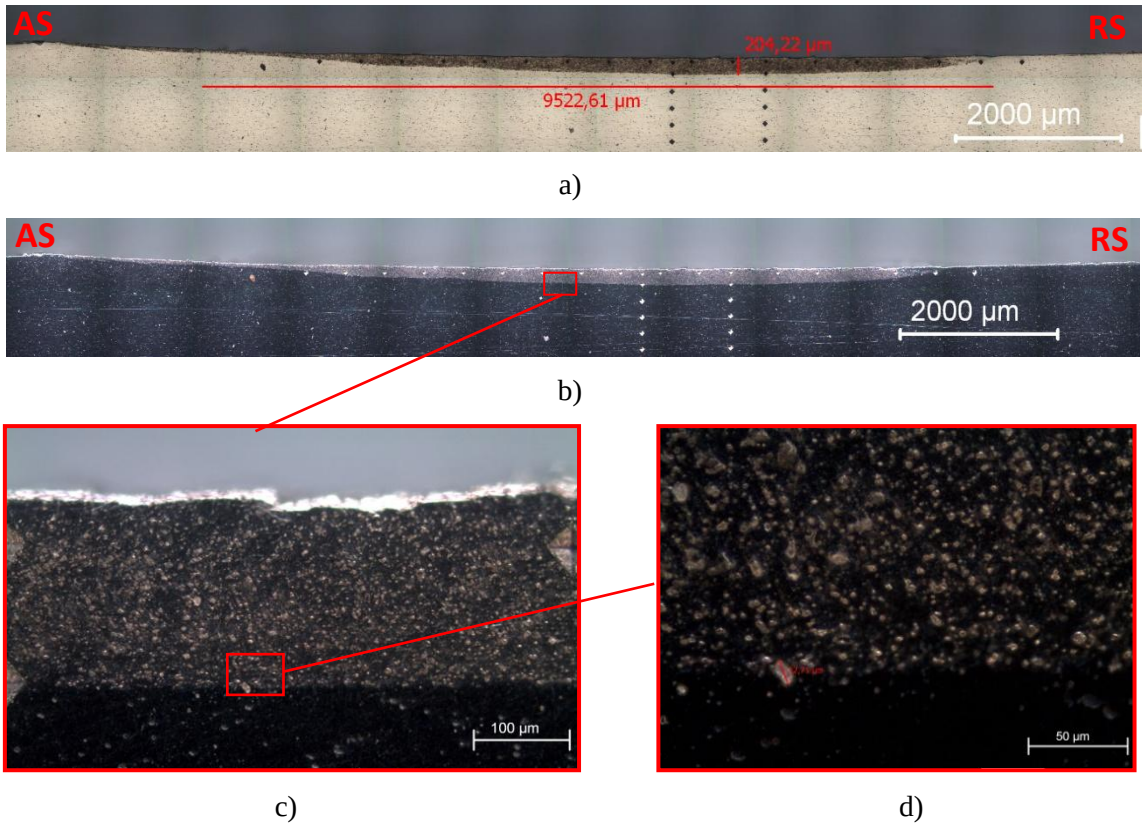

Figure 4.3 - Cross section micrographs of test sample P1_A_TS1. (A) Macrographs of bead cross section in BF, (B) Macrographs of bead cross section in DF, (C,D) Details of interface zone.

In test sample P1_A_TS2 it was also observed a thin and homogenous reinforced layer, with an extension of 8.4 mm and a depth of 200 µm, as depicted in Figure 4.4 a). The alumina particles seen in Figure 4.3 f) have been fragmented to smaller particles with an average size of 10 µm. Figure 4.4 b) and c) shows a good bounding between BM and processed zone with no observed defects.

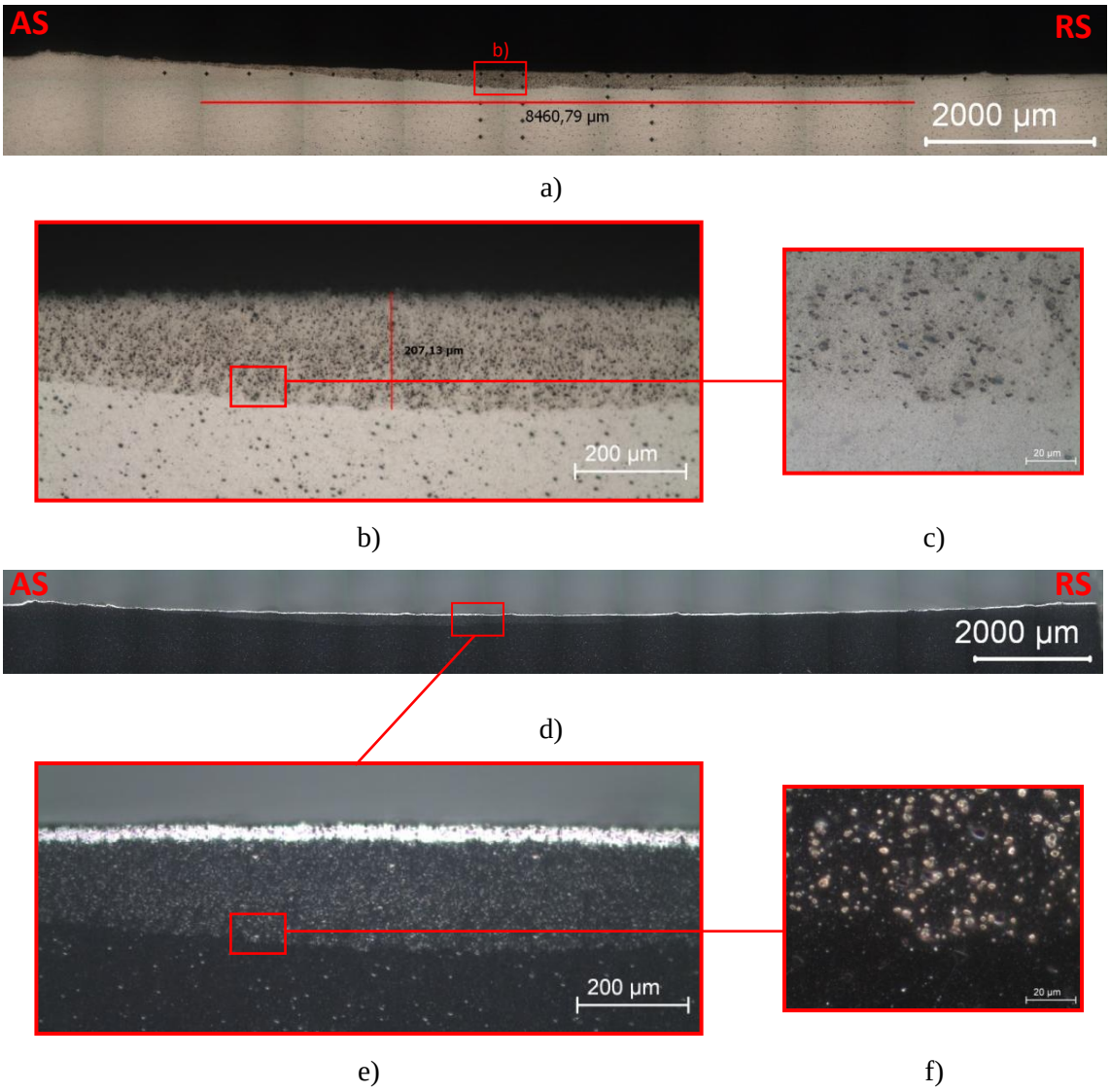

Figure 4.4 - Cross section micrographs of test sample P1_A_TS2. (A) Macrographs of bead cross section in BF, (B) Macrographs of bead cross section in DF, (B,C) Details of reinforced layer in BF, (E,F) Details of reinforced layer in DF.

Figure 4.5 shows micrographs from cross section of test sample P1_A_TS3, these micrographs show an irregular reinforced layer with concentrations of alumina particles as well as some zones in which there was no material consolidation, as depicted in Figure 4.5 b) and c) in the form of cracks. The lack of consolidation is most probably due to a low ratio Ω/Vx. This ratio indicates that this test was performed under cold conditions that did not originate enough heat to achieve a viscoplastic condition necessary to disperse alumina particles in the substrate.

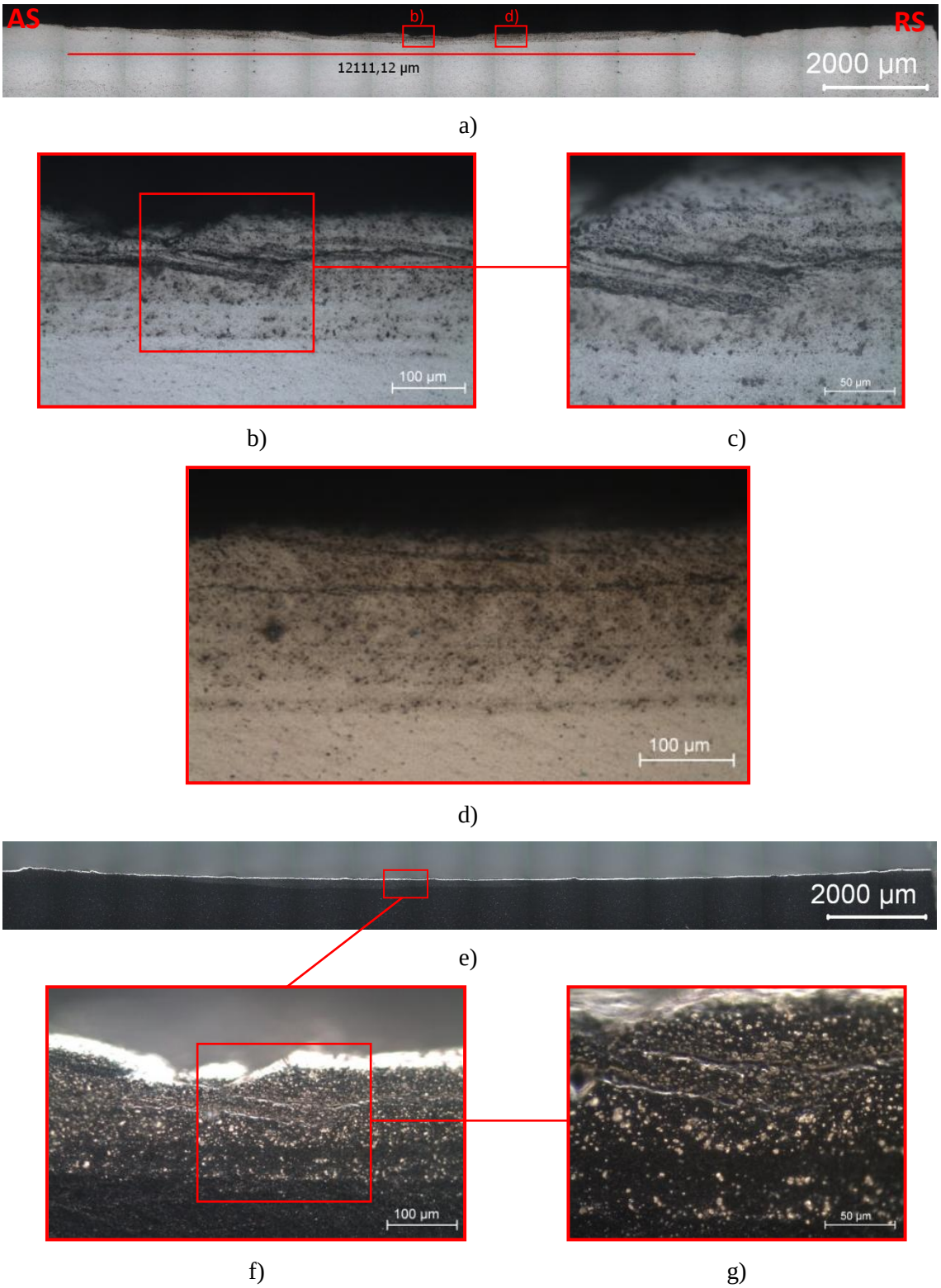

Figure 4.5 - Cross section micrographs of test sample P1_A_TS3. (A) Macrographs of bead cross section in BF, (B) Macrographs of bead cross section in DF, (B,C) Poor consolidation cracks in BF, (E,F) Poor consolidation cracks in DF.

Unlike test P1_A_T3, test P1_A_T4 was preformed in hot condition. High ratio Ω/Vx originates a non-homogeny distribution, as well, as some sliding of reinforced material layer as can be seen in Figure 4.6 b) and f). A thick burr was seen in this track, with some alumina

particles incrusted, as depicted in Figure 4.6 g). This may be due to the fact that the thin reinforced layer was removed by the high temperature and speeds used in this test. Some aligned distribution of alumina particles can be seen in Figure 4.6 d) and e).

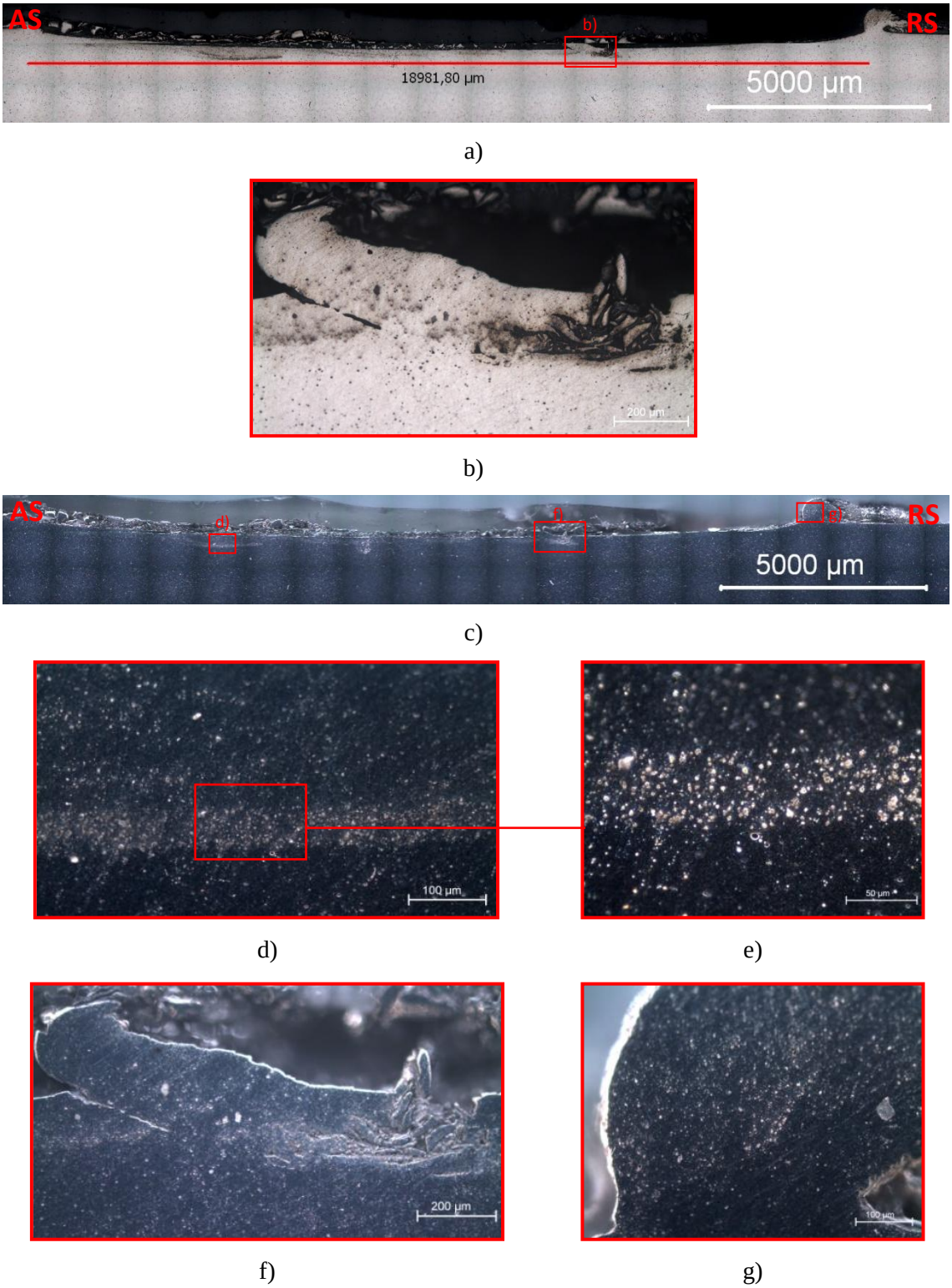

Figure 4.6 - Cross section micrographs of test sample P1_A_TS3. (A) Macrographs of bead cross section in BF illumination, (B) Sliding of reinforced layer in BF, (C) Macrographs of bead cross section in DF illumination, (D,E) Details of interface zone in DF, (F) Sliding of reinforced layer in DF, (G) Burr with alumina particles

From the test conducted, in P1_A it is noticeable that the parameters have a strong influence in homogenization of the reinforced thin layer. In test samples P1_A_T1 and P1_A_T2 a homogeneous reinforced thin layer was produced, the alumina particles were well distributed and a reasonable depth was achieved. Test samples P1_A_T3 and P1_A_T4 show defects due to low and high ratios of Ω/Vx respectively. This confirms that to reinforce the BM there is a small window of ratios Ω/Vx. In all tests the alumina particles fragmented into smaller particles with a slight difference in final sizes between tests.

4.1.2.3 Scanning electron microscopy (SEM) and Energy dispersive x-ray spectroscopy (EDS)

EDS analysis in test sample P1_A_T1 confirmed the presence of alumina particles in the thin processed zone as shown in Figure 4.7 points 1 and 4. The dark and round particles observed in point 2 are likely to be precipitates of Al_2Mg_2 , and the white phases observed and marked as point 3 correspond to iron inclusions, due to tool wear.

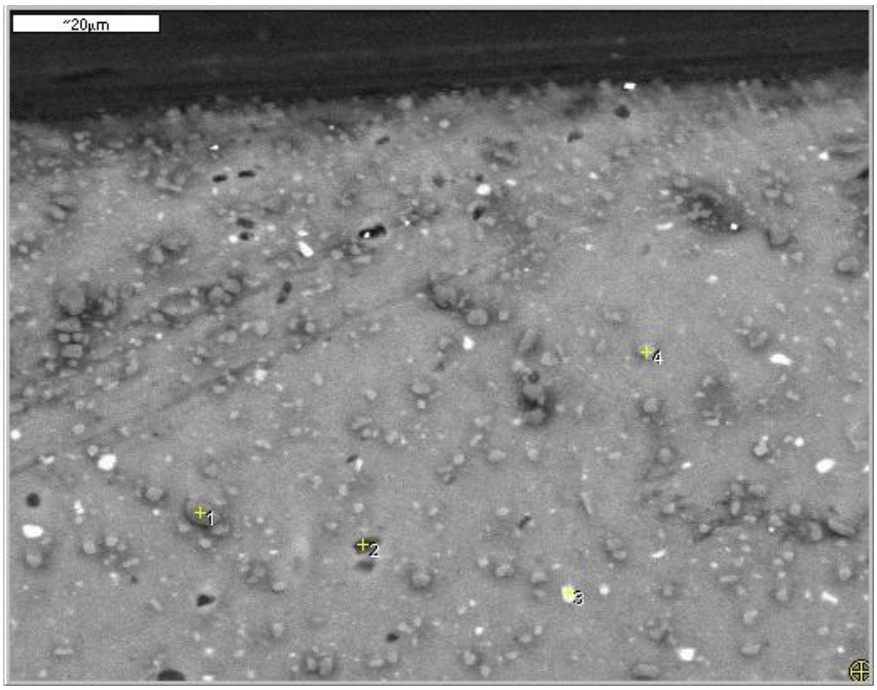

Point 1

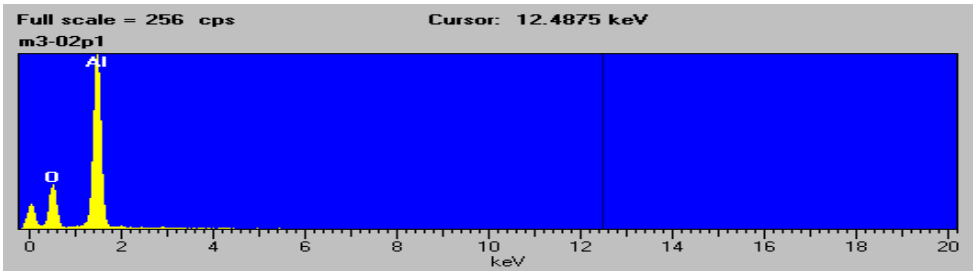

Point 2	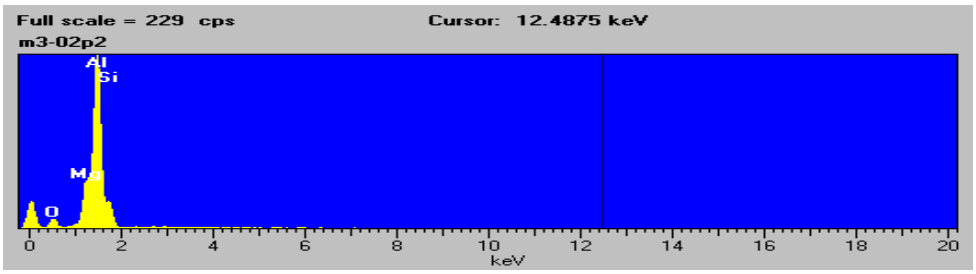
Point 3	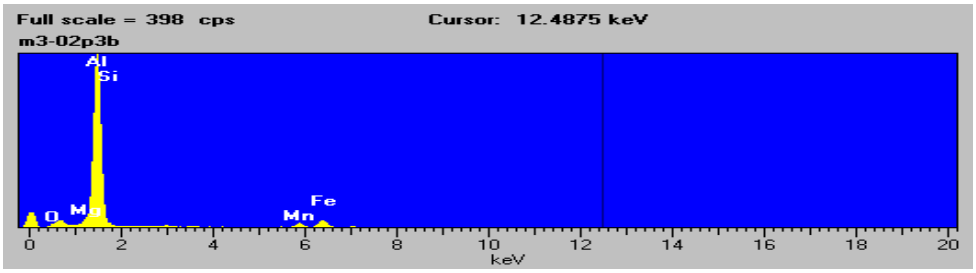
Point 4	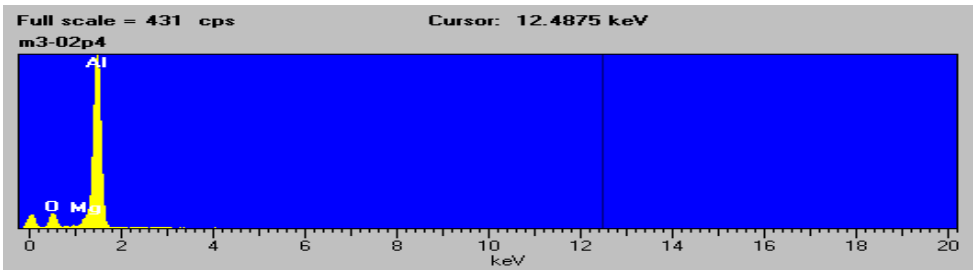

Figure 4.7 – EDS image and points of analyses.

SEM analysis preformed in tests samples P1_A_TS1 to TS3 confirmed that alumina particles are just encrusted. Table 4.2 shows several images corresponding to reinforced and interface zones. Images a) to c) correspond to test sample P1_A_TS1, and demonstrates a good distribution of alumina particles. Images a) and b) also show that no defects were found in interface zone. Images d) to f) correspond to test sample P1_A_TS2 with the same overall observations, but comparing image c) with f), it is noticeable that a higher concentration of particles is seen in image c) that correspond to test sample P1_A_TS1. Test sample P1_A_TS3 is represented in images g) to i) and shows some impurities, as well as a non homogeneous reinforced layer that was originated by cold processing conditions.

Comparing all test samples especially images c), f), and i), P1_A_TS1 shows better results, and P1_A_TS3 shows several defects that invalidates further test using this set of parameters.

Table 4.2 – SEM analyses from process one, reinforced with alumina particle

Test Sample nº	Interface with 100 µm	Interface with 50 µm	Process zone 50 µm
P1_A_TS1	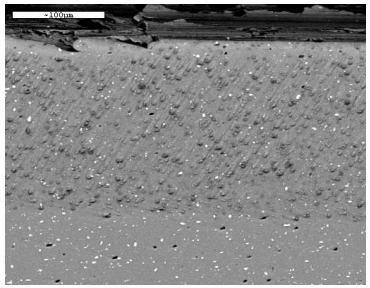 a)	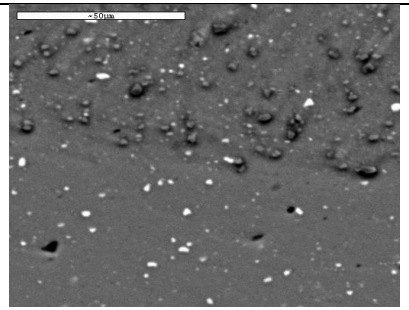 b)	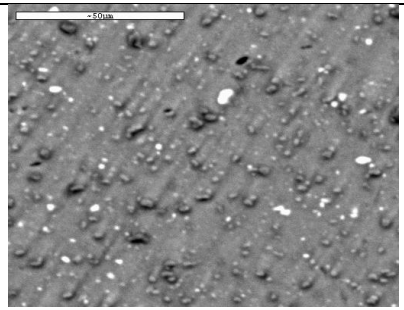 c)
P1_A_TS2	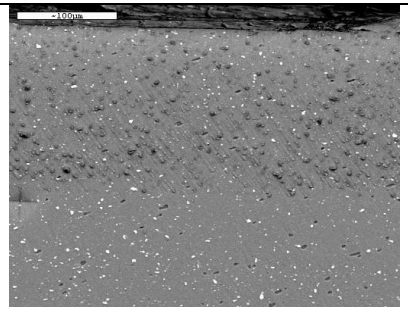 d)	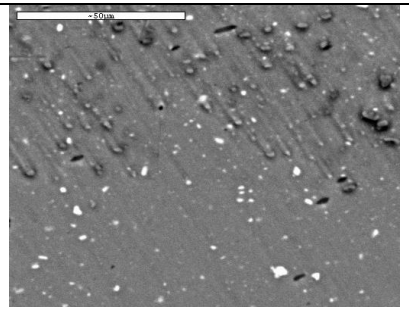 e)	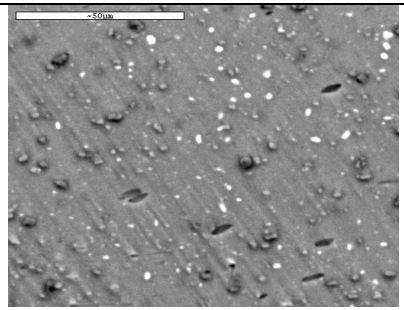 f)
P1_A_TS3	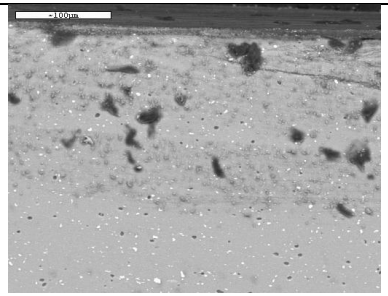 g)	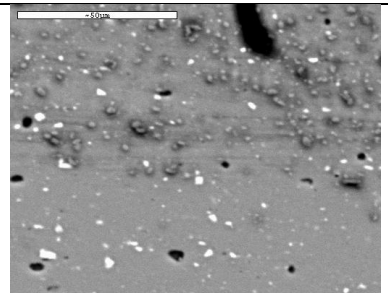 h)	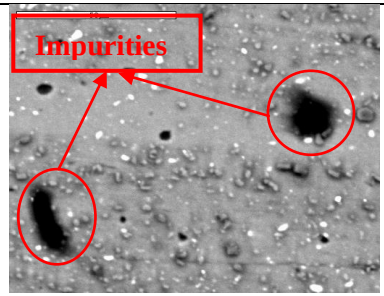 i)

4.1.2.4 Hardness tests

Hardness profiles show an increase as it approaches the beads surfaces. The thin reinforced layer has a constant hardness profile, where the highest hardness values are registered near the surface. Test sample P1_A_TS3 registered higher hardness than the other test sample; due to, higher concentrations of less fragmented particles.

Figure 4.8 represents vertical hardness profiles in cross sections along vertical lines, as well as, macrographs with the positions of the profiles. Values obtained in vertical profiles shows an increase of approximately of 60 % in comparison with BM.

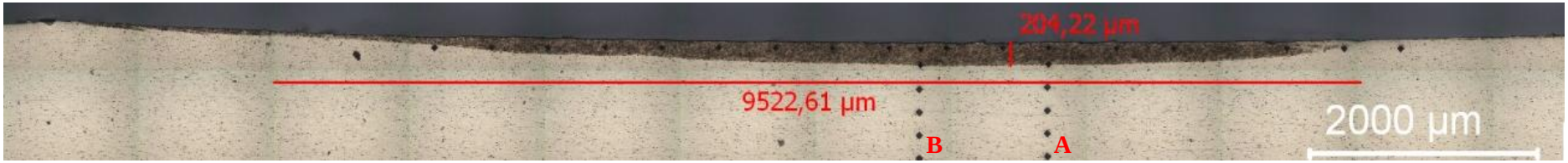

a)

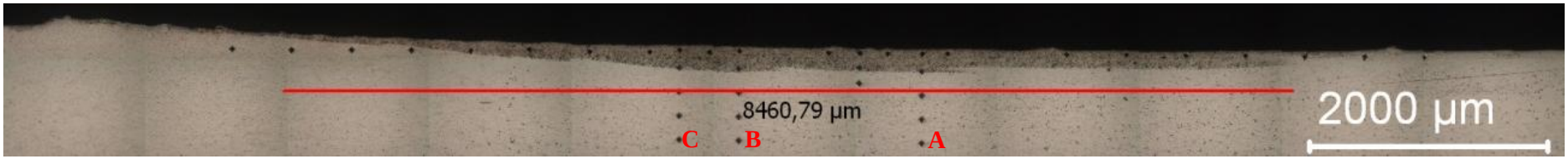

b)

c)

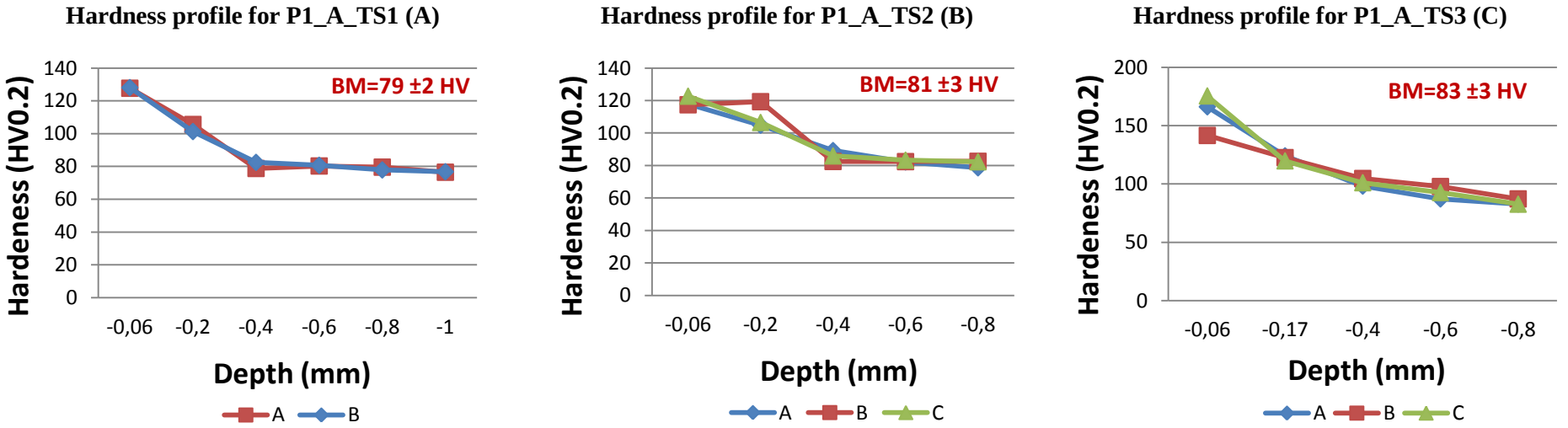

Figure 4.8 - – Hardness profiles from test samples: (A) P1_A_TS1, (B) P1_A_TS2, (C) P1_A_TS3

Figure 4.9 shows hardness profile along beads cross sections and irregular hardness profiles were seen. Comparing the three samples is noticeable that test sample P1_A_TS3 is the most irregular as expected, due to the irregularity of the thin reinforced zone, noticeable in some indentations like X=5.5, where the value of hardness almost correspond to BM hardness, and for X=5 mm that is of 164 HV.

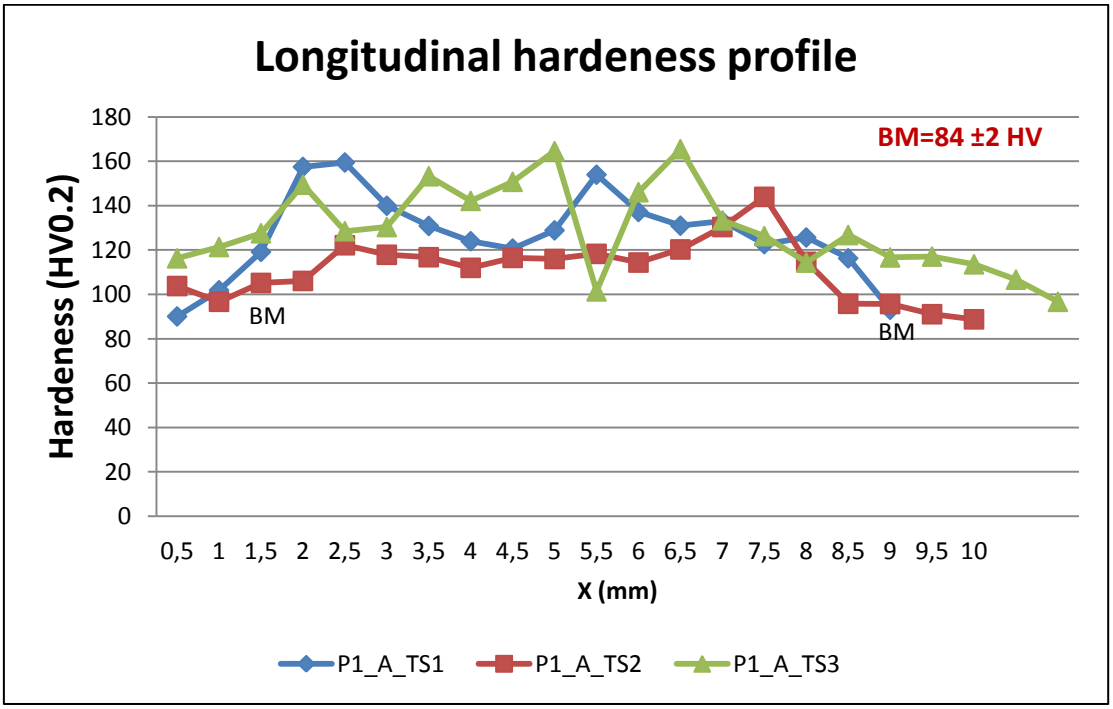

Figure 4.9 - Hardness profile along cross section for P1_A_TS1 to TS3.

4.1.3 Friction stir process reinforced with silicon carbide particles (P1_S).

For this set of tests and considering the test performed in P1_A, different parameters were used, displayed in Table 4.3.

Table 4.3 - Parameters of process one with silicon carbide.

Tests nº	ω(rev)	Vx (mm/min)	ω/Vx	Angle ()
P2_S_T1	1120	180	6,222	0
P2_S_T2	710	224	3,170	0
P2_S_T3	1120	180	6,222	2
P2_S_T4	710	224	3,170	2

4.1.3.1 Macroscopic characterization

Macroscopic characterization of all tracks shows there is almost no waviness, but a small burr is observed in tracks 3 and 4, as depicted in Figure 4.10 due to attack angle.

Figure 4.10 - Macroscopic observation from tracks for trial group P1_S.

4.1.3.2 Microscopic characterization

Figure 4.11 shows several micrographs of sample P1_S_T1 cross section, with a thin layer of processed zone with a maximum depth of 100 µm and an extension of 18.5 mm. This thin layer shows a homogeneous distribution of silicon carbide particles as seen in Figure 4.11 a) and b). Most of the silicon carbide particles have fragmented into smaller particles, but in Figure 4.11 d) it can be seen some larger particles with an average size of 20 µm, and most of these particles are incrusted on the surface. In the AS the processed zone has several layers of reinforcing material depicted in Figure 4.11 c). The layer at the surface and the layer in the interface have more silicon carbide particles then the second layer. In this cross section is also possible to observe a good bounding between the layer with reinforce and BM.

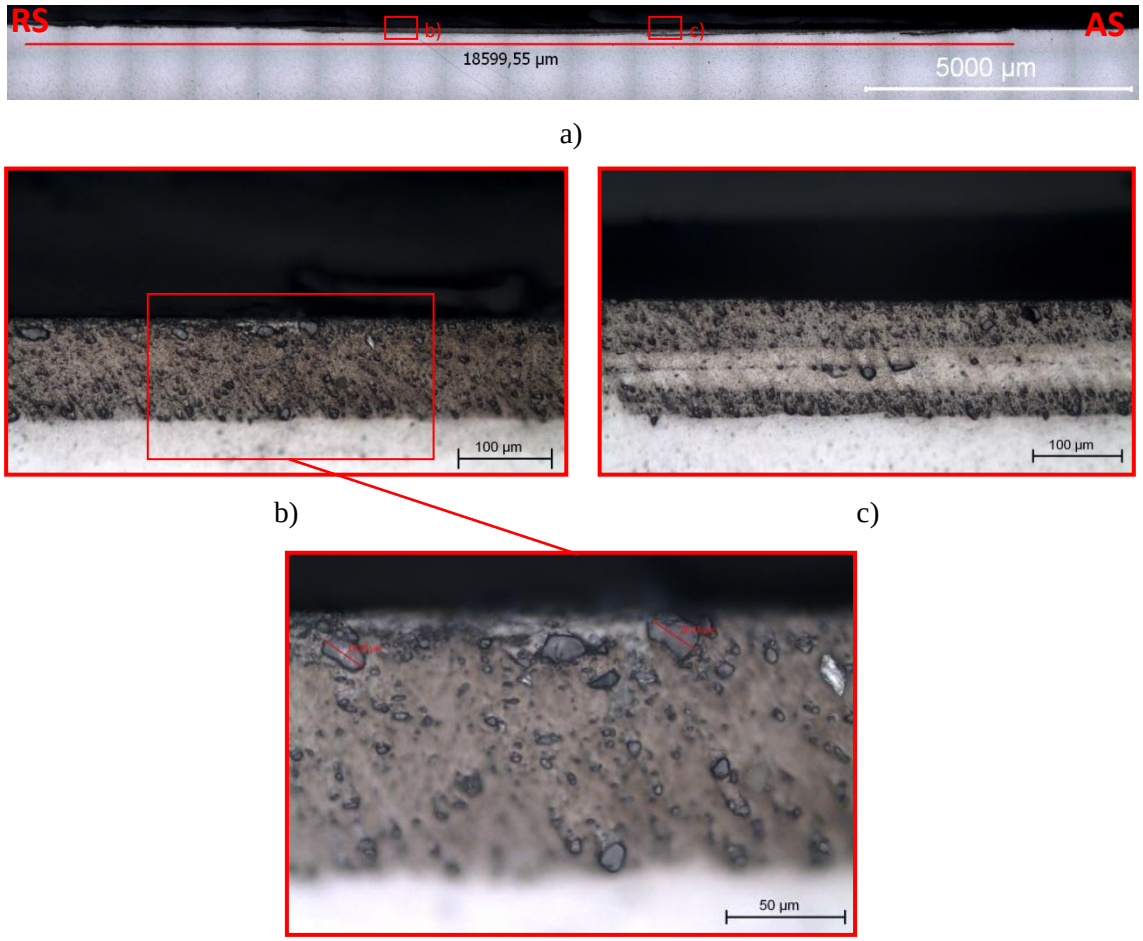

Figure 4.11 - Cross section micrographs of test sample P1_S_TS1. (A) Macrographs of bead cross section, (B,D) Details of interface zone in RS, (C) Details of interface zone in AS.

Figure 4.12 depicts cross sections of test sample P1_S_T2. A thin reinforced layer was also obtained with a maximum depth of 133.8 µm and an extension of 17.2 mm, the extension of the layer isn't homogeneous, showing some waviness, more pronounced in the AS, as seen in Figure 4.12 a) and d). Silicon carbide particles are well distributed, but like test sample P1_S_TS1, larger particles are found on the processed zone. These particles have an average size of 20 µm.

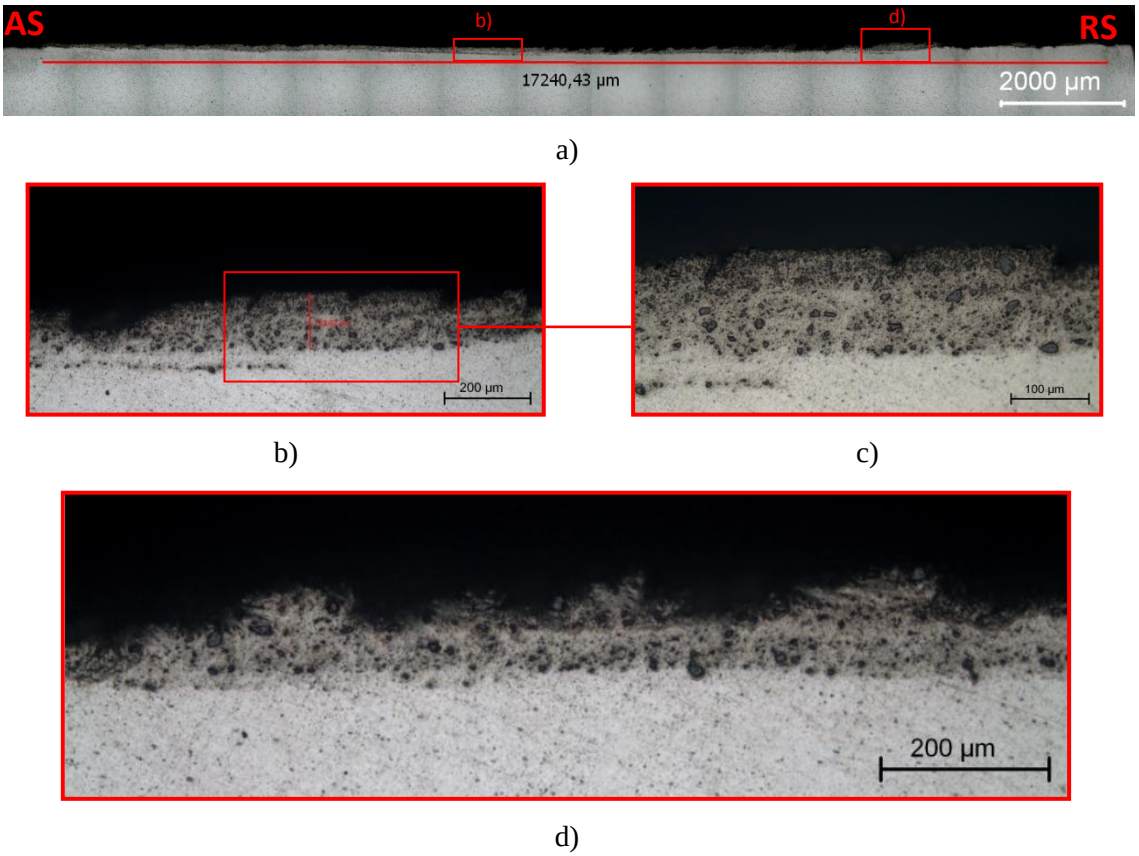

Figure 4.12 - Cross section micrographs of test sample P1_S_TS2. (A) Macrographs of bead cross section, (B,C) Details of interface zone in RS, (D) Details of interface zone in AS.

Test sample P1_S_TS3 was processed with an attack angle of 2°. Like in previous tests a thin layer was achieved with a less extension. Also a very perceptible waviness in the interface in the AS is observed in Figure 4.13 a) and e). The thin layer has a maxim deep of 90 µm and an extension of 7.9 mm. Silicon carbine particles are less fragmented and the larger particles have an average size of 30 µm. A higher concentration of the bigger SiC particles is observed in the reinforced layer than in other test samples. The two attack angle provokes shredding in reinforced layer as observed in Figure 4.13 a) and e) in the AS. This allows to concluded that an attack angle provokes an improvement in particles concentration, but is also responsible for the defects observed.

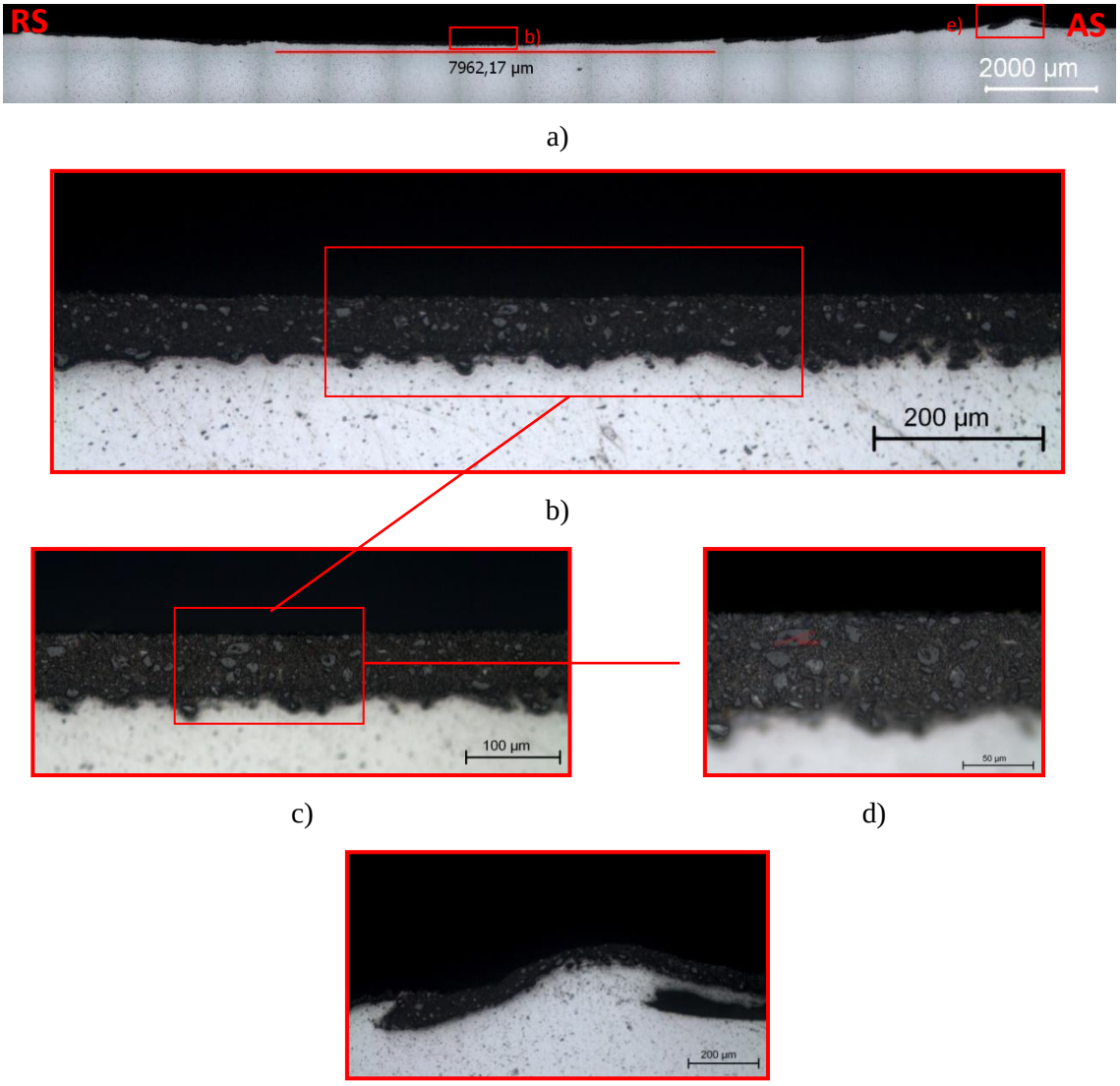

Figure 4.13 - Cross section micrographs of test sample P1_S_TS3. (A) Macrographs of bead cross section, (B,C,D) Details of interface zone, (E) Details of burr in AS.

Figure 4.14 presents micrographs from cross section test sample P1_S_TS4. Some interesting observations can be made: due to an attack angle of 2° combined with test parameters, material flows outside the processed zone and the interface region is homogeneous as shown in Figure 4.14 a). Large agglomerations of alumina particles are seen in Figure 4.14 b) to d). These agglomerations are composed by fragmented particles but like in the other test samples some larger particles can be observed. These particles have an average size of 25um. Like test sample P1_A_TS3 the attack angle provokes more downsides than improvements to the reinforced zone.

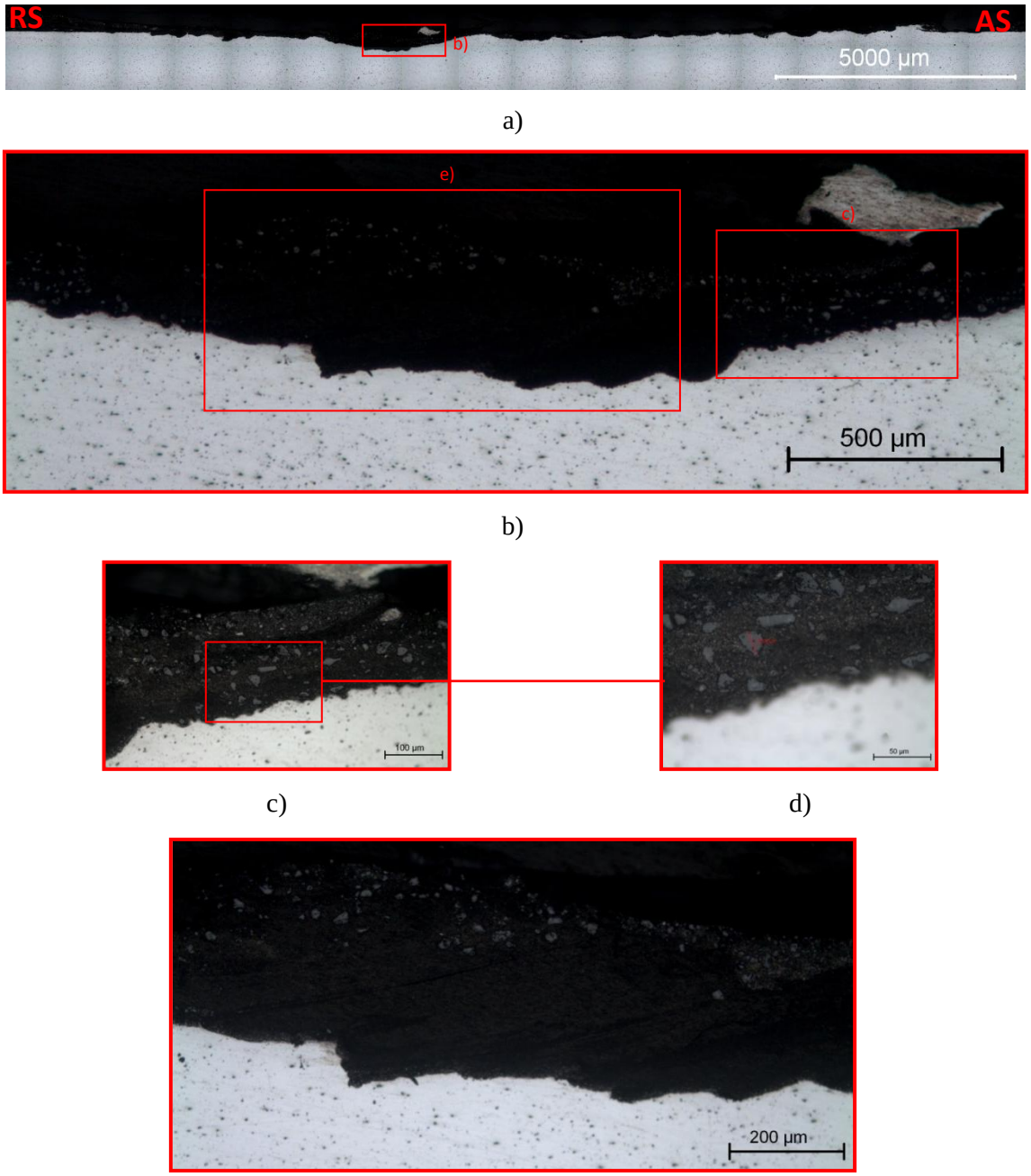

Figure 4.14 - Cross section micrographs of test sample P1_S_TS4. (A) Macrographs of bead cross section, (B,C,D,F) Details of interface zone in RS.

4.1.3.3 Hardness tests

Hardness profiles presented in Figure 4.15 indicates that higher hardness values were obtained in the thin reinforced layer in all test samples. In test sample P1_S_TS3 on vertical hardness profile A in Y=0,06 mm a irregular point was obtained with a hardness of 1400 HV. This indention was preformed on a big particle of SiC. Values obtained in vertical profiles show an increase of approximately of 300 % in comparison with BM.

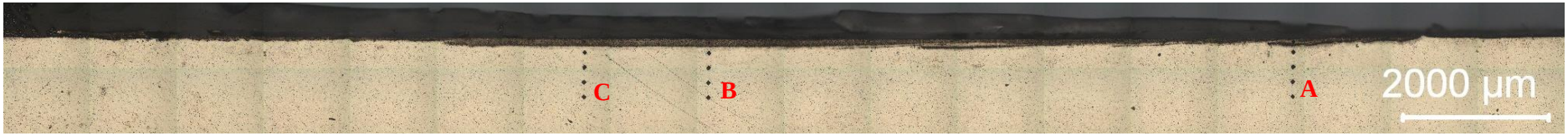

a)

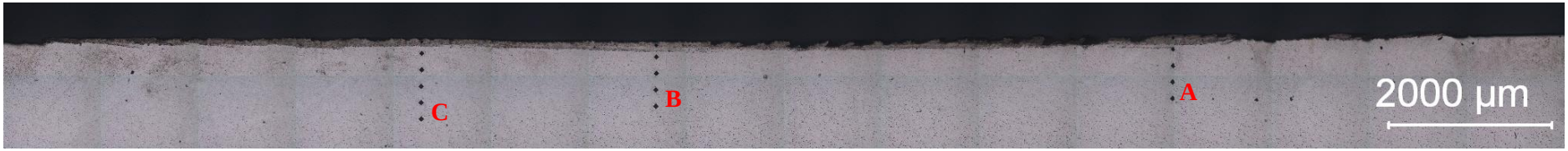

b)

c)

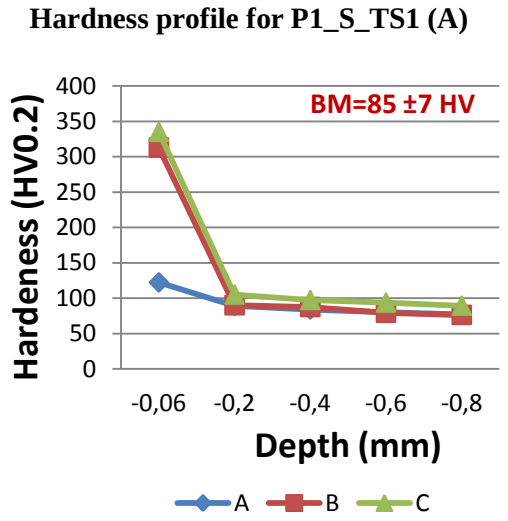

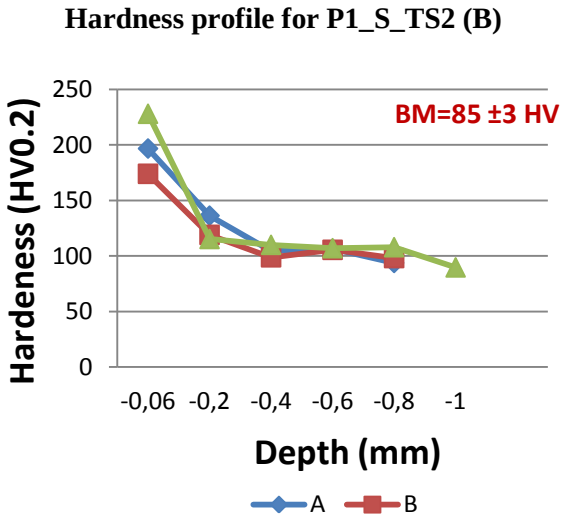

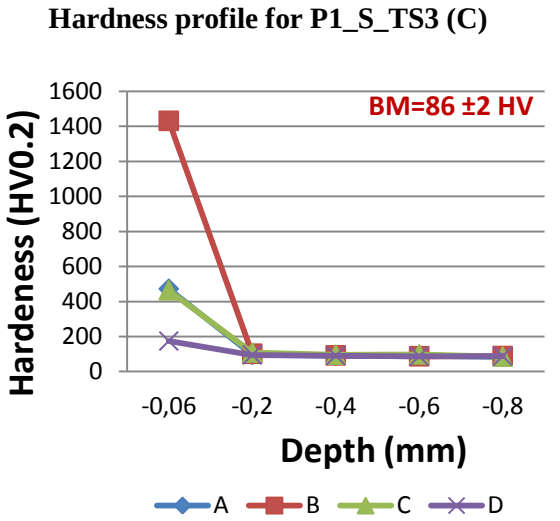

Figure 4.15 – Hardness profiles from test samples: (A) P1_S_TS1, (B) P1_S_TS2, (C) P1_S_TS3

4.2 Friction stir process with consumable driller tool packed with particles (P2).

4.2.1 Evaluation of parameters in process (P2_P)

A number of preliminary tests were preformed varying functional parameters, as can be seen in Table 4.4. A K index was calculated in order to better comprehend the small window of parameters in with the tests presents a continua's cord.

Table 4.4 - Parameters of process two.

Test nº	ω (rev)	V_x (mm/min)	α (º)	Pino	V_y (mm/min)	ω/V_y	K= ω/V_x
P2_P1	900	280	5	1	24,497	11,430	3,214
P2_P2	900	45	5	1	3,937	11,430	20,000
P2_P3	1120	45	2,5	1	1,965	22,904	24,889
P2_P4	1400	71	2,5	1	3,100	22,904	19,718
P2_P5	1400	90	2,5	1	3,929	22,904	15,556
P2_P6	1400	112	5	2	9,799	11,430	12,500
P2_P7	1400	224	5	2	19,597	11,430	6,250
P2_P8	1400	280	5	2	24,497	11,430	5,000
P2_P9	1400	280	5	3	24,497	11,430	5,000
P2_P10	1400	280	5	3	24,497	11,430	5,000
P2_P11	1800	280	5	3	24,497	11,430	6,429
P2_P12	1800	355	5	3	31,058	11,430	5,070
P2_P13	1800	355	5	4	31,058	11,430	5,070
P2_P14	1400	355	5	4	31,058	11,430	3,944
P2_P15	1400	450	5	4	39,370	11,430	3,111

In Figure 4.16 it can be seen the evolution of K index and the numbers of test preformed. This graphic allows to see that better results are obtain with a lower index K

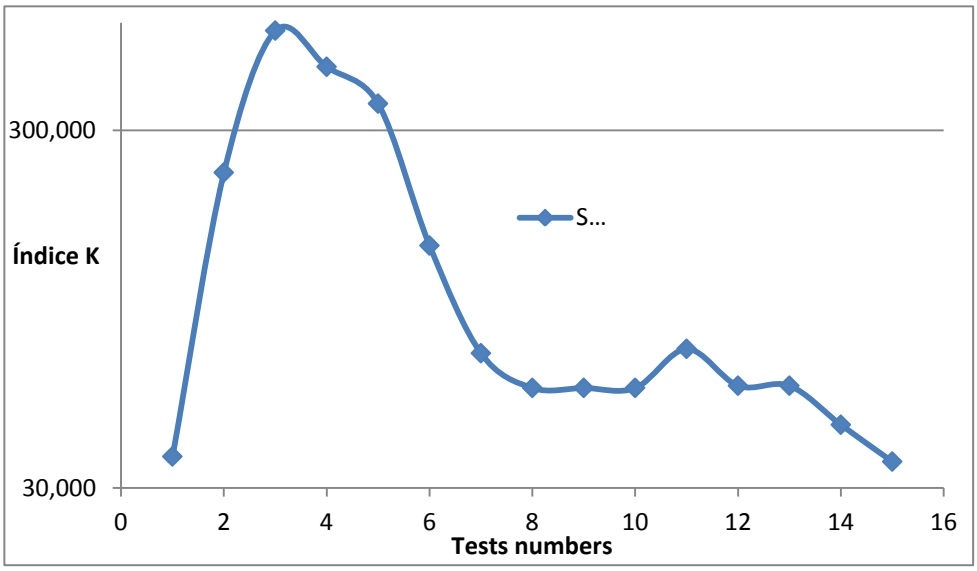

Figure 4.16 – K índice variation in test.

In tracks from 1 to 7 continuous beads were not achieved. This was due to a low rotation speed, low travel speed and a high ratio between the rotating speed and travel speed, thus, low index K. This caused interruptions in the beads, as seen in Figure 4.17. In all tracks the AS correspond to the top of the tracks and the bottom to the RS.

P2_P9
P2_P8
P2_P1 to P4
P2_P7
P2_P5
P2_P6

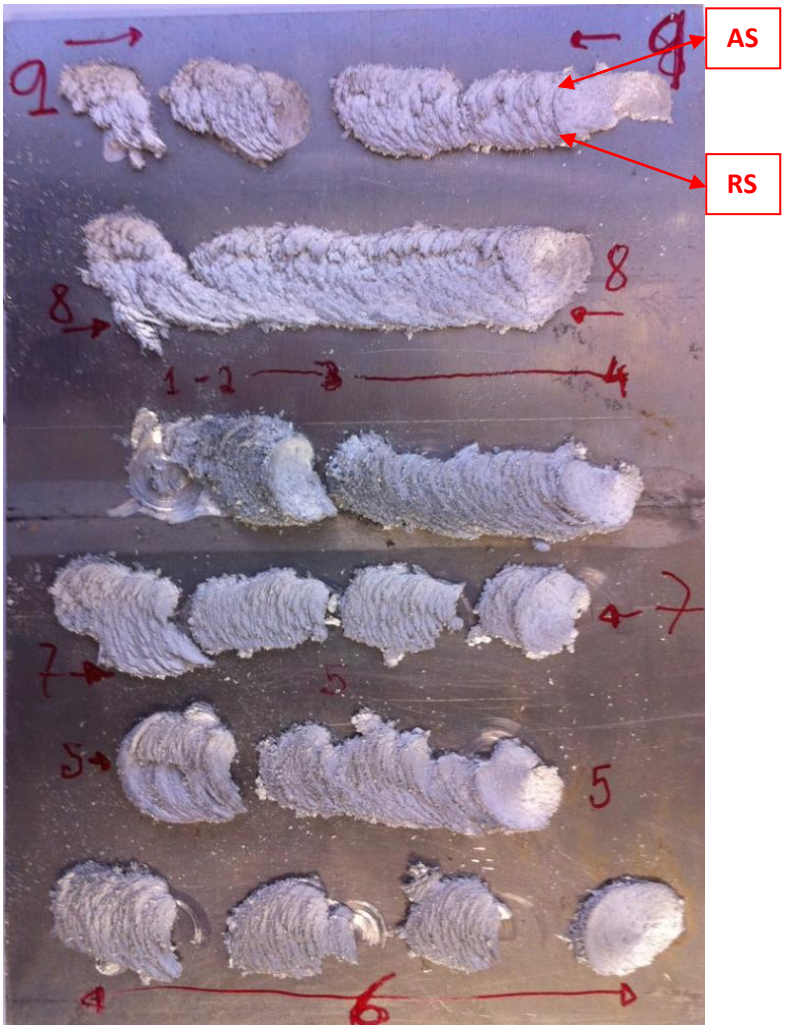

Figure 4.17 - Macrograph observation from tracks for trial group P2_P1 to P9.

From test 10 to 15 a continuous bead was achieved, but this process originates a high waviness as seen in Figure 4.18 . Track 14 and 15 reveals larger and a more regular material deposition. Like in previous figure the AS correspond to the top of tracks, and RS to the bottom.

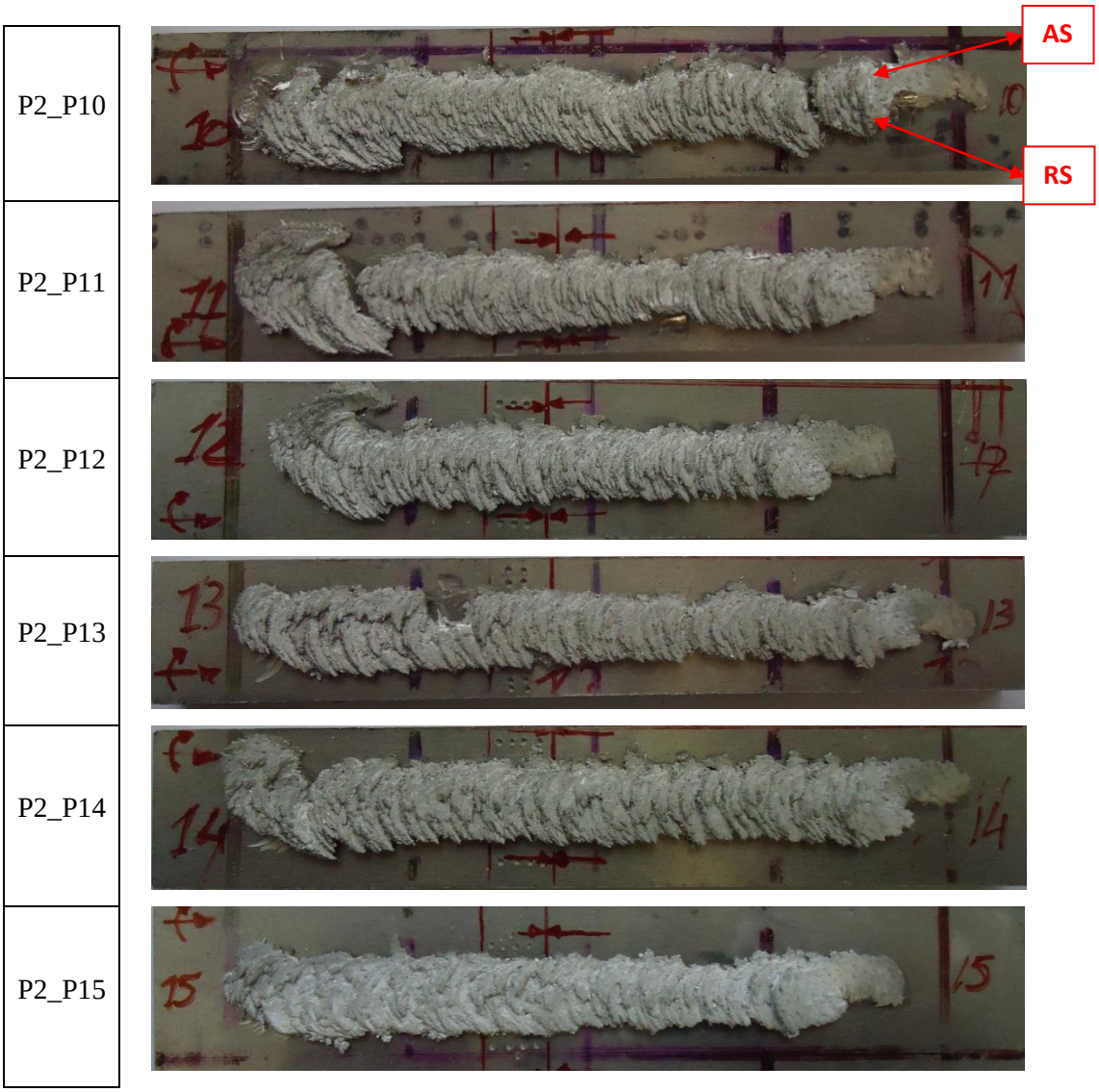

Figure 4.18 - Macrograph observation from tracks for trial group P2_P10 to P15.

A macro and microscopic analysis of cross sections from tracks 10 to 15 reveals good bonding between the AW 2007-H4 consumable pin and BM as depicted in Table 4.5. Also in this table are observed values for material deposition extension and height. These values were obtained for zones that presented good bonding with base material. Tests 13 and 15 showed better results, being these parameters the ones used in further testing.

Table 4.5 – Macrographs from test group P2_P, and values for extension and height.

P2_P10 L=8,41 mm; h=2,27 mm 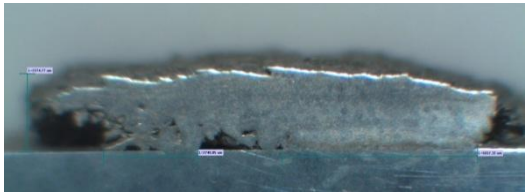	P2_P11 L=5,85 mm; h=2,26 mm 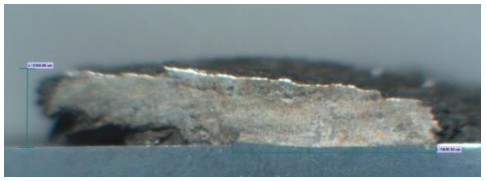	P2_P12 L=8,45 mm; h=2,13 mm 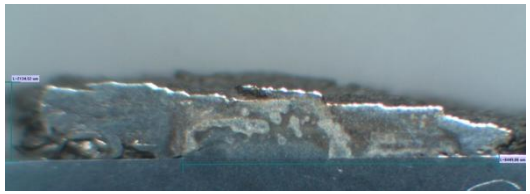
P2_P13 L=9,83 mm; h=2,27 mm 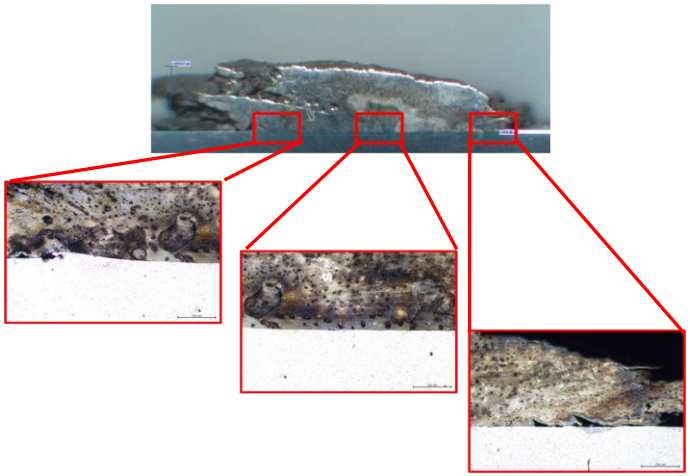	P2_P14 L=8,73 mm; h=2,36 mm 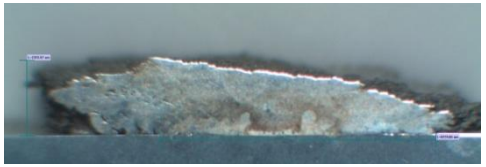	P2_P15 L=10, mm; h=2,27 mm 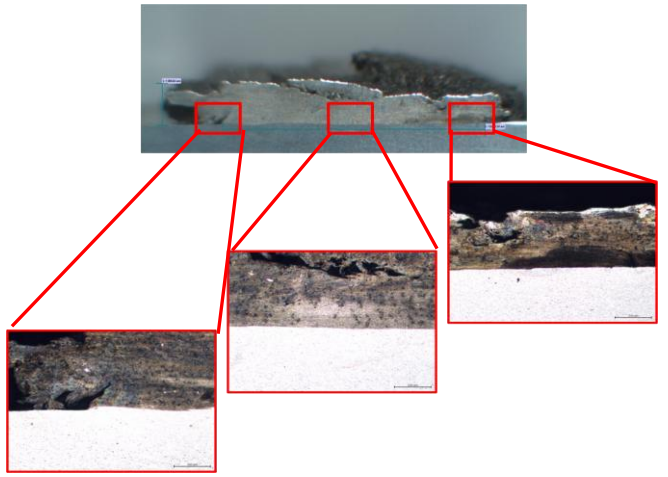

4.2.2 Friction stir process with consumable driller tool packed with alumina particles (P2_A).

Taking into account the results observed in test group P2_P, especially in test samples P2_P_TS10 to 15, parameters depicted in Table 4.6 were selected for this test group.

Table 4.6 - Parameters of process two with alumina powders.

Test nº	ω (rev)	V_x (mm/min)	α_2 (º)	α_1 (º)	Pino	V_y (mm/min)	ω/V_y	K= ω/V_x
P2_A_T1	1400	450	2,5	5	T_H4_HD4	39,370	35,560	3,111
P2_A_T2	1800	355	2,5	5	T_H4_HD4	31,058	57,955	5,070
P2_A_T3	1800	280	2,5	5	T_H4_HD4	24,497	73,479	6,429
P2_A_T4	1800	355	2,5	5	T_H1_HD4	31,058	57,955	5,070
P2_A_T5	1400	355	2,5	5	T_H1_HD4	31,058	45,076	3,944
P2_A_T6	1400	450	2,5	5	T_H1_HD4	39,370	35,560	3,111

During this process with alumina particles, it was noticed high concentrations of alumina powders, preventing bounding between consumable pin and substrate This was compensated by reducing hole diameter in order to accommodate less volume of alumina powders. With a smaller hole diameter the bounding to the substrate increased, but alumina powders still prevented bounding to the substrate, especially compared to test group P2_P.

4.2.2.1 Macroscopic characterization

Figure 4.19 presents macrographs of processed beads from trial group P2_A, on a first observation is noticed a non-continuous bead, on tests P2_A_T1 to T4. This is a consequence of the lack of bounding provoked by a high volume of alumina powders inserted in the drilled holes of the consumable pin. As referred, a new profile of consumable pin was used with smaller holes to reduce powder volume and improve bounding. Tests P2_A_T4 to T6 were performed using pin profile T_H1_HD4 and a significant improvement was noticeable with a continuous bead.

Pin T_H1_HD4	P2_A_T6
	P2_A_T5
	P2_A_T4
Pin T_H4_HD4	P2_A_T3
	P2_A_T2
	P2_A_T1

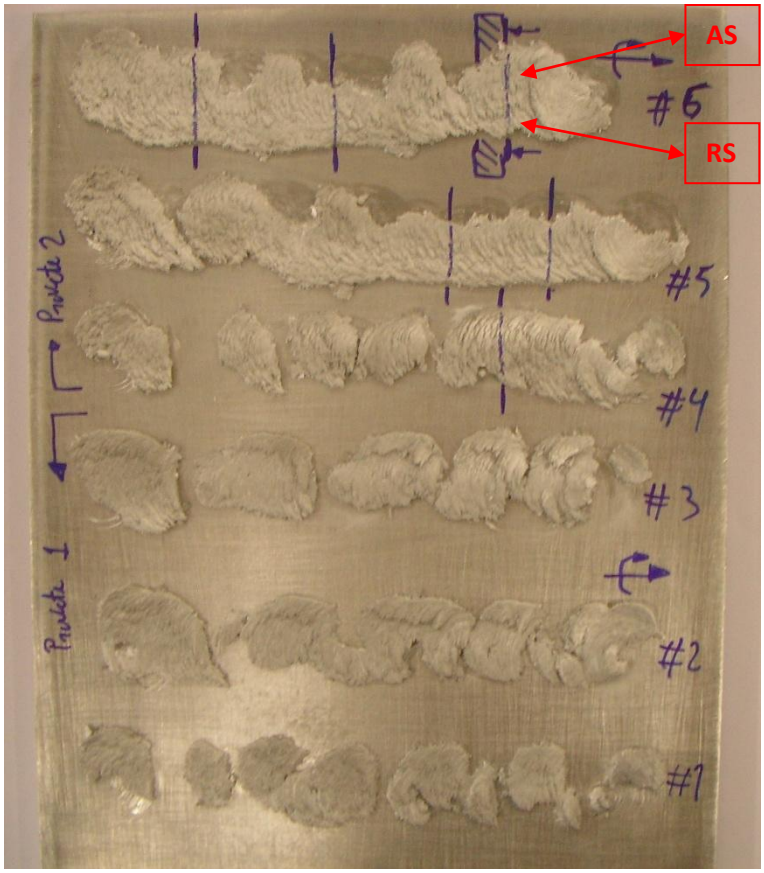

Figure 4.19 – Macrograph observation from tracks for trial group P2_A.

Figure 4.20 presents a closer image of test group P2_A, where it is seen a relevant waviness in all tests from trial group.

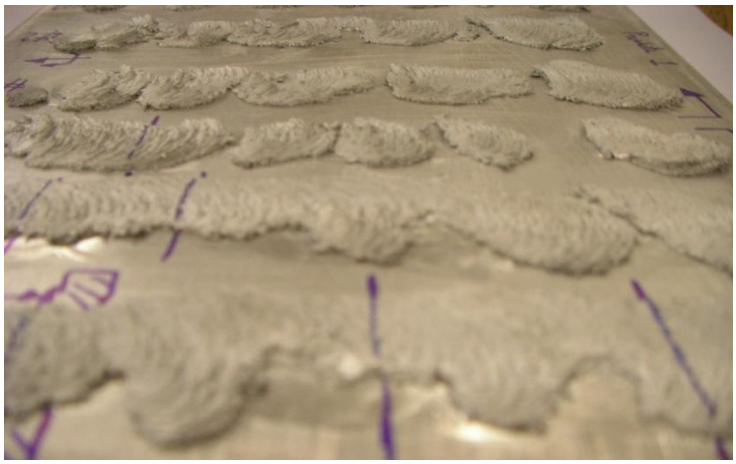

Figure 4.20 – Macroscopic detail from test group P2_A.

4.2.2.2 Microscopic characterization

Microscopic characterization of test group P2_A, no cross sections from tests P2_A_T1 to 3 were taken because of a non continuous bead, that prevented further characterization.

Figure 4.21 shows a macrographs images from cross sections taken from P2_A_T4 to T6, This images depicts the poor bonding of Al1100 to BM due to alumina powders, especially on

Figure 4.21 a) and b). Alumina particles are concentrated and aligned along test sample on deposited material in test sample P2_A_TS3 and some particles are located in the interface between materials in all test samples, concluding that alumina particles are responsible for the lower bounding to BM, in comparison with P2_P.

This process shows a large waste in material deposition due to the low bounding verified especially in the retreating side.

P2_A_TS1 – L=5,37 mm, h=1,36 mm

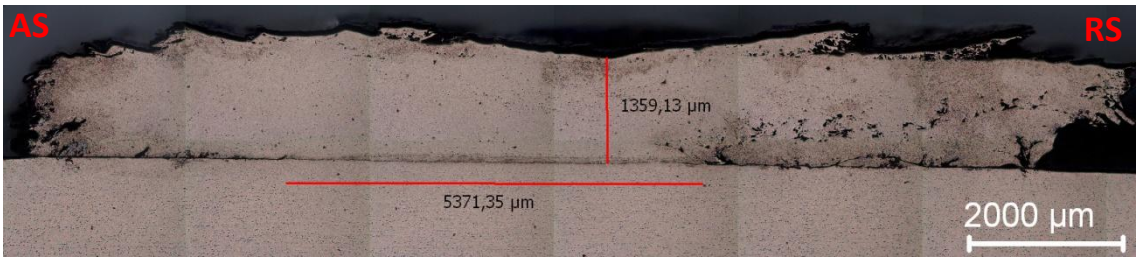

a)

P2_A_TS2 - L=2,3 mm, h=1,39 mm

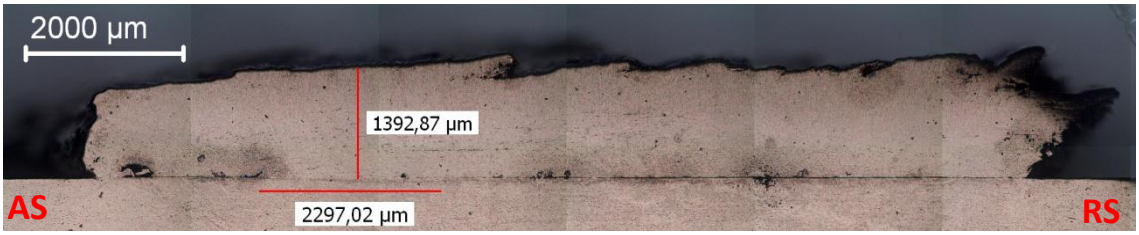

b)

P2_A_TS3 - L=6,9 mm, h=1,23 mm

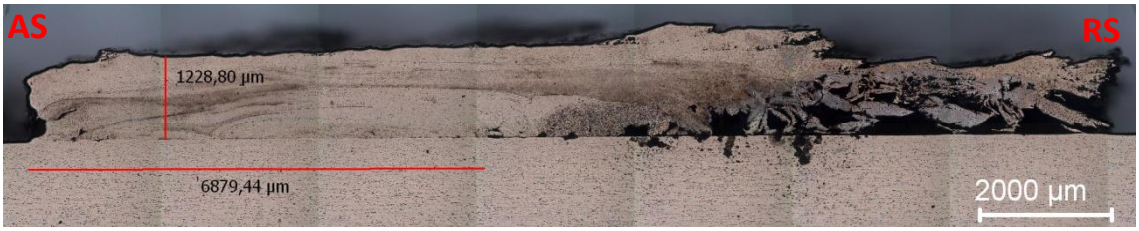

c)

Figure 4.21 - Macrographs of bead cross section for test group P2_A.

Observation in dark mode illumination of test sample P2_A_TS3, shows the presence of fragmented alumina particles, as depicted in Figure 4.22 d). These particles have an average size of 15 µm.

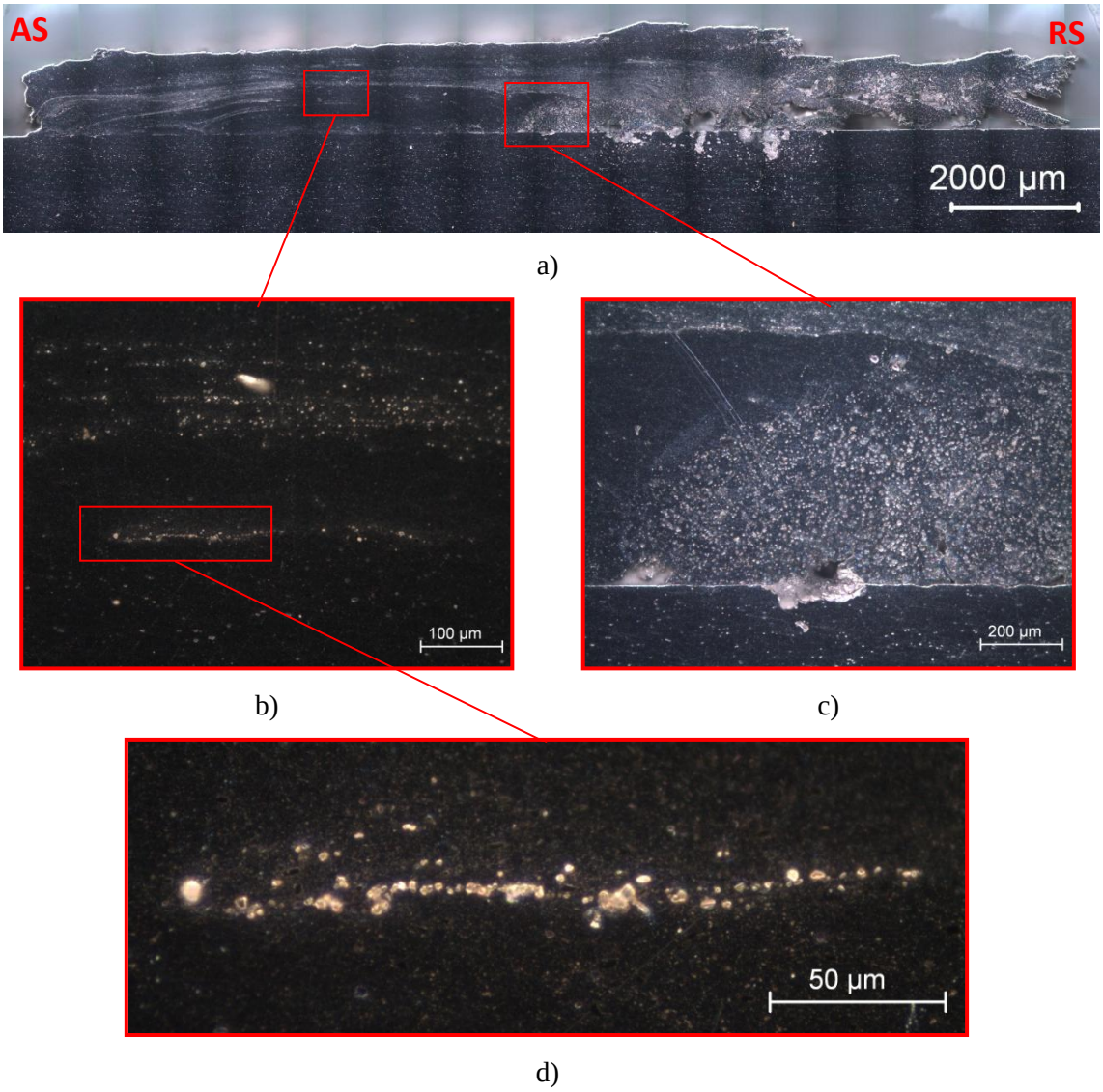

Figure 4.22 - Cross section micrographs of test sample P2_A_TS3 in DF. (A) Macrographs of bead cross section, (B,D) Concentration of alumina particles, (C) Detail of interface zone in AS.

4.2.2.3 Hardness testing

Hardness profiles from test samples depicted in Figures 4.23 to 4.25 are very similar. In the interface zone hardness between BM and AA1100 was obtained in the order of 90 HV. In the zone closer to the surface of the layer, higher values of hardness of about 140 HV were measured that correspond to a raise of 15%. Some abnormal high values in hardness correspond to zones with concentration of alumina particles.

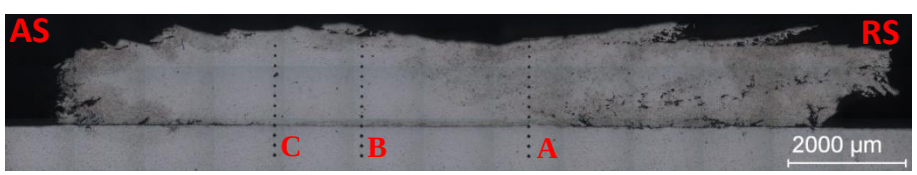

a)

b)

Hardness profile from P2_A_TS1

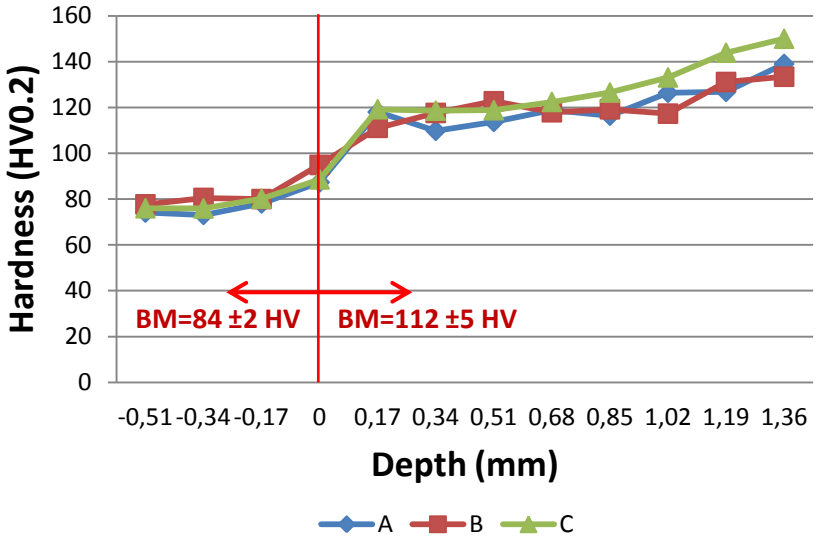

Hardness profile from P2_A_TS2

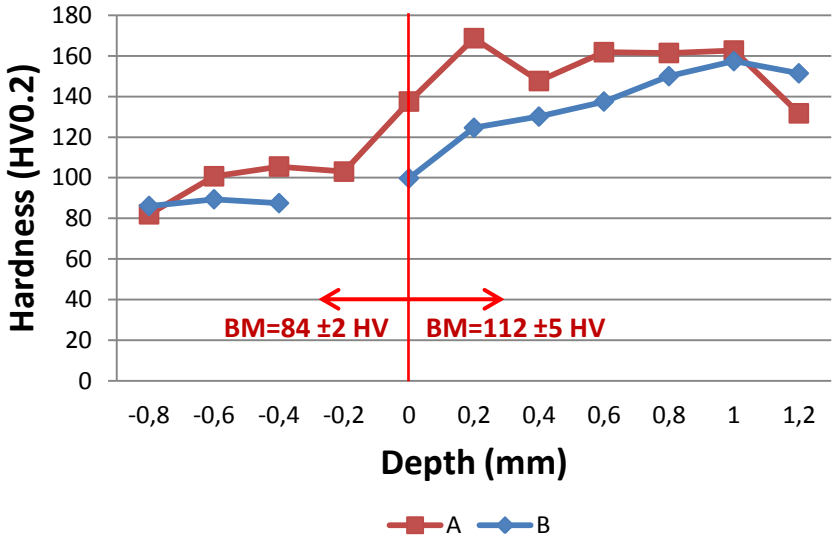

Figure 4.23 – Hardness profiles from test samples: (A) P2_A_TS1, (B) P2_A_TS2.

Hardness profile from P2_A_TS3

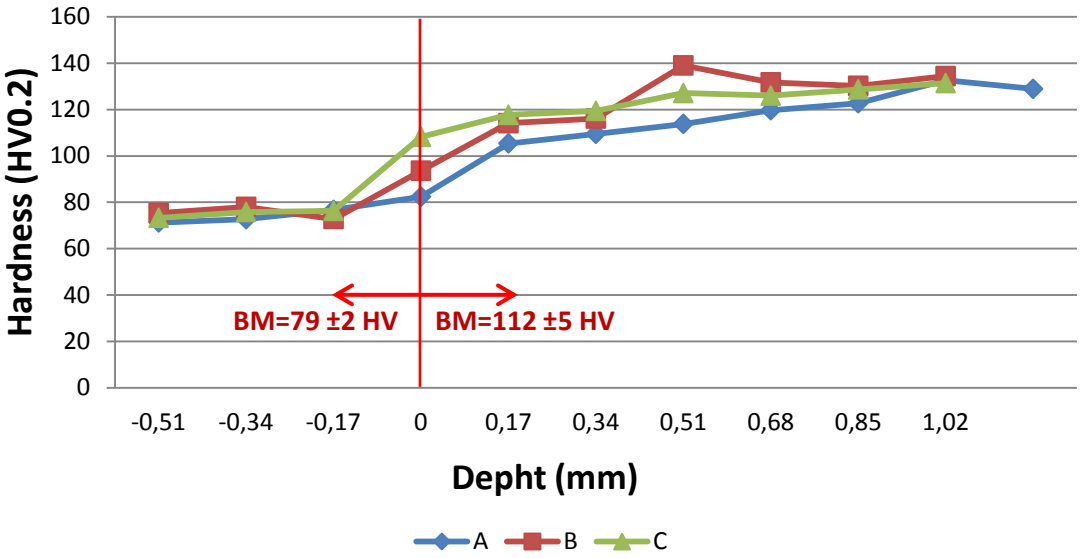

Figure 4.24 - – Hardness profiles from test sample P2_A_TS3.

4.2.3 Friction stir process with consumable driller tool packed with silicon carbide particles (P2_S)

Taking into account the results verified in test group P2_P and P2_A, the parameters depicted in Table 4.77 were chosen for this test group.

Table 4.7 - Parameters of process two with silicon carbide particles.

Test nº	ω (rev)	V_x (mm/min)	α_2 (º)	α_1 (º)	Pino	V_y (mm/min)	ω /V_y	K= ω/V_x
P2_S_T1	1800	355	2,5	5	T_H2_HD2	31,058	57,955	5,070
P2_S_T2	1400	450	2,5	5	T_H2_HD2	39,370	35,560	3,111
P2_S_T3	1800	355	2,5	5	T_H1_HD2	31,058	57,955	5,070
P2_S_T4	1400	450	2,5	5	T_H1_HD2	39,370	35,560	3,111
P2_S_T5	1800	280	2,5	5	T_H1_HD2	24,497	73,479	6,429
P2_S_T6	1800	180	2,5	5	T_H1_HD2	15,748	114,301	10
P2_S_T7	900	450	2,5	5	T_H1_HD2	39,370	22,860	2
P2_S_T8	1400	450	2,5	5	T_H1_HD2	39,370	35,560	3,11

During the process and due to the pin profile chosen fewer concentrations of SiC powders were noticeable and a better bonding was achieved in the first test in comparison with the first tests from P2_RA. For test P2_RS_T5 to T7. The parameters were slightly different in order to observe the influence in a high ratio K with reinforcing particles.

4.2.3.1 Macroscopic characterization

Figure 4.25 represents macrographs of beads from test group P2_RS. In spite of the consumable pin used in tests P2_RS_T1 and T2, with less volume of powders, a non continuous bead is still obtained. For this test group, T_H1_HD2 pin profile with half the volume in reinforcing powders was used and better results were obtained, especially in test P2_RS_T4 and T8 where a continuous bead was obtained. The tests processed with a high and low ratio K confirmed that outside the window of K values, a non continuous bead is obtained with or without reinforcing powders.

T_H1_HD4	P2_RS_T1
	P2_RS_T2
T_H1_HD2	P2_RS_T3
	P2_RS_T4
	P2_RS_T5
	P2_RS_T6
	P2_RS_T7
	P2_RS_T5

Figure 4.25 - Macrograph observation from tracks for trial group P2_S.

Like previous test from P2 a relevant waviness was observed as depicted in Figure 4.26.

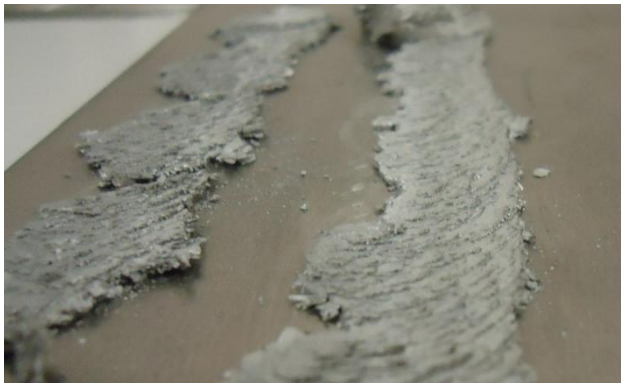

Figure 4.26 – Macrograph of waviness from test group P2_S.

4.2.3.2 Microscopic characterization

Comparing all test samples depicted in Figure 4.27 to 4.29, it can be seen aligned distributions of SiCp in AA1100 along the test samples. Samples removed from tests performed using pin profile T_H1_HD2 show an improved bonding especially in tests samples P2_S_TS4 and TS5, and although this pin profile compact less volume of SiCp, good concentrations of SiCp were observed in AA1100 although aligned along test samples. Also larger concentrations of SiCp are observed in the RS with the exception of P2_S_TS1

Like other test groups, test group P2_S shows a high waste of deposited material, as seen in the RS. Figure 4.27 b) shows a good example with a large area of deposited material but without consolidation.

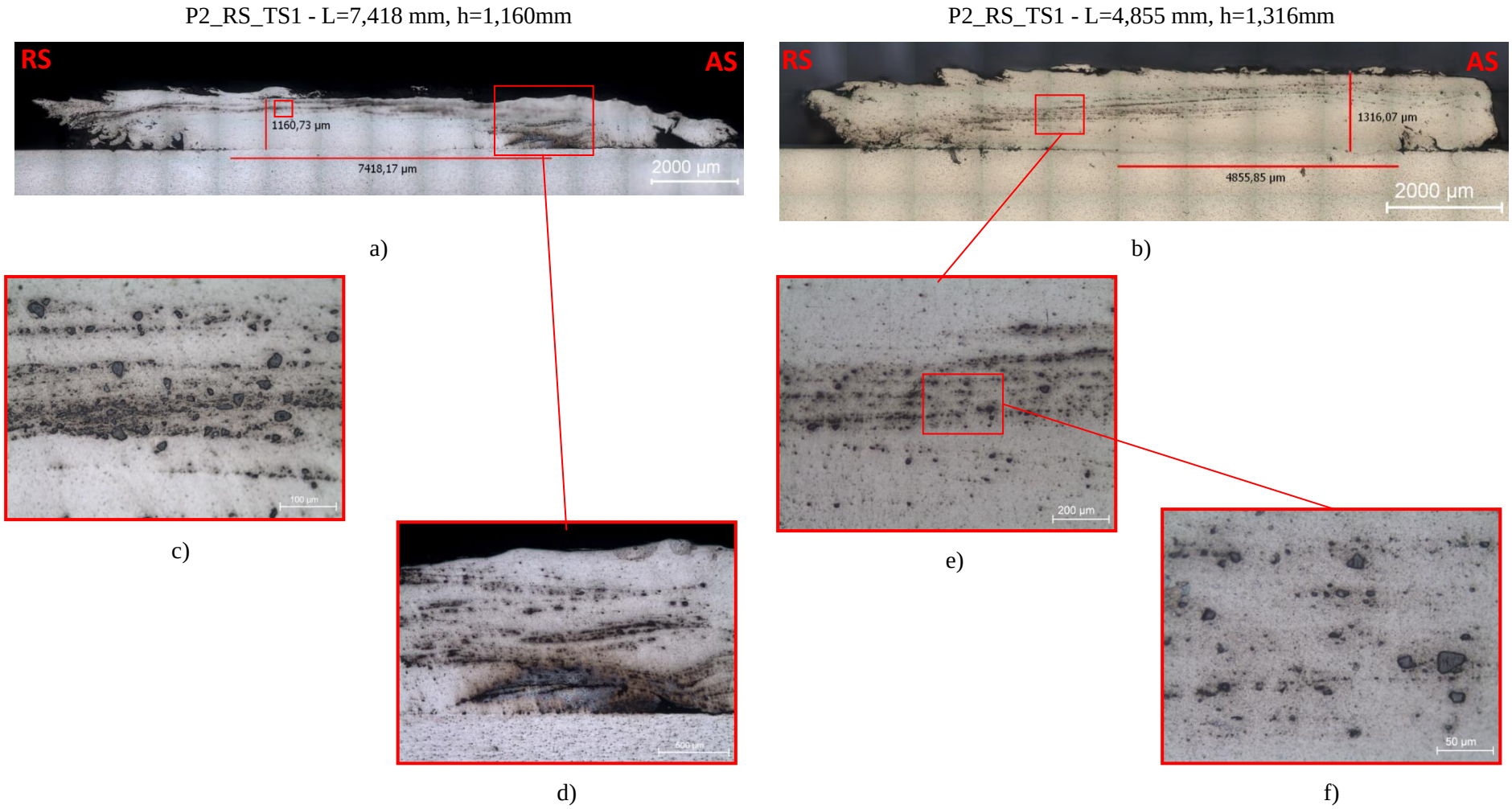

Figure 4.27 - Cross section micrographs of test sample P2_S_TS1 and P2_S_TS2. (A) Macrographs of bead cross section from P2_S_TS1, (B) Macrographs of bead cross section from P2_S_TS2, (C) Detail of alumina particles concentrations,(D) Details of interface zone, (E, F) Detail of alumina particles concentrations.

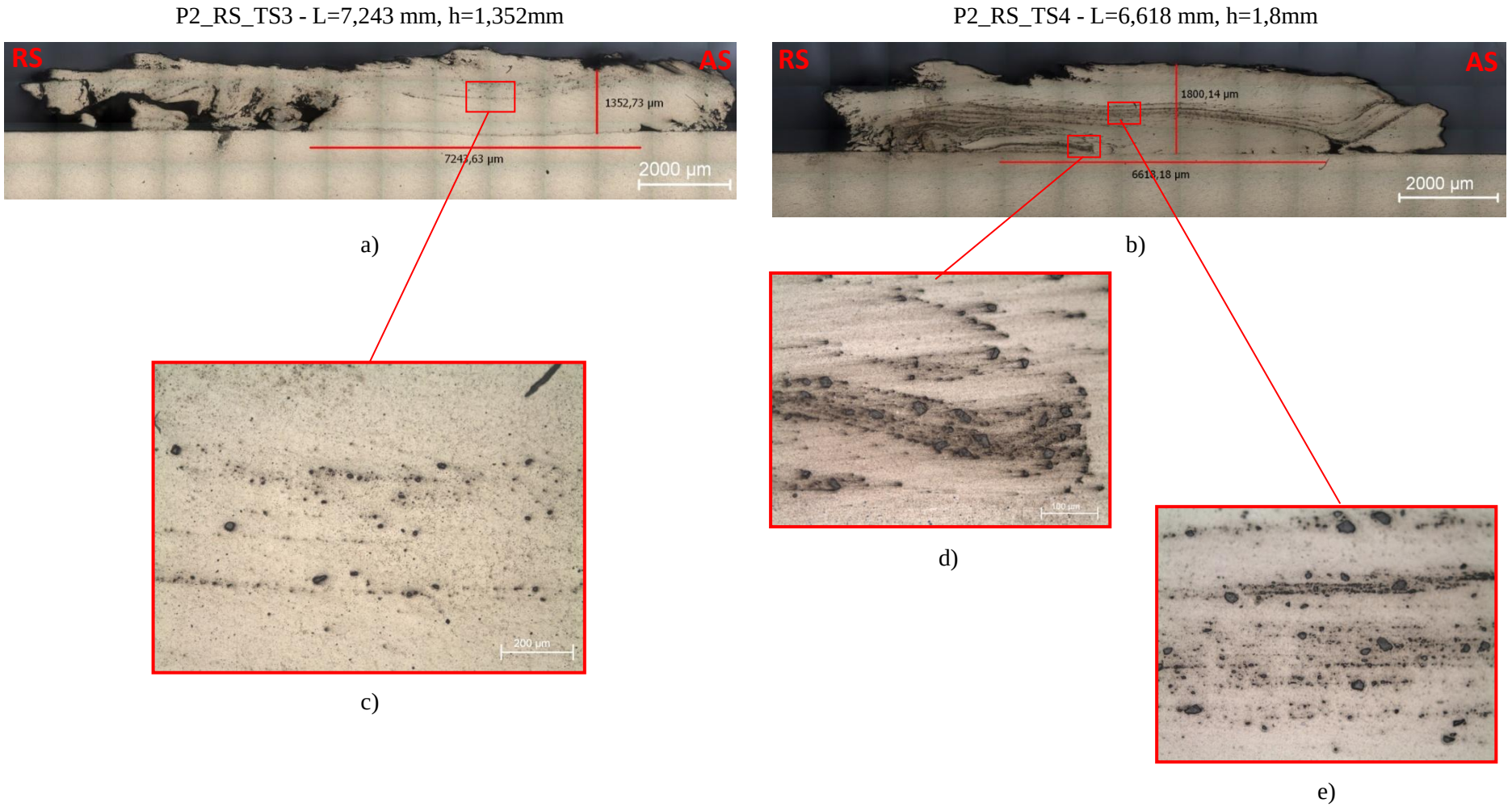

Figure 4.28 - Cross section micrographs of test sample P2_S_TS1 and P2_S_TS2. (A) Macrographs of bead cross section from P2_S_TS3, (B) Macrographs of bead cross section from P2_S_TS4,(C) Detail of alumina particles concentrations, (D, E) Detail of alumina particles concentrations in interface zone.

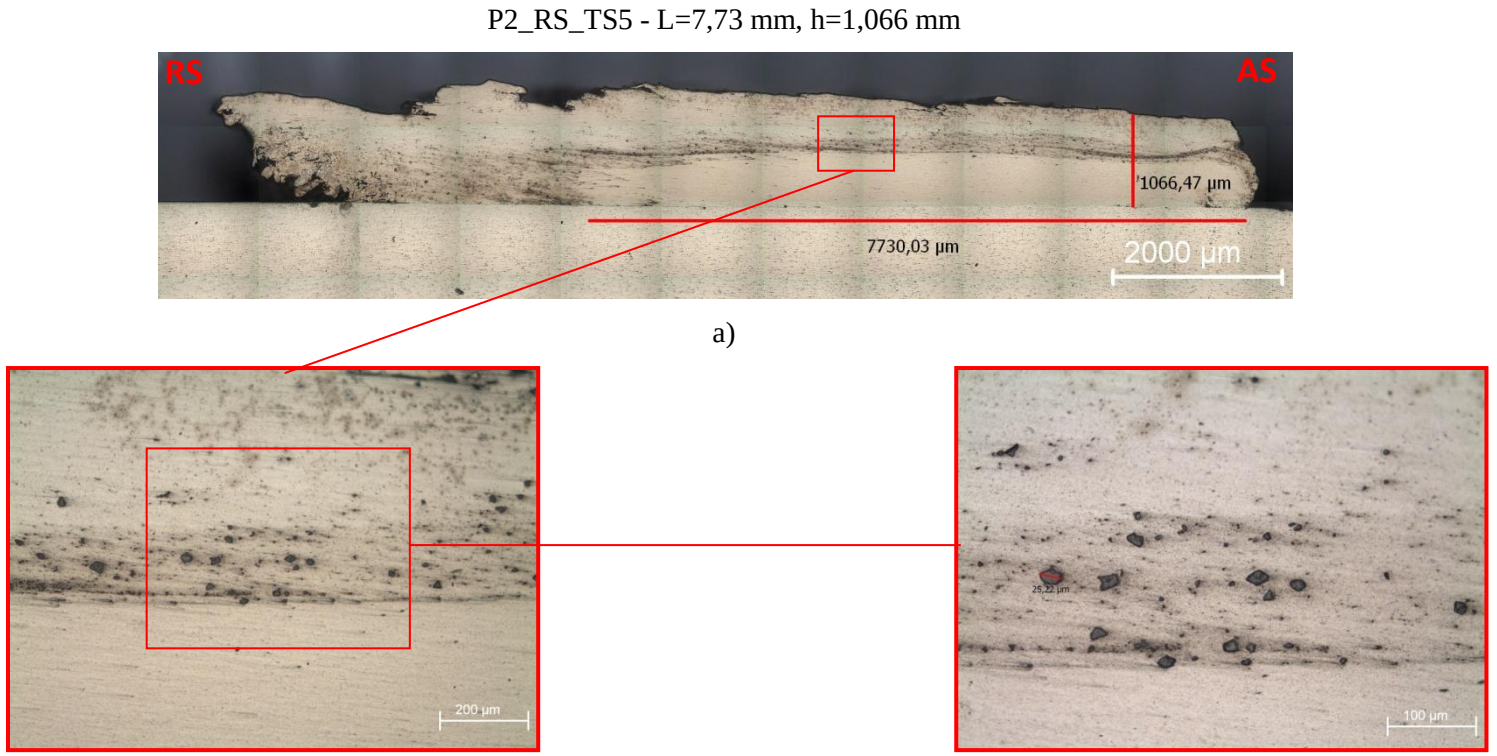

Figure 4.29 - Cross section micrographs of test sample P2_S_TS5. (A) Macrographs of bead cross section, (B, C) Detail of alumina particles concentrations.

4.2.3.3 Hardness testing

Figure 4.30 to 4.31 shows hardness profiles from test group P2_S. A significant increase in hardness was achieved, but the increase in hardness is mostly due to hardness of aluminium alloy deposited on surface of BM. Some exceptions are noticeable in the indentations preformed, such as P2_S_TS1 in Y=0,68 mm in vertical hardness profile B, and in P2_S_TS5 in Y=1,02 mm in vertical hardness profile C, in these two cases a higher values were observed because the indentations were preformed in zones where SiCp were concentrated.

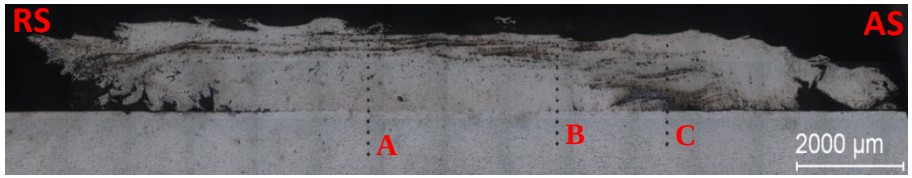

a)

Hardness profile from P2_S_TS1

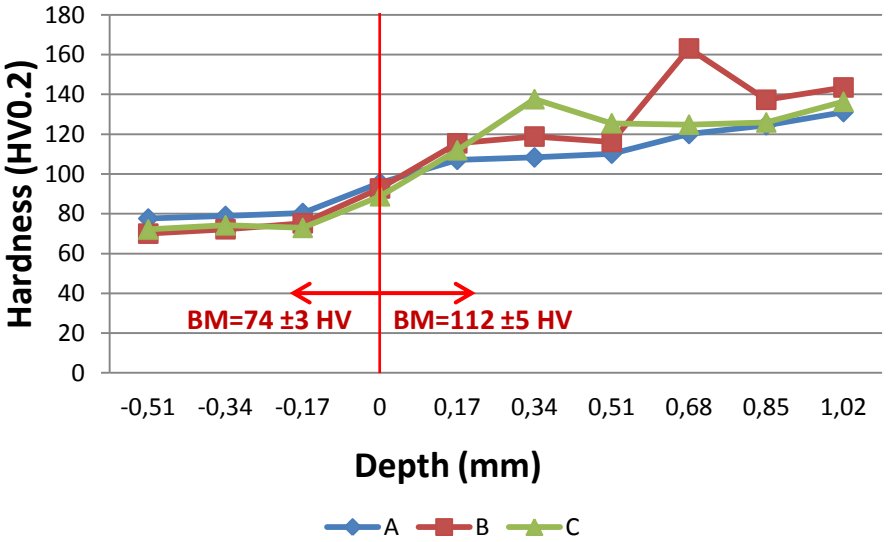

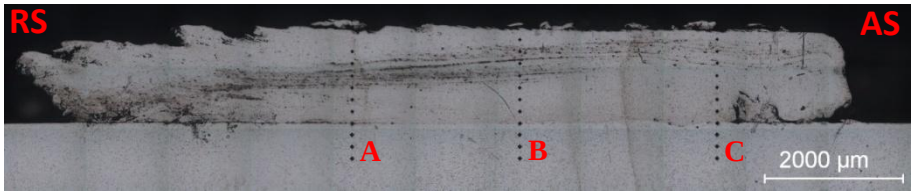

b)

Hardness profile from P2_S_TS2

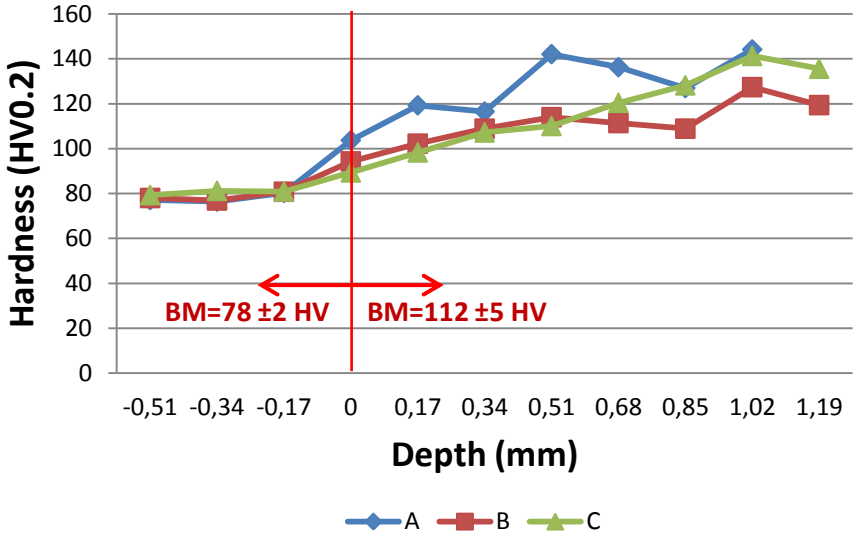

Figure 4.30 - Hardness profiles from test samples: (A) P2_S_TS1, (B) P2_S_TS2.

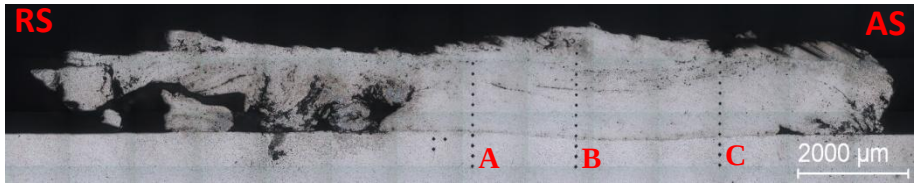

a)

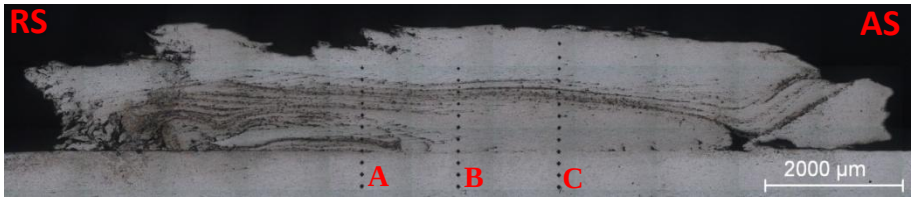

b)

Hardness profile from P2_S_TS1

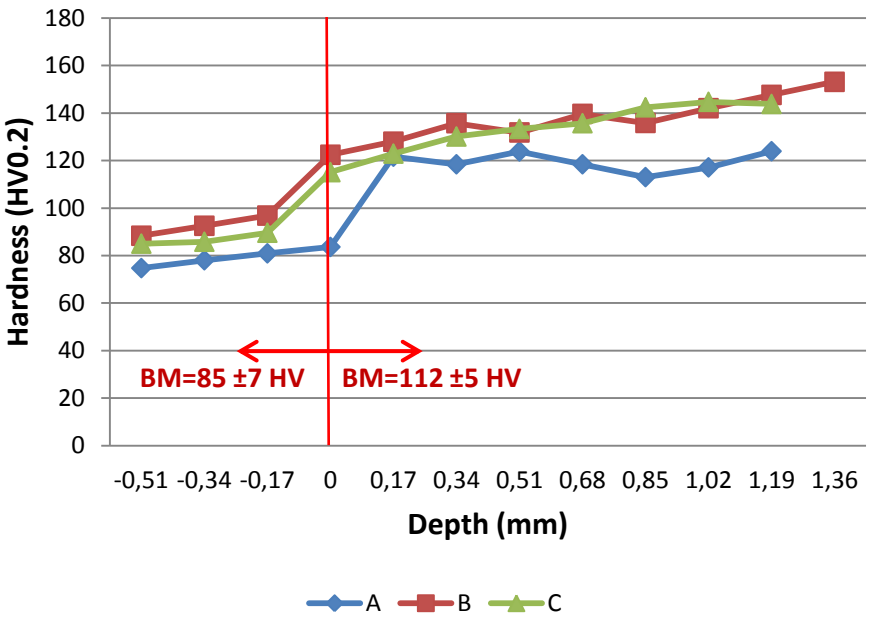

Hardness profile from P2_S_TS2

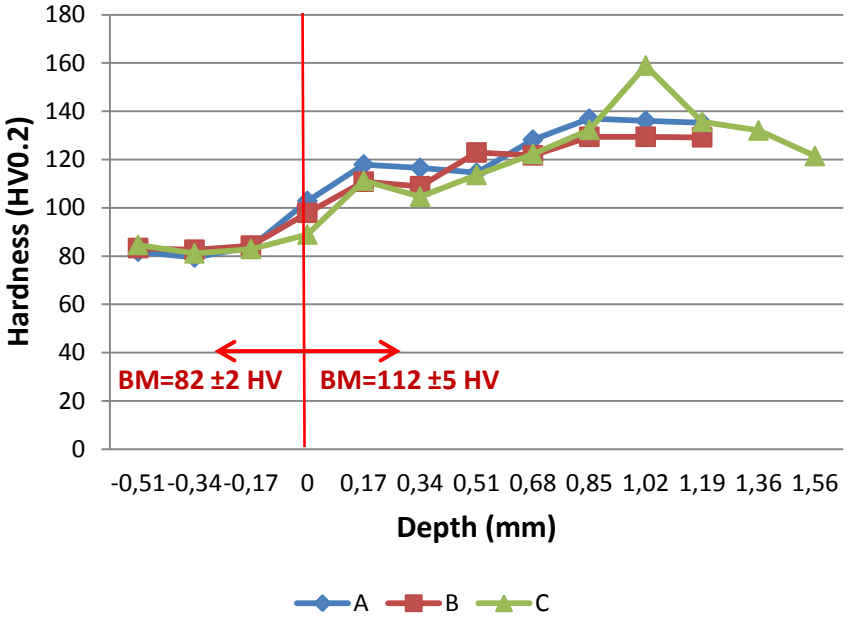

Figure 4.31 - Hardness profiles from test samples: (A) P2_S_TS3, (B) P2_S_TS4.

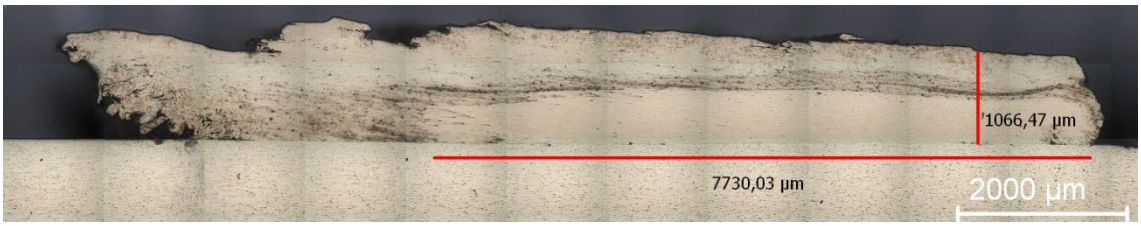

Hardness profile for P2_S_TS5.

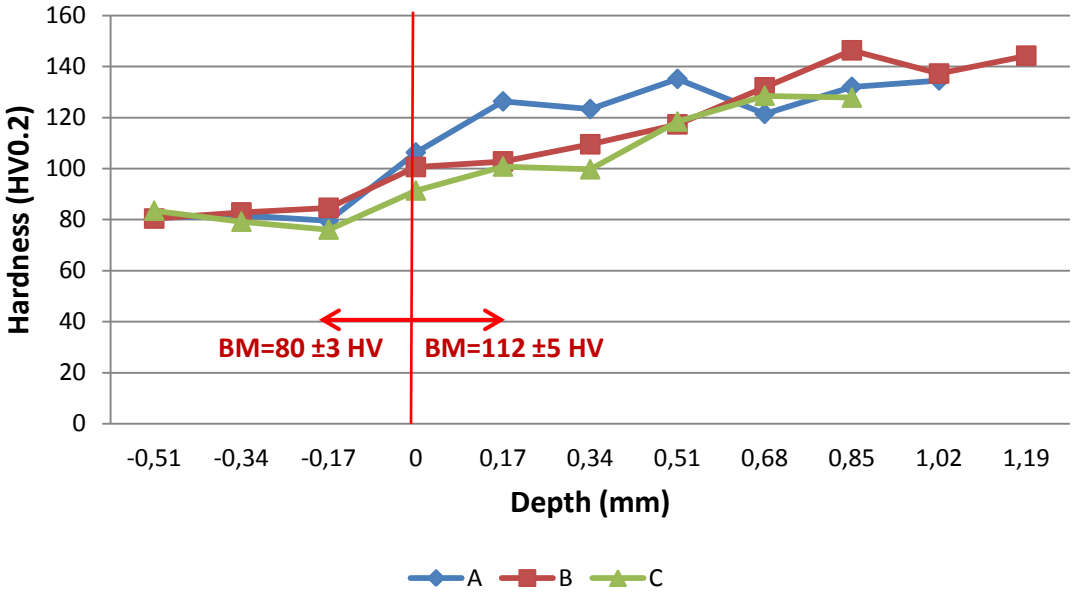

Figure 4.32 - Hardness profile for P2_S_TS5.

4.3 Friction stir process with predeposition of reinforcing particles using electric current (P1_E).

4.3.1 Friction stir process with predeposition of reinforcement with alumina (P1_E_A).

The parameters used for this tests were chosen according to the results presented in process P1_A and are depicted in Table 4.8. These were chosen due to good results in distributions, homogeneity, and size of superficial reinforced layer obtained.

For each test preformed with electric current there was a segment before and after without the assistance of electric current, to compare results.

Table 4.8 - Parameters of P1_E_RA

Tests nº	ω (rev)	Vx (mm/min)	ω/Vx	Angle (º)
P2_E_A_TS1 to TS6	1120	180	6,222	0
P2_E_A_TS7 to TS 13	710	224	3,170	0

4.3.1.1 Macroscopic characterization.

Due to the pre deposition of particles and the lack of tool force in the equipment used, there were some difficulties in process control; this is visible in the waviness obtained in beads that appears to be due to a small tool vertical force thus lacking contact between tool and BM.

Figure 4.33 presents macroscopic images from beads. Due to excess of powders it is difficult to see the tracks and this lack of visibility difficult process control. Tracks 1 and 2 correspond to tests sample P1_E_A_TS1 to TS6, and tracks 3 and 4 correspond to the remaining test samples.

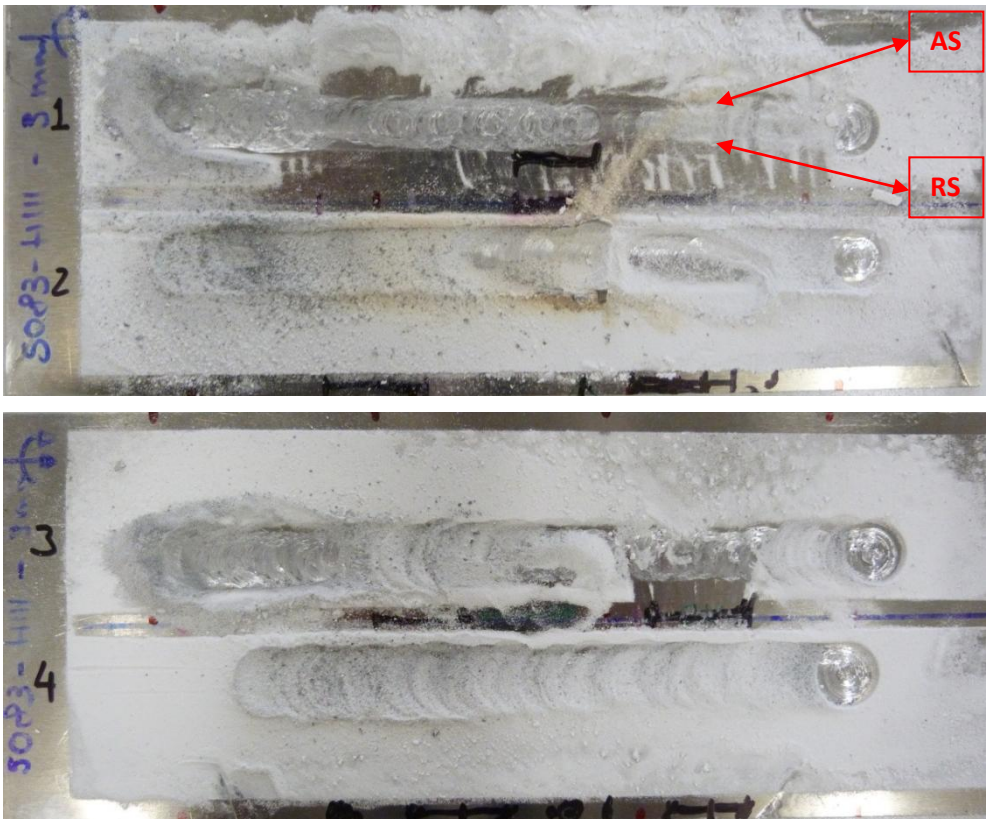

Figure 4.33 - Macrograph from tracks for trial group P1_E_A.

4.3.1.2 Microscopic characterization.

Figure 4.34 depicts the zones where test samples were removed for characterization. Samples were always taken in pairs to compare the process with and without electric variant. The zones with the letter C correspond to zones processed with electric variant, and in red is marked where test sample was removed.

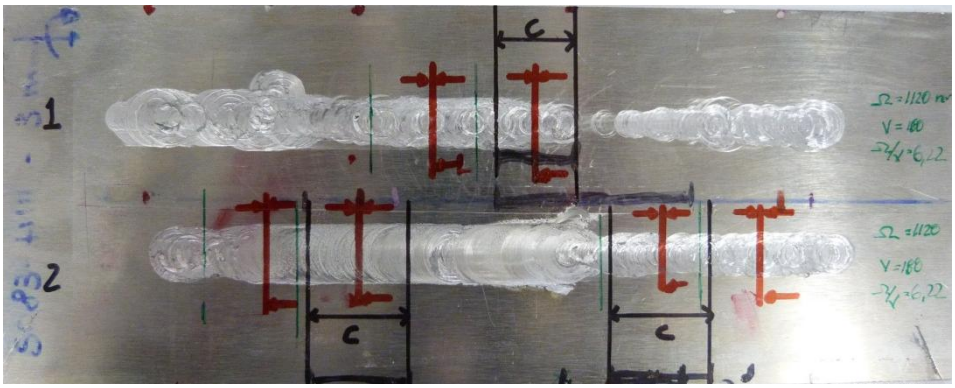

a)

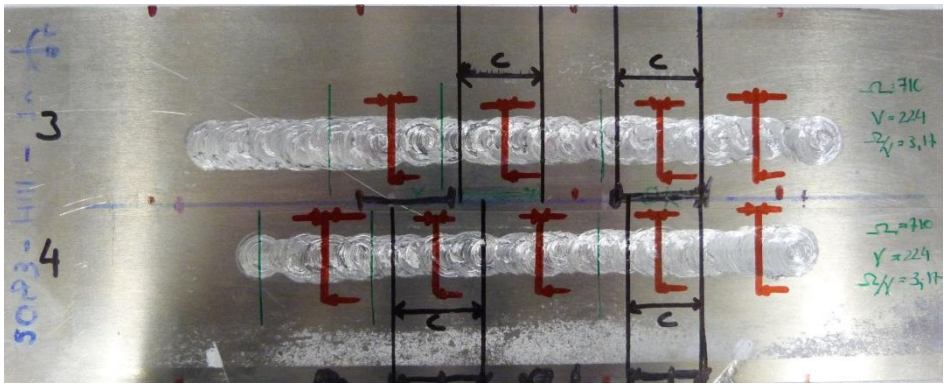

b)

Figure 4.34 - Macrograph from tracks with test samples removable zones, (A) test samples from TS1 To TS6, (B) test samples from TS7 to TS13

Figure 4.35 represent several micrographs from cross sections using parameters P1_E_A_T1, and P1_E_A_T2. In these micrographs is observed a lack of thin reinforced layer with and without the assistance of electric current, depicting the difficulty in process control mentioned above. A number of defects like tearing is visible in test samples.

a)

b)

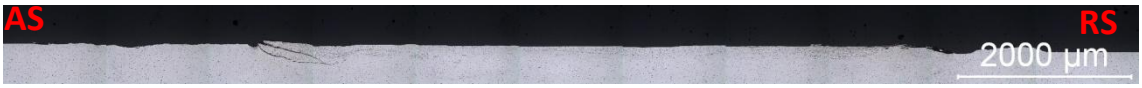

c)

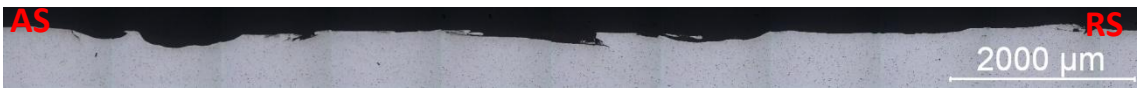

d)

Figure 4.35 – Macrographs from cross sections tests samples, (A) P1_E_A_TS1, (B) P1_E_A_TS2, (C) P1_E_A_TS7, (D) P1_E_A_TS8.

Figure 4.36 depicts test samples P1_E_A_TS3, which was removed from a track produced without assistance of electric current. Test sample P1_E_A_TS3 shows a thin reinforced layer as expected with a depth around 200 µm and an extension of 5800 µm. These results are similar with the ones obtained in P1_A, but the difference is in the shoulder diameter used in this process that decreased the layer extension. Particles are well distributed in reinforced layer and have fragmented into smaller particles as in process P1_A as depicted in Figure 4.36 g) and h). Figures 4.36 c) and d), shows larger concentrations of alumina particles on the bead surface. Interface zone depicted in Figures 4.36 e) and f) shows smaller concentrations of alumina particles as expected due to the viscoplastic behaviour.

Test sample P1_E_A_TS4, was removed from a zone in the bead produce with the assistance of electric current. Figure 4.47 depicts micrographs from cross section of test sample P1_E_A_TS4. Micrographs taken from this test sample shows a large increase of reinforced thin layer with a depth of 1224 µm, and extension of 8000 µm. Figure 4.47 c) to g) shows the surface of the bead, in with a higher concentration of alumina particles is verified, but alumina particles are well distributed in all visible reinforced zone. Alumina particles have also fragmented in to smaller particles as depicted in Figure 4.47 d).

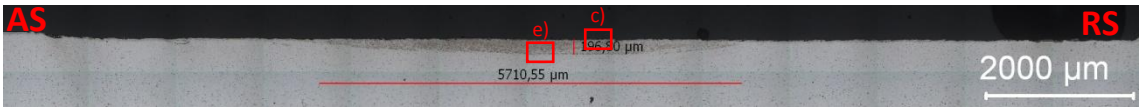

a)

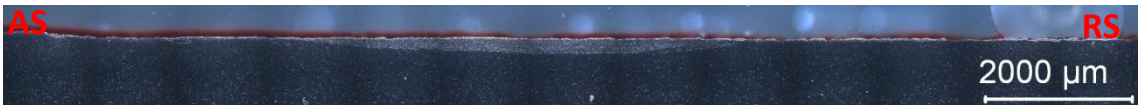

b)

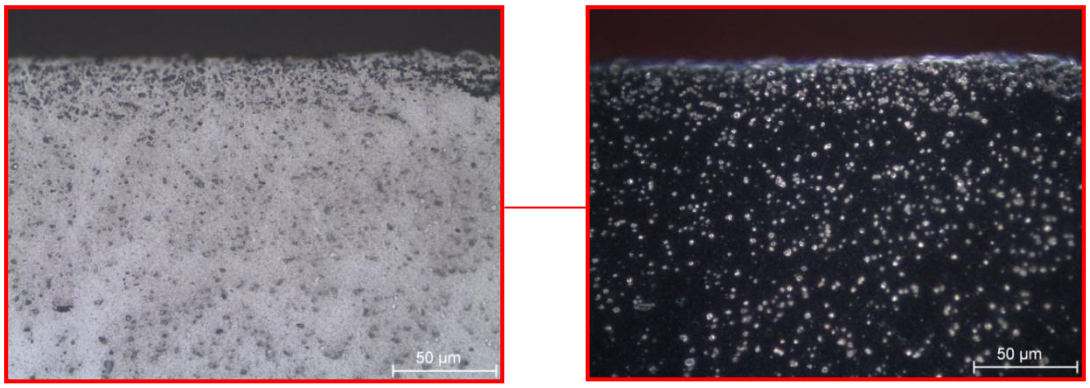

c) d)

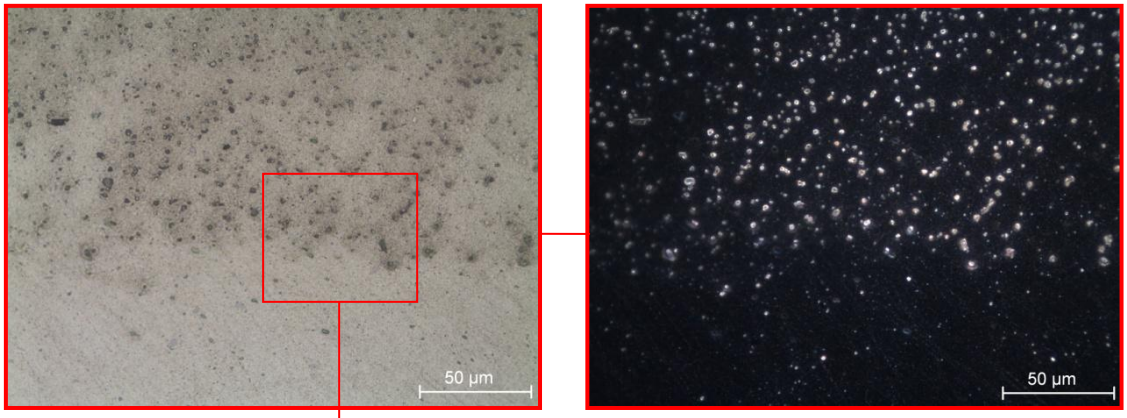

e) f)

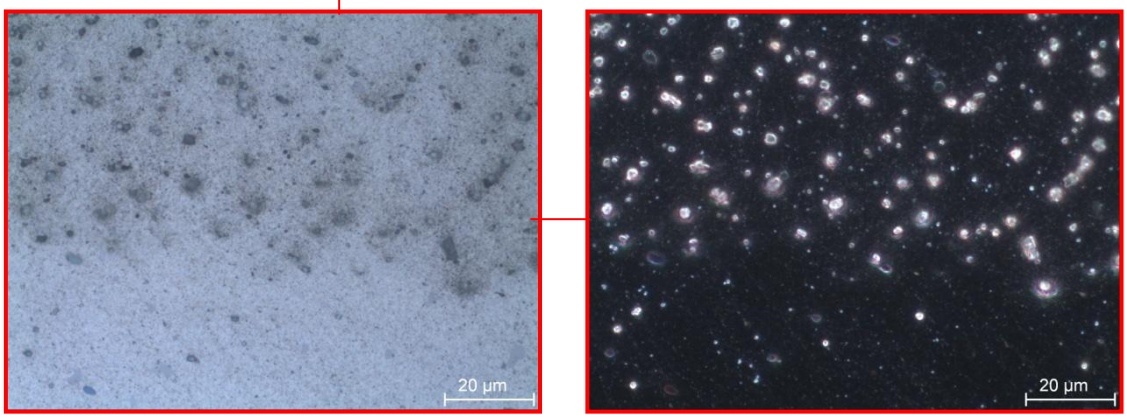

g) h)

Figure 4.36 - Cross section micrographs of test sample P1_E_A_TS3. (A) Macrographs of bead cross section in BF, (B) Macrographs of bead cross section in DF, (C,D) Details of surface zone in BF and DF respectively, (E,F,G,H) Details from interface zone BF and DF respectively.

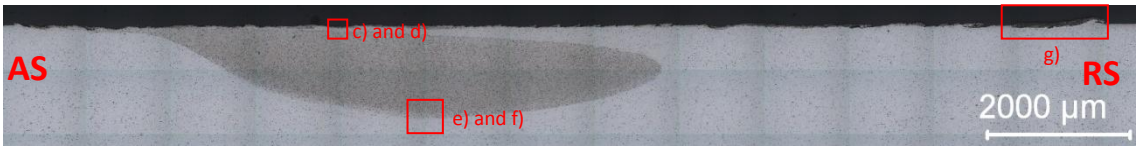

a)

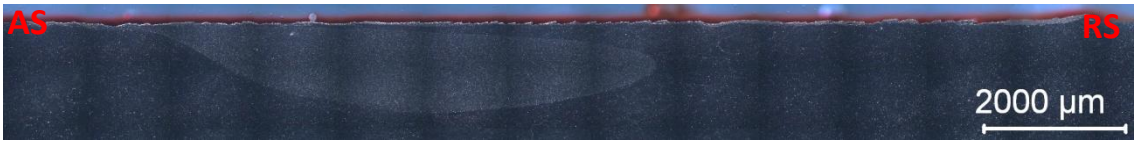

b)

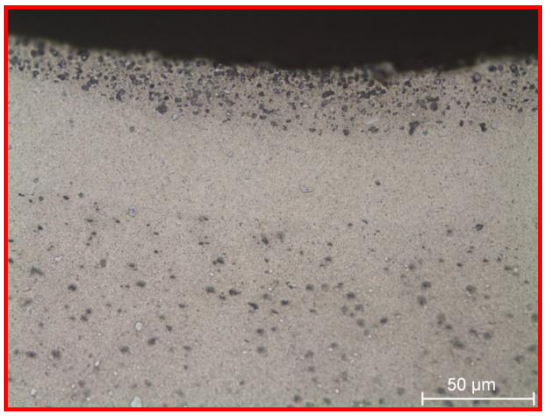

c)

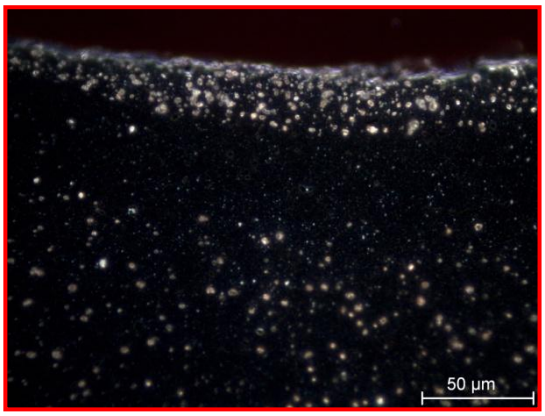

d)

e)

f)

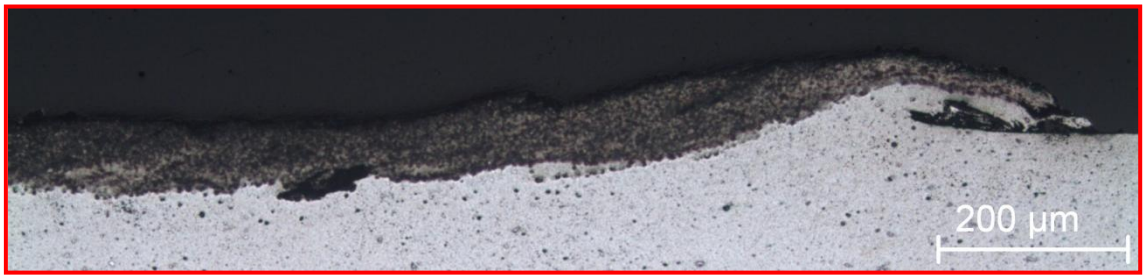

g)

Figure 4.37 - Cross section micrographs of test sample P1_E_A_TS4. (A) Macrographs of bead cross section in BF, (B) Macrographs of bead cross section in DF, (C,D) Details of surface zone in BF and DF respectively, (E,F) Details from interface zone BF and DF respectively, (G) Detail from surface zone in the RS.

Comparing the two test samples it is noticeable that electric current assistance resulted in a increase of reinforced area zone, with an increase in approximate 500% in depth and of 40% in extension. This result shows the smoothing effect on BM improving particles penetration. Figure 4.38 represents a comparison of micrographs taken from test samples P1_E_A_TS3 and TS4. These micrographs allow the comparison of particles concentration between the two samples. It can be verified that TS4 has a lower particle concentration than TS3. Increasing reinforced area provokes a decrease of concentration because particles volume maintains constant during both process.

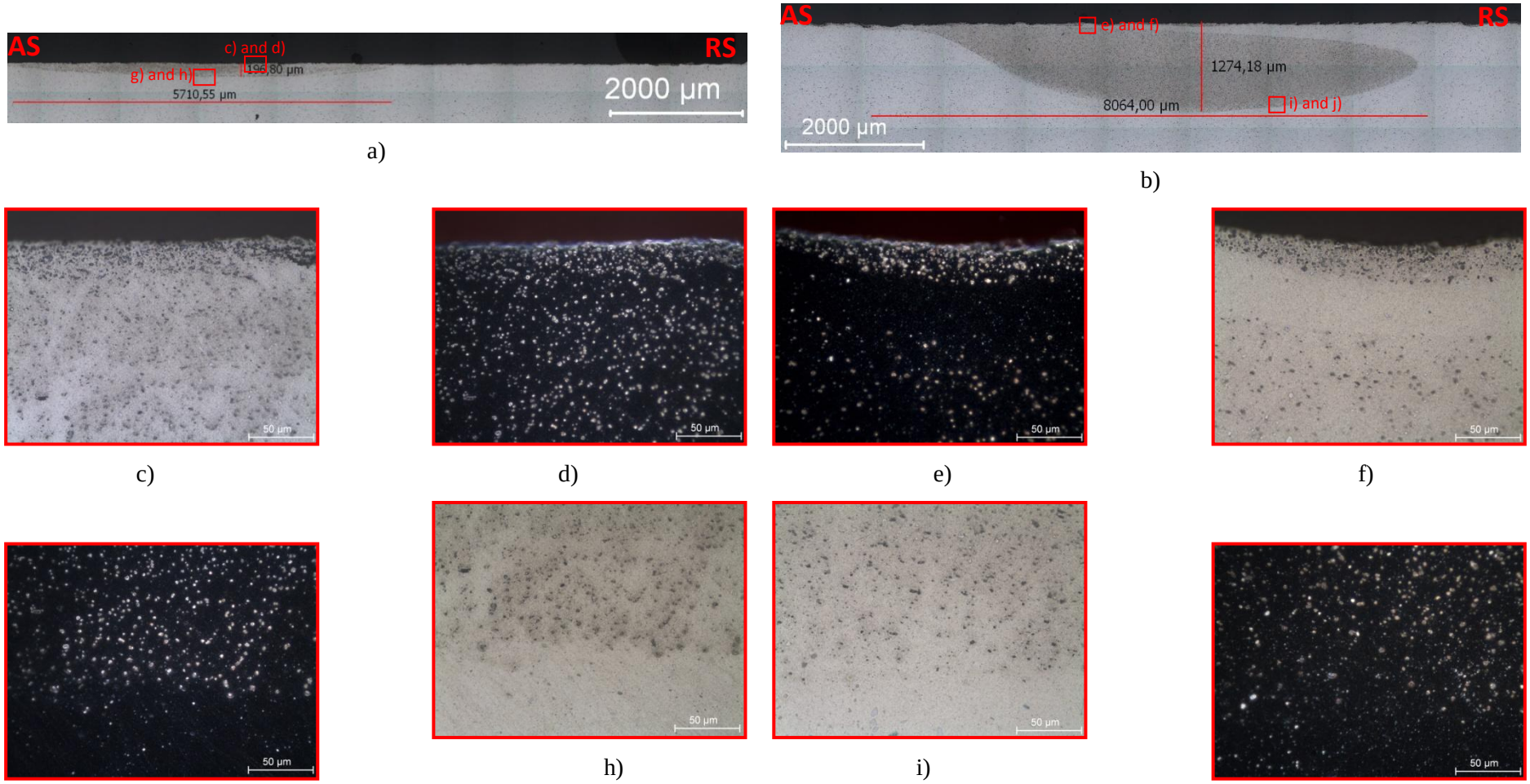

Figure 4.38 - Cross section micrographs of test sample P1_E_A_TS4. (A) Macrographs of P1_E_A_TS3, (B) Macrographs of P1_E_A_TS4, (C,D) Details of surface of P1_E_A_TS3, (E,F) Details of surface of P1_E_A_TS4, (G,H) Detail from interface of P1_E_A_TS3, (I,J) Detail from interface of P1_E_A_TS4.

4.3.1.3 Hardness testing.

Hardness profiles were only taken, from test samples that showed a reinforced zone. The group of samples P1_E_A_TS3 and TS4 were the only samples where there was a reinforced zone, with test samples showing an increase of approximately 39 % and 29 % in hardness in comparison with BM.

Figure 4.38 shows vertical hardness profiles taken from both test samples. Comparing the two, it is noticeable where vertical profiles enters the BM, and also test sample P1_E_A_TS3 shows a higher hardness than test sample P1_E_A_TS4. This fact shows that although a larger area of reinforcing zone has been achieved, the lower concentration of alumina particles verified on test sample P1_E_A_TS4 decreases hardness by 10 % compared with P1_E_A_TS3.

Figure 3.39 represents longitudinal hardness profiles for both test samples, and this profile confirms what was observed in vertical hardness profiles, that test sample processed without the assistance of electric current demonstrates a higher hardness due to alumina particles concentrations.

The difference in hardness is explain by the difference in particle concentration, that can be explain by the difference in reinforced area with the same volume of alumina particles.

a)

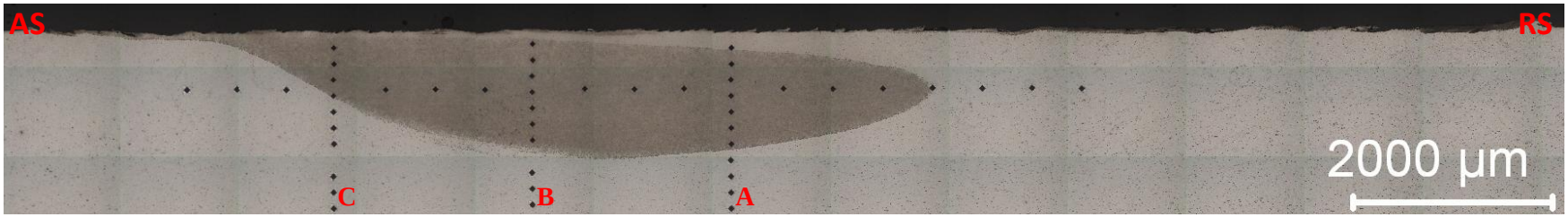

b)

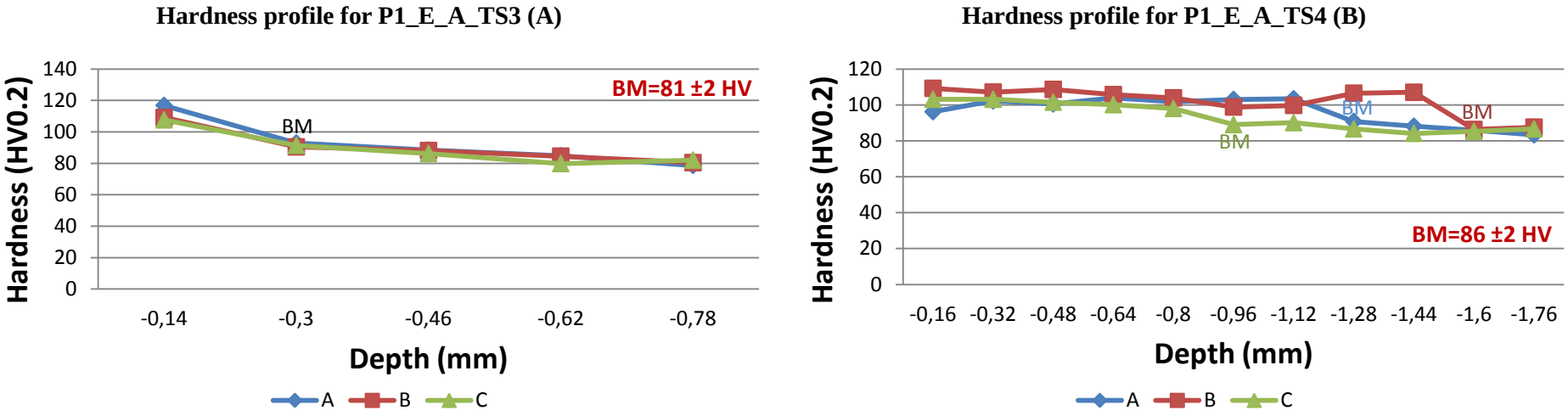

Figure 4.39 - Hardness profiles from test samples: (A) P1_E_A_TS3, (B) P1_E_A_TS4

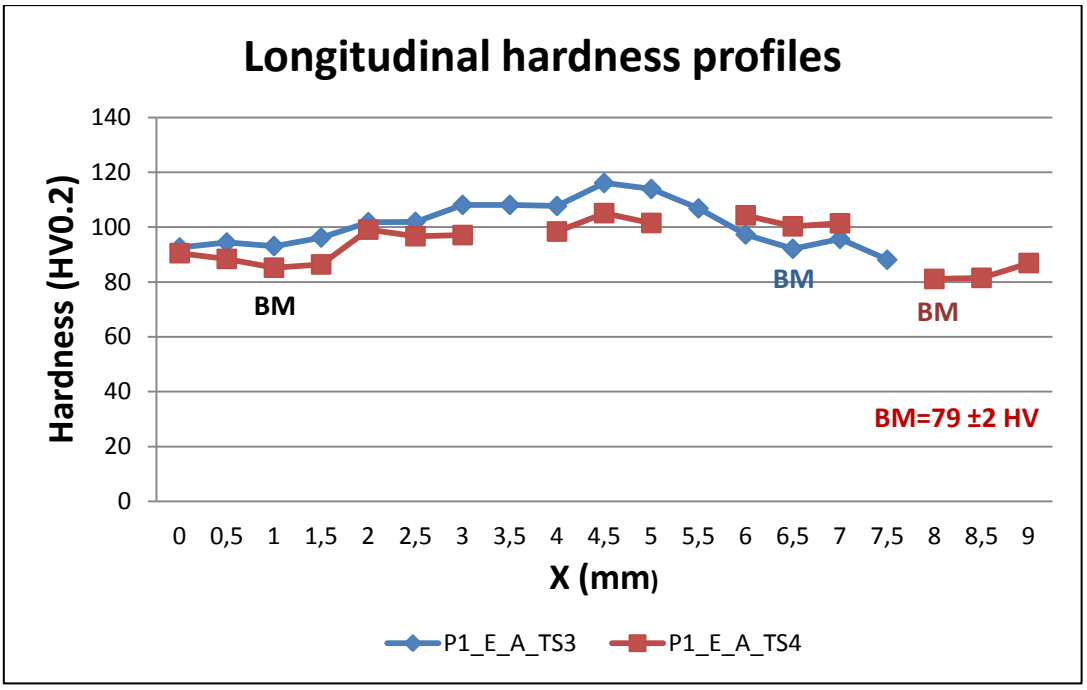

Figure 4.40 – Hardness profile along cross section for P1_RA_TS3 to TS4.

4.3.2 Friction stir process with predeposition of reinforcing silicon carbide particles using electric variant (P1_E_S).

Due to severe wear observed in pin and shoulder during P1_S, this process assisted with electric current reinforced with silicon carbide particles was discarded.

4.4 Friction stir process with consumable driller tool with electric variant (P2_E).

Simulations using CST software were performed to better understand the effect of heat input. Through these simulations, temperature raised by 10 ºC, which is insufficient to improve the process significantly.

Using thermocouples to evaluate temperature evolution, the same values for heat input were obtained. The initial system was developed to conduct current in a copper pin with a diameter of 3 mm, and for this process, a consumable pin of aluminium with 20 mm was used. This means that amperage values should be much higher than the ones used, by an order of magnitude higher. Tests preformed showed a constant value of 12 V, and a maxim value of amperage of 500 A. Optimal values should be of 5000 A.

Figure 4.42 depicts T evolution. Temperature in thermocouple 2 shows a rapid increase as soon as current passed through the system, reaching a maximum value of 34.4 ºC. Thermocouple 1 that correspond to the plate, shows a small increase reaching a maximum value of 22.84 ºC. Current was applied between the instant t = 11.6 s and t = 62.6 s represented in Figure 4.42 by the letters A and B.

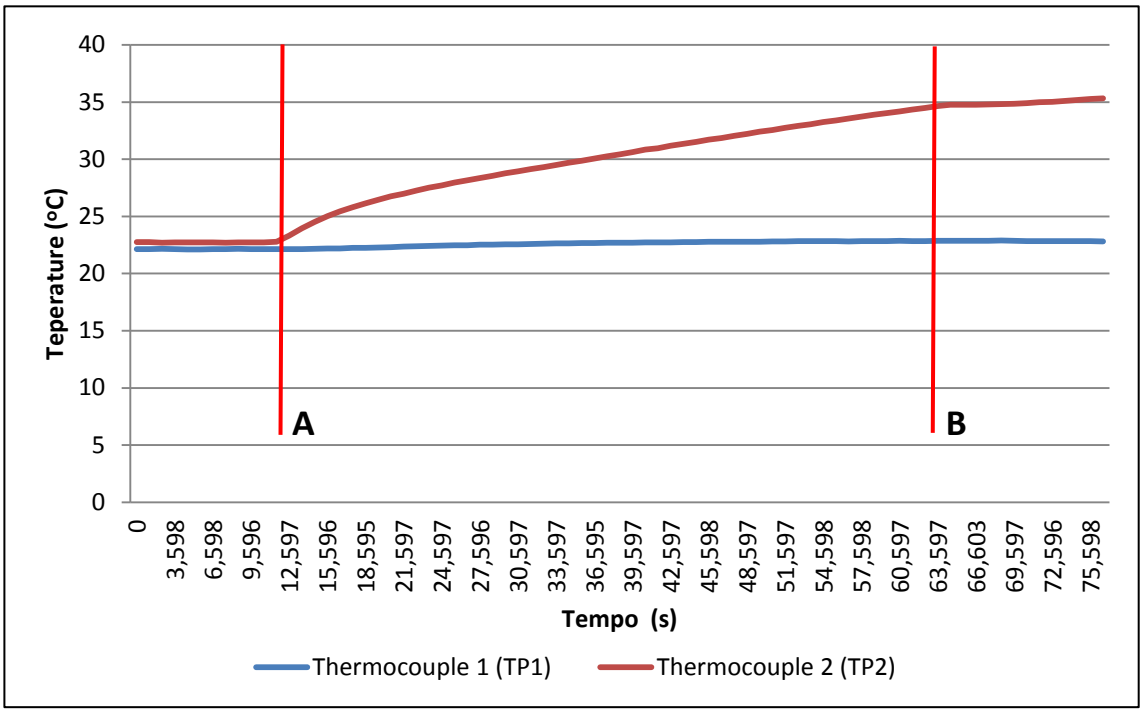

Figure 4.41 – Heat input in process P2_E.

5 Final conclusions and suggestions for future work

From the study conducted the following overall conclusions can be drawn:

Predeposition of reinforcing particles process:

- Reinforced surface layers are achievable with hard ceramic particles SiC and Al_2O_3 by means of FSP processing
- Parameters were optimized and both the extensions and depths where measured.
- Hard ceramic particles have fragmented to smaller particles in reinforced surface layers.
- High and homogeneous distributions of particles where observed in reinforcing layers in samples processed with specific parameters.
- Hardness measurements are consistent with image processing results, where surface hardness is increased in reinforced layers
- Surface layers reinforced with SiC particles shows higher hardness values that surfaces reinforced with Al_2O_3, with medium values of 200 HV and 135 HV, respectively.
- Surface layers reinforced with SiC particles shows larger particles than surfaces reinforced with Al_2O_3.
- High tool wear is observed in processed tests using SiC particles.

Consumable tool with drilled holes packed with particles:

- Continuous material deposition can only be achieved in a narrow window of rotational and advance speeds ratios
- High volumes of reinforcing particles originated poor bonding between deposited material and substrate.
- High concentrations of reinforcing particles were observed in deposited material.

- Consumable pin profiles with less holes and smaller diameter shows better results in bounding areas between.
- This process shows a large waste of deposited material.
- Lack of vertical tool control also originates poor bounding between deposited material and substrate.

Predeposition of reinforcing particles process assisted with electric current:

- A large increase in extension and depth of reinforced zone was achieved in test samples produced with the assistance of electric current.
- Smaller concentration of alumina particles were observed in test samples produced with the assistance of electric current, provoking a small decrease in hardness, but still a increase in hardness when compared with BM.
- Due to lack in process control, more specifically in toll vertical control force, only a few test samples were successfully produce.

Consumable tool with drilled holes packed with particles assisted with electric current:

- Simulations using software CST demonstrates that electric current that passes through the system is not enough to significantly improve the process.
- Preliminary test using thermocouples shows a small heat contribution to the process

The following is suggested for future work:

- Address the effect of initial particles size. Using smaller reinforcing particles may produce better results.
- Wear characterization should be performed in future investigations for the validation of strategies used, with the purpose of wear resistance in light weighted aluminium composites.
- Surface reinforcement with multi step over surfaces must be investigated to validate strategies for industrial applications.
- New strategies should be developed to increase bonding between deposited material and substrates.
- For process one with the electric variant, the used of equipment with tool control force should improve the beads consistency.
- Further testing should be preformed to validate results in the increasing of reinforced area.
- New strategies should be developed to increase values of the electric current that passes through the process. New equipment should by developed to allow higher values.

References

[1] F. M. Nascimento. "Processamento por fricção – Caracterização e analise de ligas de alumínios processadas". Lisboa, 2007, Dissertação (Mestrado em Engenharia de Materiais) – Instituto superior técnico, Universidade técnica de Lisboa

[2] R.S.Mishra, Z.Y. Ma, I. Charit, "Friction stir processing: a novel technique for fabrication of surface composite", Materials Science and Engineering A., 341, (2003), pp. 307-310.

[3] Lim SC, Gupta M, Ren L, Kwok JKM, "The tribological properties of Al–Cu/SiCp metal-matrix composites fabricated using the casting technique", Mater. Process Technology., (1999), pp. 80–90:591–6.

[4] Y. Morisada, H Fujii, T Nakata, M Fukusumi, "Effect of friction stir processing with SiC particles on microstructure and hardness of AZ31", Materials Science and Engineering A., 433, pp. 50-54.

[5] Y. Morisada, H. Fujii, T. Nagaoka, M. Fukusumi, " MWCNTs/AZ31 suface composites fabricated by friction stir processing", Materials Science and Engineering A., 419, (2006), pp. 344-348.

[6] C.I. Chang, Y.N. Wang, H.R. Pei, C.J. Lee, C.H. Du, J.C. Huang, "Microstructure and mechanical properties of Nano-ZrO2 and Nano-SiO2 particulate reinforced AZ31-Mg based composites fabricated by friction stir processing", Key Engineering Materials, Composite. Materials., 351, (2007), pp. 114-119.

[7] C.I. Chang, Y.N. Wang, H.R. Pei, C.J. Lee, J.C. Huang, "On the hardening of friction stir processed Mg-AZ31 based composites with 5-20% nano-ZrO2 and nano-SiO2 particles", Materials Transactions., 47, (2006), pp. 2942-2949.

[8] B.M. Darras, M.K. Khraisheh, F.K. Abu-Farha, M.A. Omar, "Friction stir processing of commercial AZ31 magnesium alloy", Journal of Materials Processing Technology., 191, (2007), pp. 77-81.

[9] W.-B. Lee, C.-Y. Lee, M.-K. Kim, J.-I. Yoon, Y.-J. Kim, Y.-M. Yoen. S.-B. Jung, Composites Science. Technology., 66, (2006), pp. 1513-1520.

[10] Y.C. Chen, K. Nakata, "Evaluation of microstructure and mechanical properties in friction stir processed SKD61 tool steel", Materials Caracterization,, 60, (2009), pp. 1471-1475.

[11] G. Faraji, P. Asadi, "Characterization of AZ91/alumina nanocomposite produced by FSP", Materials Science and Engineering A., 528, (2011), pp. 2431-2440.

[12] M. Barmouz, M. Givi, J. Seyfi, "On the role of processing parameters in producing Cu/SiC metal matrix composites via friction stir processing: Investigating microhardness, wear and tensile behaviour", Science Direct., 62, (2011), pp. 108-117.

[13] Zhu j, Liu L, Zhao H, Shen B, Hu W. "Microstructure and performance of electroformed Cu/nano-SiC composite", Material Design., 28, (2000), pp. 1958-62

[14] Ramesh CS, Noor Ahmed R, Mujeebu MA, Abdullah MZ. "Development and performance analysisi of novel cast copper-SiC-Gr hybrid composites", Material Design., 30, (2009), pp.1957-65.

[15] Lekka M, Koumoulis D, Kouloumbi N, Borona PL. "Mechanical and anticorrosive properties of copper matrix micro and nano-composite coatings", Electrochim Acta., 54, (2009), pp. 2540-6.

[16] Zhan Y, Zhang G. The effect of interfacial modifying on the machanical and wear properties of SiCp/Cu composites. Mater Lett., 57, (2003), pp. 4583-91.

[17] Tjong SC, Lau KC. Tribological behaviour of SiC particle-reinforced copper matrix composites. Mater Lett, 43, (2000), pp. 274-80.

[18] R.S. Mishra, M.W. Mahoney, S.X. McFadden, N.A. Mara, A.K. Mukherjee, "High strain rate superplasticity in a friction stir processed 7075 Al alloy", Scripta Materialia, 42, (2000), pp. 163-168.

[19] Z.Y.Ma, R.S.Mishra, M.W.Mahoney, "Superplasticity in cast A356 induced via friction stir processing", Scripta Materialia, 50, (2004), pp. 931-935.

[20] K. Elangovan, V. Balasubramanian, "Influences of pin profile and rotational speed of the tool on the formation of friction stir processing zone in AA2219 aluminium alloy", Materials Science Engeriring A, 459, (2007), pp. 7–18.

[21] Stephens JR, "High temperature metal matrix composites for future aerospace system", NASA TM 1987, pp. 100-212.

[22] I. S. Lee, P. W. Kao, M. J. Mo, "Microstructure and mechanical properties of Al-Fe in situ nanocomposite produced by friction stir processing", Intermatallics, 16, (2008), pp. 1104-1108.

[23] A. S. Zarghani, S. F. K. Bozorg, A. Z. Hanzaki, "Wear assessment of Al/Al_2O_3 nano-composite srface layer produced using friction stir processing", Wear, 270, (2011), pp. 403-412.

[24] D. Yadav, R. Bauri, "Processing, microstructure and machanical properties of nickel particles embedded aluminium matrix composite", Materials Science and Engineering A, 528, (2011), pp. 1326-1333.

[25] M. Sharifitabar, A. Sarami, S. Khorshahian, M. S. Afarami, "Fabrication of 5052Al/ Al_2O_3 nanoceramic particle reinforced composite via friction stir processing route", Material and Design, 32, (2011), pp. 4164-4172.

[26] S. Mukherjee, A. K. Ghosh, "Friction stir processing of direct metal deposited copper nickel 70/30", Materials Science and Engineering A, 528, (2011), pp. 3289-3294.

[27] S. A. Alidokht, A. Abdollah-zadeh, S. Soleymani, H. Assadi, “Microstructure and tribological performance of na aluminium alloy based hybrid composite produced by friction strir processing”, Materials and Design, 32, (2011), pp. 2727-2733.

[28] J. P. M. Gandra. “Preliminary Study on the Production of Functionally Graded Materials by Friction Stir Processing” Lisboa, 2010, Dissertação (Mestrado em Engenharia Mecânica) – Faculdade de Ciências e Tecnologia, Universidade Nova de Lisboa

[29] H. Fujii, L. Cui, M. Maeda and K. Nogi, “Effect of tool shape on mechanical properties and microstructure of friction stir welded aluminum alloys”, Materials Science Engeriring A, 419, (2006), pp. 25–31.

[30] Scialpi, L.A.C. De Filippis, P. Cavaliere, “Influence of shoulder geometry on microstructure and mechanical properties of friction stir welded 6082 aluminium alloy”, Materials and Design, Vol. 28, (2007), pp. 1124-1129.

[31] Y. Zhao, S. Lin, L. Wu, F. Qu, “Integral and layered mechanical properties of friction stir welded joints of 2014 aluminium alloys”, Materials Science and Technology, 59, (2006), pp. 2948– 2952.

[32] Y. Tozaki, Y. Uematsu and K. Tokaji, “Effect of tool geometry on microstructure and static strength in friction stir spot welded aluminium alloys”, Internacional Journal of Machine Tools & Manufacture, 47, (2007), pp. 2230–2236.

[33] L. Karthikeyan, V.S. Senthilkumar, K.A. Padmanabhan, “On the role of process variables in the friction stir processing of cast aluminium A319 alloy”, Materials and Design, Vol. 31, (2010), pp. 761-771.

[34] K. Elangovan, V. Balasubramanian, “Influences of tool pin profile and tool shoulder diameter on the formation of friction stir processing zone in AA6061 aluminium alloy”, Materials and Design, Vol. 29, (2008), pp. 362-373.

[35] K. Surekha, B.S. Murty, K.Prasad Rao, “Effect of processing parameters on the corrosion behaviour of friction stir processed AA 2219 aluminum alloy”, Solid State Sciences, Vol. 11, (2009), pp. 907-917.

[36] E.R.I. Mahmoud, M. Takahashi, T. Shibayanagi and K. Ikeuchi. “Effect of friction stir processing tool probe on fabrication of SiC particle reinforced composite on aluminium surfasse”. Science and Techonology of welding and Joining, 14, 5, (2009), pp. 413-425.

[37] Scialpi, L.A.C. De Filippis, P. Cavaliere. Influence of shoulder geometry on microstructure and mechanical properties of friction stir Welded 6082 aluminium alloy. Materials and Design, Vol. 28; (2007); pp. 1124-1129.

[38] Rajiv S. Mishra, Murray W. Mahoney. Friction stir welding and processing. Ohio: ASM International;2007;1° Edition, ISBN-10: 087170840X.

[39] M. Yang, C. Xu, C. Wu, K. Lin, Y. J. Chao, L. An, "Fabrication of AA6061/ Al_2O_3 nano ceramic particle reinforced composite coating by using stir processing", J. Mater. Sci., 45, (2010), pp. 4431-4438.

[40] K. Nakata, Y.G.Kim, H.Fujii, T.Tusumura, T.Komazaki, "Improvement of mechanical properties of aluminium die casting alloy by multi-pass friction strir processing", Materials Science and Engineering A, 437, (2006), pp. 274-280.

[41] L.B. Johannes, R.S. Mishra, "Multiple passes of frivtion stir processing for creation superplastic 7075 aluminim", Materials Science and Engeneering A, 464, (2007), pp. 255-260.

[42] Z.Y. Ma, S.R. Sharma, R.S. Mishra, "Effect of multiple-pass friction stir processing on microstructure and tensile properties of a cast aluminium-silicon alloy" Scripta Materialia, 54, (2006), pp. 1623-1626.

[43] Lee C.J. Huang JC, Hsieh PJ, "Mg based nano-composites fabricated by friction stir processing", Sripta Mater, 54, (2006), pp. 1415-20.

[44] B. Zahmatkeesh, M.H. Enayati, "A novel approach for development of surfasse nanocomposite by friction stir processing", Materials Science and Engineering A, 527, (2010), pp. 6734-6740.

[45] D. Yadav, R. Bauri, "International conference na Advances in Materials and Processing Technologies (AMPT2010)"

[46] R.S. Mishra, Z.Y. Ma, "Friction stir welding and processing", Materials Science and Engineering R, 50, (2005), pp. 1-78.

[47] A. Kurt, I. Uygur, E. Cete, "Surface modification of aluminium by friction stir processing" Journal of Materials Processing Technology, 211, (2011), pp. 313-317.

[4] Garcia-Cordovilla C, Narciso J, Louis E, "Abrasive wear resistance of aluminium alloy/ceramic particulate composites", Wear, 192, (1996), pp. 170-177.

[50] Basavarajappa S, Chandramohan G, Mukund K, Ashwin M, Prabu M, "Dry sliding wear behaviour of Al 2219/SiCp–Gr hybrid metal matrix composites", Mater Eng Perform 15 ,(2006), pp. 668–74.

[51] Riahi AR, Alpas AT, "The role of tribolayers on sliding wear behavior of graphitic aluminium matrix composites". Wear, 251, (2001), pp. 1396–407.

[52] Basavarajappa S, Chandramohan G, Mahadevan A, "Influence of sliding speed on the dry sliding wear behaviour and the subsurface deformation on hybrid metal matrix composite". Wear, 262, (2007), pp. 1007–12.

[53] S. Mukherjee, A. K. Ghosh, "Friction stir processing of direct metal deposited copper nickel 70/30", Materials Science and Engineering A, 528, (2011), pp. 3289-3294.

[54] Shafei-Zarghani, A , Kashani-Bozorg, SF , Zarei-Hanzaki, "Microstructures and mechanical properties of Al/ Al_2O_3 surface nano-composite layer produced by friction strir process", Materials Science and Engineering A, 500, (2009), pp. 84-91.

[55] X.N. Zhang, L. Geng, G.S. Wang, "Fabrication of Al-based hybrid composites reinforced with SiC whiskers and SiC nanoparticles by squeeze casting", Journal of Materials Processing Technology, 176, (2006), pp. 146-151.

[56] H. Ahlatci, T. Kocer, E Candan, H Cimenoglu, "Wear behaviour of Al/(Al2O3p+SiCp) hybrid composites", Tribology International, 39, (2006), pp. 213-220.

[57] E. Mahmoud, M. Takahashi, T. Shibayanagi, K. Ikeuchi, "Wear characteristics of surfasse-hybrid-MMCs layer fabricated on aluminum plate by friction stir processing", Wear, 268, (2010), pp. 1111-1121

[58] W. L. E. Wong, M. Gunpta and C. Y. H. Lim, Sol. Stat. Phenomena 111, (2006), pp. 39-42.

[59] J. Singh, S.K. Goel, V.N.S. Mathur, M.L. Kapoor, J. Mater. Sci. 26 (1991) 2750–275

[60] A.R.E. Singer, S. Ozbek, "Metal matrix composites produced by spray codeposition", Powder Metallurgy, 28, (1985), 72–78.

[61] K.L. Tee, L. Lu, M.O. Lai, "In situ processing of Al-TiB2 composite by the stir-casting technique", Journal of Materials Processing Technology, 89–90, (1999), pp. 513–519.

[62] D. Satpathi, A.K. Maji, in: International Conference on Intelligent Materials, Tchnomic Pub. Co., Williamsburg VA, 1994

[63] S. M. Tuominen, A. R. Pelton, in: US-Japan workshop on Smart Materials and Structures, Warrendale, PA, TMS, 1997

[64] M. Dixit, J. W. Newkirk, R. Misha, "Properties of friction stir-processed Al 1100-NiTi composite", Scripta Materialia, 56, (2007), pp. 541-544.

[65] C.F. Deng, Y.X. Ma, P. Zhang, X.X. Zhang, D.Z. Wang, "Thermal expansion behaviors of aluminum composite reinforced with carbon nanotubes", Materials Letters, 62, (2008), pp. 2301–2303.

[66] E.T. Thostenson, C. Li, T.W. Chou, "Nanocomposites in context", Composites Science and Technology, 65, (2005), pp. 491–516.

[67] E.T. Thostenson, Z. Ren, T.W. Chou, "Advances in the science and technology of carbon nanotubes and their composites: a review", Composites Science and Technology, 61 (2001) 1899–1912.

[68] D. K. Lim, T. Shibayanagi, A. P. Gerlich, "Synthesis of multi-walled CNT reinforced aluminium alloy composite via friction stir processing", Materials Science and Engineering A, 507, (2009), pp. 194-199.

Annexes

A1 – Technical drawing of FSP tool body.

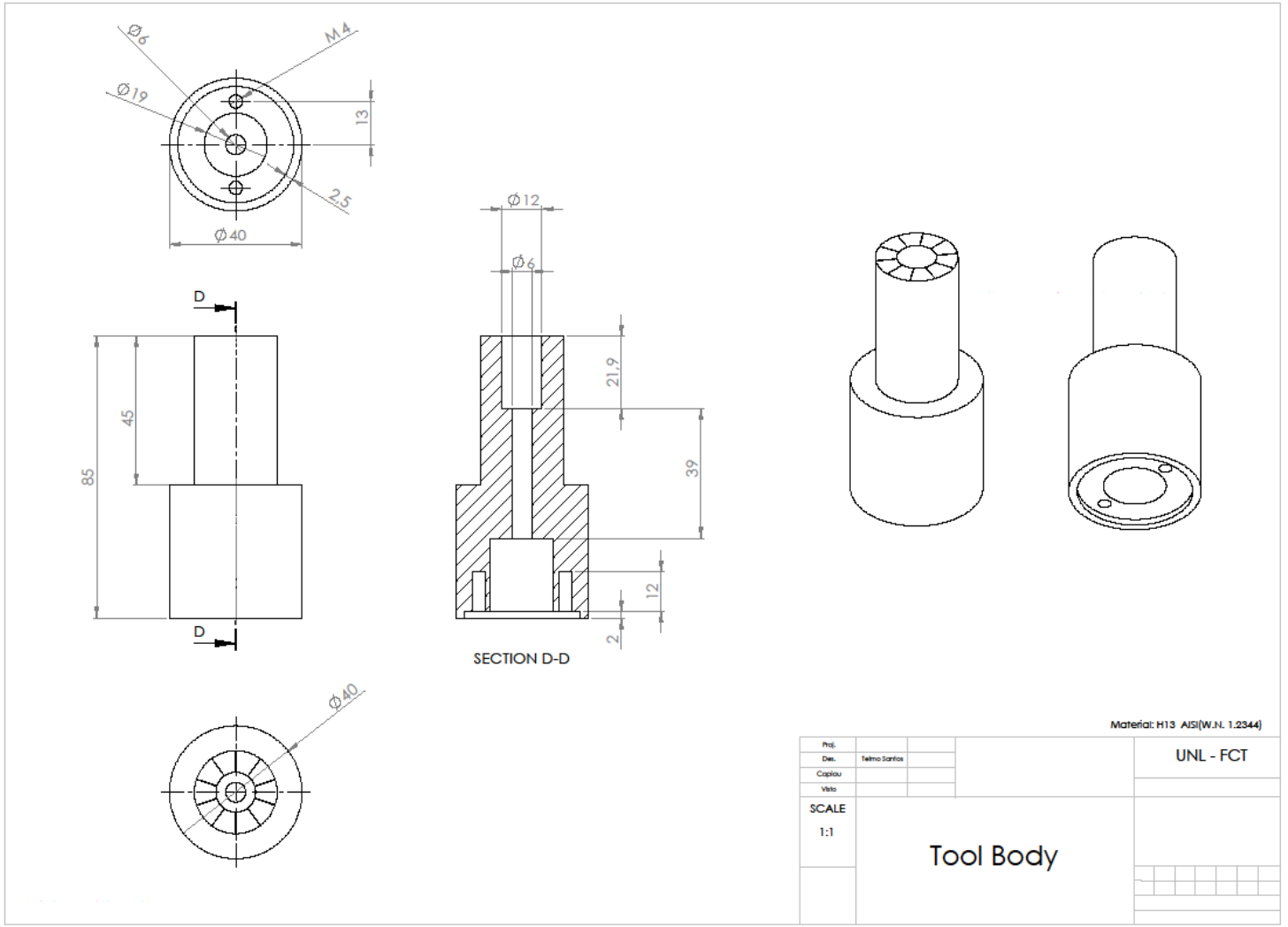

A2 – Technical drawing of FSP tool shoulder profiles.

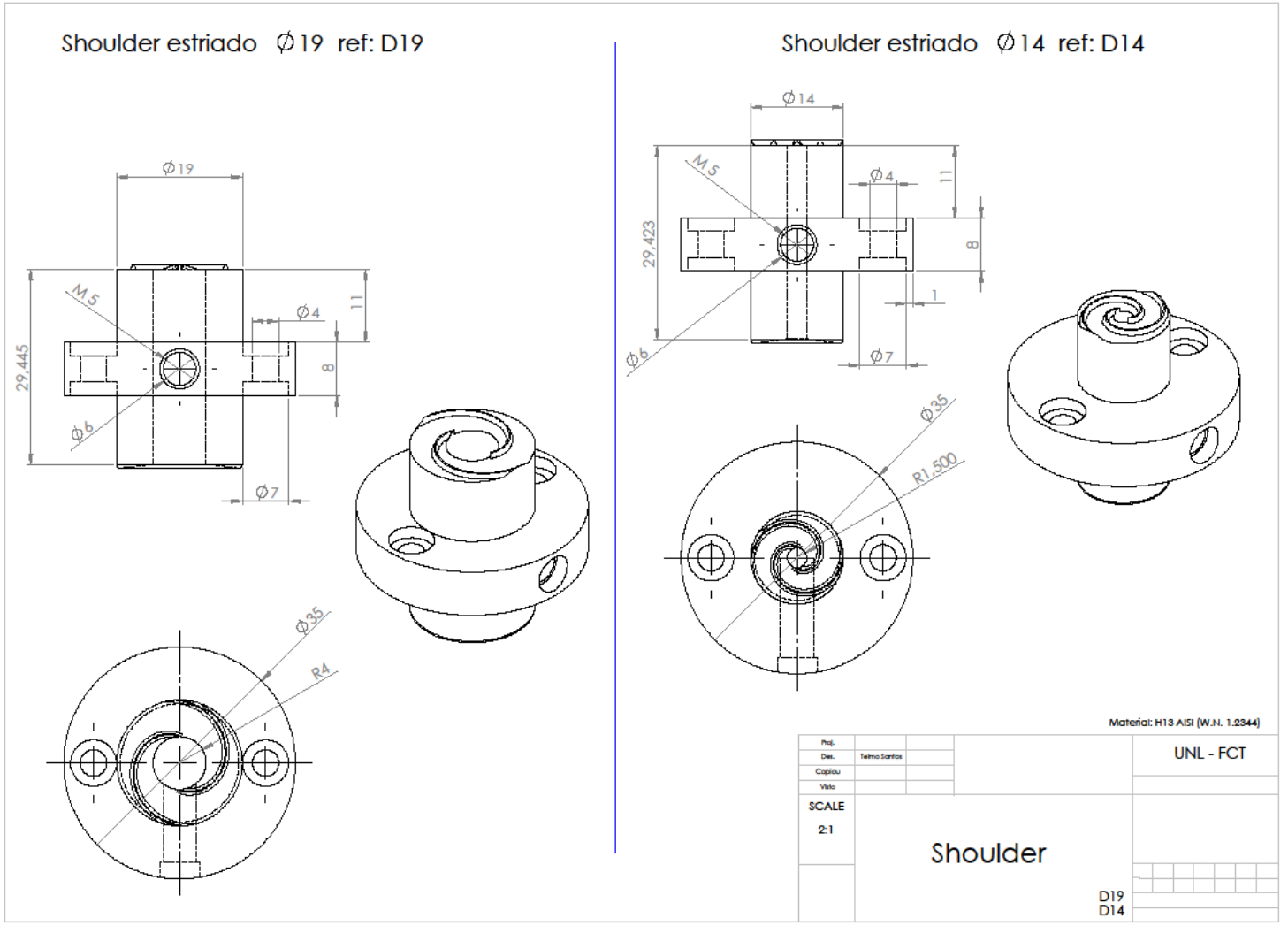

A3 - Metallography samples were prepared according with the following polishing procedure:

1. Sample section from processed surface.

2. Removal of edge shaving.

3. Sample marking.

4. Sample cold mounting in moulds filled with epoxy resin.

5. Polish each sample according to the sequence: SiC gridding paper 80, 240, 400, 600, 1200 and 2500 lubricated with running water.

6. Proceed with polishing using a PRESI SUPRA 5 cloth impregnated with Buehler Topol alumina solution of 1 and 0.3 μm. Perform circular motions against polisher rotation direction to eliminate comets.

7. Etch samples with Keller‟s reagent prepared according to Table E.1.

Table E.1 – Keller`s reagente composition and use.

Reagent	Composition	Etching procedure
Keller	5 mL HNO_3 3 mL HCI 2 mL HF 190 mL H_2O	Dip the samples for 10 seconds. Wash with running water. Blow dry with hairdryer. In case of unsatisfactory contrast, repeat process for 3 second time intervals.

8. Photograph with several magnifications the most relevant features observed.

Guide lines:

- The grinding papers must be exclusively used for aluminium alloy polishing.
- The samples should be washed with running water between each polishing step, following alcohol cleaning and blow dry.
- The cloths must be washed with water and detergent whenever excessive contamination is observed.
- Etching time duration is lower for micrographs than for macrographs.
- Ultrasonic cleaning is not advised, since the poor bonding between the particles and material substrate may lead to their release.